NAVAL POSTGRADUATE SCHOOL

MONTEREY, CALIFORNIA

THESIS

SIMULATION OF CYLINDER IMPLOSION INITIATED BY AN UNDERWATER EXPLOSION

by

Seth R. Krueger

June 2006

Thesis Advisor:	Young Shin
Second Reader:	Jarema Didoszak

Approved for public release; distribution is unlimited

THIS PAGE INTENTIONALLY LEFT BLANK

REPORT DOCUMENTATION PAGE		Form Approved OMB No. 0704-0188

1. AGENCY USE ONLY *(Leave blank)*	2. REPORT DATE	3. REPORT TYPE AND DATES COVERED
	June 2006	Master's Thesis

4. TITLE AND SUBTITLE Simulation of Cylinder Implosion Initiated by Underwater Explosion	5. FUNDING NUMBERS
6. AUTHOR(S) Seth R. Krueger	
7. PERFORMING ORGANIZATION NAME(S) AND ADDRESS(ES) Naval Postgraduate School Monterey, CA 93943-5000	8. PERFORMING ORGANIZATION REPORT NUMBER
9. SPONSORING /MONITORING AGENCY NAME(S) AND ADDRESS(ES) N/A	10. SPONSORING/MONITORING AGENCY REPORT NUMBER

11. SUPPLEMENTARY NOTES The views expressed in this thesis are those of the author and do not reflect the official policy or position of the Department of Defense or the U.S. Government.

12a. DISTRIBUTION / AVAILABILITY STATEMENT	12b. DISTRIBUTION CODE
Approved for public release; distribution is unlimited.	A

13. ABSTRACT (maximum 200 words)

The traditional study of underwater explosions (UNDEX) with respect to ship damage became of interest during World War II when torpedo explosions near a ship created more damage than a direct hit. Following the war, many full scale ship shock trials were conducted that provided much of the empirical data that is used in the field today. However, one type of shock phenomena became of interest in the late 1960s that potentially could be more damaging than a typical underwater explosion; an implosion. Crude implosion experiments were conducted in the late 1960s. Although these experiments collected data on pressure waves, more emphasis was placed on the acoustical properties associated with an implosion event. Today, one of the Navy's concerns is about the potential for the implosion of a pressure vessel in close proximity to a submarine hull. A computational approach is desired that will predict the source strength of an implosion.

This thesis will cover the basic principals of underwater shock phenomena, including explosions and implosions. Drawing from previous experiments and computational simulations, a detailed investigation of the implosion event will be made using, DYSMAS, a coupled Eulerian-Lagrangian solver. DYSMAS will be used to compare the characteristics of implosion and explosion events.

14. SUBJECT TERMS Implosion; UNDEX; Submarine; Shock Simulation; DYSMAS	15. NUMBER OF PAGES 119
	16. PRICE CODE

17. SECURITY CLASSIFICATION OF REPORT	18. SECURITY CLASSIFICATION OF THIS PAGE	19. SECURITY CLASSIFICATION OF ABSTRACT	20. LIMITATION OF ABSTRACT
Unclassified	Unclassified	Unclassified	UL

NSN 7540-01-280-5500 Standard Form 298 (Rev. 2-89)
Prescribed by ANSI Std. 239-18

THIS PAGE INTENTIONALLY LEFT BLANK

Approved for public release; distribution is unlimited

SIMULATION OF CYLINDER IMPLOSION INITIATED BY AN UNDERWATER EXPLOSION

Seth R. Krueger
Ensign, United States Navy
B.S. United States Naval Academy, 2005

Submitted in partial fulfillment of the
requirements for the degree of

MASTER OF SCIENCE IN MECHANICAL ENGINEERING

from the

NAVAL POSTGRADUATE SCHOOL
June 2006

Author: Seth R. Krueger

Approved by: Young S. Shin
Thesis Advisor

Jarema M. Didoszak
Second Reader

Anthony J. Healey
Chairman, Department of Mechanical and
Astronautical Engineering

THIS PAGE INTENTIONALLY LEFT BLANK

ABSTRACT

The traditional study of underwater explosions (UNDEX) with respect to ship damage became of interest during World War II when torpedo explosions near a ship created more damage than a direct hit. Following the war, many full scale ship shock trials were conducted that provided much of the empirical data that is used in the field today. However, one type of shock phenomena became of interest in the late 1960s that potentially could be more damaging than a typical underwater explosion; an implosion. Crude implosion experiments were conducted in the late 1960s. Although these experiments collected data on pressure waves, more emphasis was placed on the acoustical properties associated with an implosion event. Today, one of the Navy's concerns is about the potential for the implosion of a pressure vessel in close proximity to a submarine hull. A computational approach is desired that will predict the source strength of an implosion.

This thesis will cover the basic principals of underwater shock phenomena, including explosions and implosions. Drawing from previous experiments and computational simulations, a detailed investigation of the implosion event will be made using, DYSMAS, a coupled Eulerian-Lagrangian solver. DYSMAS will be used to compare the characteristics of implosion and explosion events.

THIS PAGE INTENTIONALLY LEFT BLANK

TABLE OF CONTENTS

LIST OF FIGURES

LIST OF TABLES

THIS PAGE INTENTIONALLY LEFT BLANK

ACKNOWLEDGMENTS

I would like to thank Professor Shin for providing me with the unique and privileged opportunity to work in the NPS Shock and Vibration Computational Laboratory. His leadership and sincerity truly encouraged me throughout my research and study. I would also like to thank him for the trust that he placed in me while working under his tutelage.

I am also indebted to the watchful, keen, encouraging, and guiding eye of Jake Didoszak. Throughout his incredibly busy day he always could take the time to answer questions, clarify the scope of my research, or offer useful criticism of my work. His professionalism and patience are to be admired. To him I am sincerely grateful.

To Jose Lepe, I wish you the best of luck as you further your studies at Cal-Poly. I thank you for your candor and knowledge as I learned the ropes of DYSMAS. It was a learning experience that I really enjoyed and I am glad that you were there as an extra set of eyes.

I would like to thank the gentlemen at Indian Head for providing extremely valuable training on DYSMAS. I would like to especially thank Roger Ilamni, whose expertise and technical prowess helped out immensely.

To the superb faculty at NPS, I thank your for your dedication and hard work. I wish Professor Kelleher the best in his well deserved retirement. In particular, I would like to thank Professor Kwon for his mastery of the finite element method. His expertise brought a full understanding to the method that is a foundation of computational analysis. Also, I would like to thank Professor P.H. Miller at USNA for his direction and assistance.

Lastly, but certainly not least, I would like to extend by sincere appreciation and thanks to my wife, Stephanie. Thank you for your patience and understanding as I completed my studies.

THIS PAGE INTENTIONALLY LEFT BLANK

I. INTRODUCTION

A. BACKGROUND

The field of underwater explosion (UNDEX) research is not a new concept. During World War II, it was noted that an UNDEX event could actually damage a vessel without directly impacting the target with a torpedo or mine. The concept of "close is close enough" was especially applicable to submarine warfare. In particular, depth charges were used to destroy submarines during this era. A depth charge did not necessarily need to physically touch the submarine in order to cause catastrophic damage.

Numerous studies were conducted on both surface ships and submarines after the war. Many of these studies focused on the vulnerabilities of ships and submarines to UNDEX phenomena. At the time, the studies focused on the initial pressure wave created by the explosion. The subsequent pressure pulses caused by bubble oscillation were also studied, but to a lesser degree.

Although less emphasis was placed on the study of the bubble oscillation, one fact remained apparent. The initial shock wave indeed excited the response of the ship or submarine, but intuitively, it does little for the low frequency response of the ship. Something else was causing the low frequency vibration of the hull girder. The explanation for this low frequency vibration, or whipping as it would be later dubbed, was indeed the oscillating bubble underneath the hull of the vessel. Researchers quickly realized the effect of whipping, which could possibly "break the back" of the ship or submarine [Ref. 1].

The cause of whipping is not necessarily the bubble oscillating, but the subsequent pressure gradients cause by the bubble oscillation. As previously stated, the initial shock wave provides the energy needed to excite many of the natural frequencies of the ship or the shipboard equipment. However, it is the gas bubble oscillation that remains the underlying cause of low frequency excitation [Ref. 1]. Whipping occurs to the extent that it does for two main reasons: 1) the bubble oscillations occur at a frequency that is roughly equal to the low mode natural frequency of the hull girder, thus

creating a resonance condition, and 2) because of the long duration flow loading from the initial bubble expansion which initiates the ship movement.

B. SCOPE OF RESEARCH

It has been established through testing that explosions near a submarine or surface vessel create a damaging initial pressure wave and a subsequent equally as dangerous oscillating gas bubble. However, an explosion is not the only method of producing a pressure wave and oscillating bubble. Perhaps an implosion event near a submarine would also create a damaging pressure wave and bubble phenomena.

For instance, suppose a submerged submarine was a host vessel to a smaller experimental pod or pressurized delivery vehicle. The interior compartment of the vehicle would be at atmospheric pressure, which would be much less than the pressure of the surrounding hydrostatic environment. If the vehicle were to encounter damage in some way or perhaps even randomly implode in close proximity to the host submarine, it would indeed create a pressure wave and oscillating bubble action that would ultimately impact the host vessel.

Computer modeling of implosion events are now becoming of interest. During the late 1960's, experiments were conducted on the implosions in pressure vessels. These experiments indicated that the maximum hydrodynamic pressure decreased as the distance from the implosion center increased [Ref. 2]. In other words, if an implosion event occurred in close proximity to a submarine, the vessel would encounter a large pressure wave. This pressure wave is a result of the surrounding water rushing inward upon the collapsing structure and low pressure air inside the structure. The surrounding water builds momentum as it rushed inward during the collapse. When the air reaches a minimum volume, the velocity of the water is forced to zero and the water compresses, resulting in a shock wave that travels back out into the water.

This thesis will investigate the pressure wave and gas bubble oscillation caused by an implosion event. The research conducted will utilize an Eulerian-Lagrangian coupled solver known as DYSMAS. In addition to studying the pressure wave cause by an implosion event, a comparative study will also be done to identify similarities between explosion and implosion events.

II. UNDERWATER EXPLOSION THEORY AND MODELING

A. ORDER OF EVENTS FOR AN UNDERWATER EXPLOSION

An underwater explosion releases a compressive shock wave which begins to move at 25,000 ft/sec and exponentially slows down to nearly 5,000 ft/sec (which is the speed of sound in water) as it moves outward. In order to simplify the mathematics of the problem, it can be assumed that the shock wave travels at the speed of sound in water, 5,000 ft/sec. By using this approximation, the following formula for a plane wave approximation in a compressible flow environment is:

$$P = \rho_0 C_0 u \qquad 1$$

where P is the fluid pressure, C_0 is the speed of sound in water, ρ_0 is the density of the fluid, and u is the fluid particle velocity.

Over time, empirical formulas have been developed to describe the fluid particle velocity and pressure during the initial shock phase of an UNDEX event cause by a specified charge type and weight. The following equation is an example of one of the empirical equations formulated to determine peak pressure at a specified distance from the charge:

$$P_{\max} = K_1 \cdot \left(\frac{W^{1/3}}{R} \right)^{A_1} \qquad 2$$

in which case P_{max} is the peak magnitude of the pressure in the shock front (measured in psi), K_1 and A_1 are parameters which are dependent on the type of charge (TNT, HBX-1, etc.), and R is the radial distance from the explosive charge to the target (measured in feet) [Ref. 3].

As the shock wave propagates through the water, it will inevitably reach either its target (a ship or submarine) or reflect off of the seafloor or the air-water interface. Shock waves that reflect off of the seafloor primarily remain compressive and reflect or transmit in accordance with Snell's Law, which states:

$$\frac{C_0}{\sin\alpha} = \frac{C_0}{\sin\alpha'} = \frac{C_0}{\sin\alpha''} \qquad (3)$$

where C_0 is the speed of sound in a given environment while the three angles are shown in Figure 1 below.

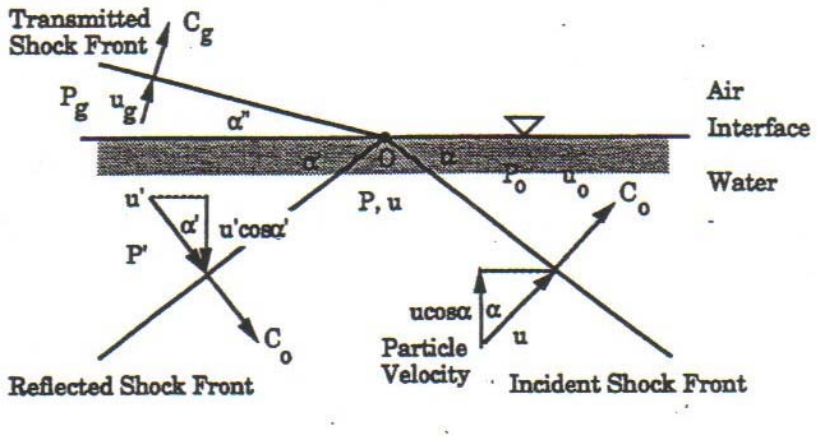

Figure 1. Illustration of Snell's Law (From Ref. 3)

The shock waves that reflect off of the air-water interface are known as surface reflection or rarefaction waves. These waves are tensile in nature. In addition, these reflection waves also follow Snell's Law. The direction and magnitude of these waves are determined by imagining an "image" charge which is equidistant of the charge below the waterline. Figure 2 illustrates the "image" charge and Snell's Law for both bottom and air-water interface reflection waves.

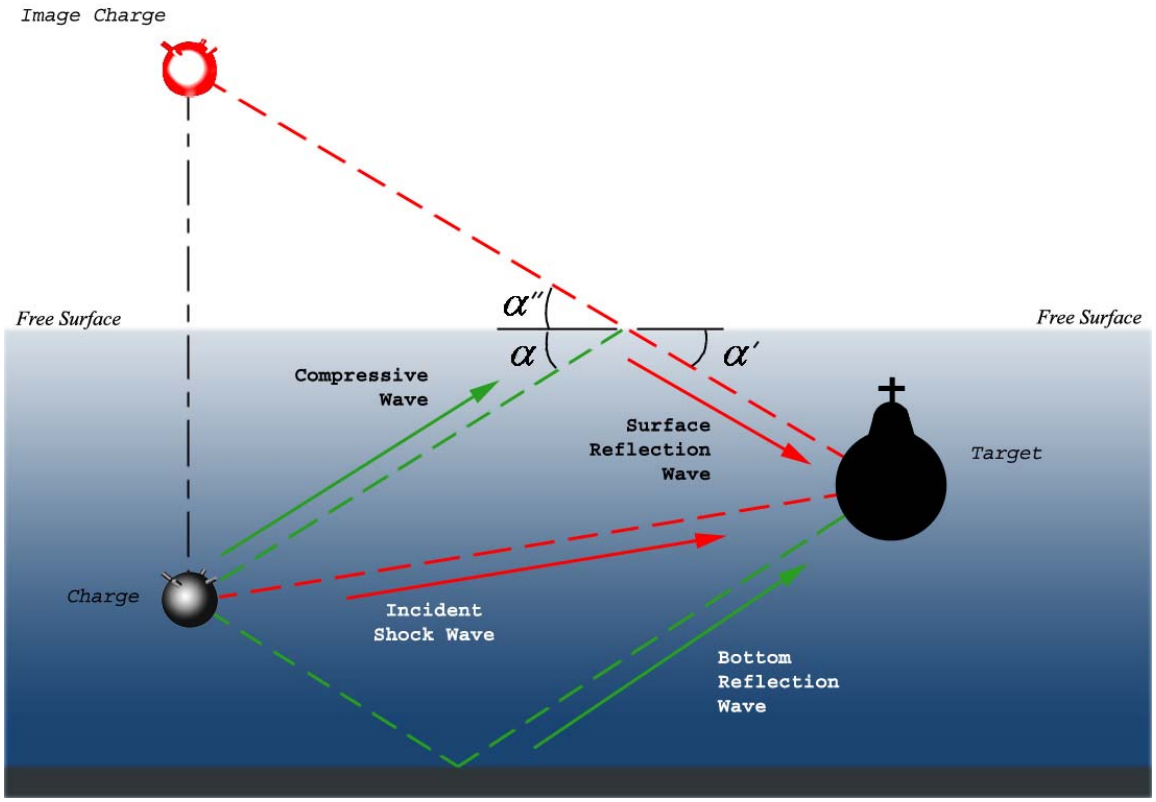

Figure 2. Typical UNDEX Phenomena Geometry (From Ref. 3)

Notice that the tensile wave as a result of surface reflection creates a tension force in the water. This tension causes a foamy appearance at the surface of the water. This phenomenon is known as bulk cavitation, where the pressure of the water is essentially equal to zero. Figure 3 is a photograph of this phenomenon.

Figure 3. Photograph of Bulk Cavitation Due to UNDEX Event

After the initial shock wave passes, subsequent pulses are experienced at time intervals that are functions of the type of explosive, charge weight, and depth of the charge. When an explosion occurs gasses are released. These gasses form a large expanding bubble which continues to expand until hydrostatic pressure halts the bubble's growth. When the bubble is finished expanding, the pressure inside the bubble is much less than that of the outside hydrostatic pressure. This causes the bubble to quickly collapse. When this bubble collapses, it releases a "bubble pulse". This pulse in turn creates another expanding bubble of lesser magnitude. The term "shock wave" is replaced with "pulse" because the pressure waves are now being created by the oscillating bubble. Recall that the initial shock wave, which causes initial damage to a ship or submarine, is of short duration and high magnitude. However, the pressure waves caused by the bubble pulses are of lower magnitude and longer duration.

Due to hydrostatics, the oscillating gas bubble migrates to the surface at varying speeds. As the bubble size decreases, the bubble moves more quickly to the surface. On the contrary, as the bubble re-expands, its velocity decreases. This varying velocity is due to the drag forces on the bubble. After many bubble oscillations, the energy from the explosion is either dissipated into a large number of small gas bubbles or the bubble reaches the surface and vents to the atmosphere [Ref. 4]. As the bubble moves toward the surface, the bubble dynamics can cause different disruptions to the water's surface depending on the initial depth of the charge. If the explosion is not at great depth, a large plume of water may occur at the surface of the water.

B. MODELING OF THE GAS BUBBLE OSCILLATIONS

As previously discussed, the initial damage done to a ship or submarine is due to the initial shock wave. The following pulses which are due to the oscillating bubble create the low frequency excitation. This low frequency excitation is known as whipping. In order to better understand whipping, one must first understand these gas bubble oscillations. Once theses oscillations are understood, mathematical models can be created and employed to predict the damage done by the bubble pulses.

Each bubble collapse results in a pulse that can be modeled as an acoustic wave. However, the pulses are not the primary means by which whipping occurs. The low frequency mode of the hull girder is primarily excited by the inertial movement of water that occurs when the gas bubble oscillates. Thus, whipping is not directly caused by the pressure waves associated with the pulses, but by the "fluid flow associated with the entire pressure field" which was in fact caused by the gas bubble oscillations [Ref. 5].

The motion of the gas bubble oscillations and the resulting pressure effects are seen in Figure 4. The vertical positions of the bubble are displayed with respect to time which is on the horizontal axis. Note that the bubble does not migrate to the right.

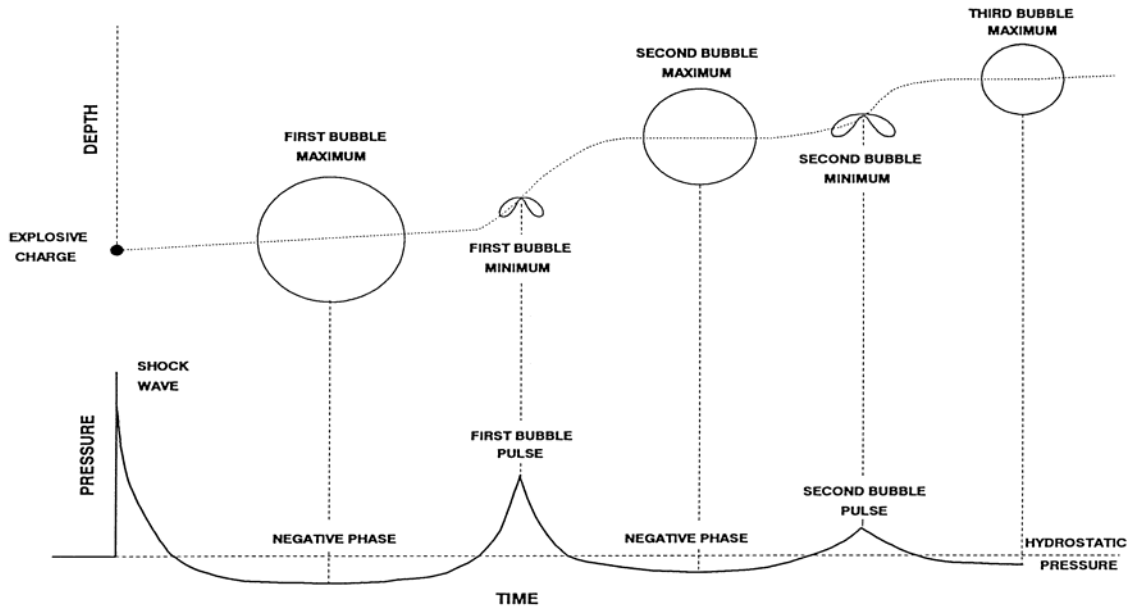

Figure 4. Bubble Oscillation and Subsequent Pressure Effects (From Ref. 3)

There are very important differences between the initial pressure wave and the subsequent gas bubble pulses. The distinctions between the two resulted in two approaches to mathematical modeling. As previously stated, the initial shock wave is modeled as an acoustic wave, which required the assumption of a compressible fluid medium. On the other hand, the bubble oscillations are modeled in an incompressible, irrotational, and inviscid fluid medium. The physical processes which occur for the initial explosion and the smaller "explosions" associated with bubble collapse are basically the same, only differing in magnitude and duration. The two mathematical models only partially capture what is occurring and are used based on the most dominant effects upon the ship at the time frame that is to be analyzed. The model for the gas bubble oscillations must capture both the pushing and pulling on the ship caused by the pressure gradients due to bubble oscillation. Therefore, a study of the field immediately surrounding the gas bubble is needed. Fortunately, the assumptions of irrotational, incompressible, and inviscid flow allows for straightforward calculations. However, the model of the initial shock wave must capture the large pressure impulse experienced by the ship. For this situation, the compressible fluid, acoustic model works well. An incompressible fluid dynamics algorithm could be employed to model the initial shock

wave, but the assumption of incompressibility would be invalid and would result in a failure to model the shock wave's large amplitude.

Chertock's original algorithms which modeled gas bubble oscillations made use of the assumption of an incompressible, irrotational, and inviscid fluid medium [Ref. 6]. When Hicks developed his modeling approach, he utilized the same assumptions. Hicks stated that the incompressibility assumption was valid because "the pressure in the gas bubble is very low during most of its pulsation cycle…" [Ref. 7]. The pressure is high only during the short period of the initial shock wave and also, but to a lesser extent, when the bubble collapses.

1. The Hicks Bubble Model

The derivation to follow on the gas bubble behavior from an UNDEX event was used by Hicks in his models, but was based on derivations by Herring and Taylor in addition to the work done by R. Cole which was completed shortly after World War II [Ref. 5, 7].

The premise of Hicks' model is the assumption of a fluid point source of strength, denoted as "e", which originates at the center of the explosion or bubble. This source approximation is used to model the gas bubble as an expanding sphere. This source refers to a volume flux, denoted as "Q", coming from a point source. The flow will spread out radially and at a specified radius, denoted as "r", will be:

$$u_r = \frac{Q}{4\pi r^2} = \frac{e}{r^2} \qquad 4$$
$$u_\theta = 0$$

where u_r and u_θ are radial and tangential particle velocities, respectively. Thus, it follows that:

$$e = \frac{Q}{4\pi} \qquad 5$$

The velocity potential is derived as:

$$\phi = \frac{e}{r} \qquad 6$$

In order to simplify the mathematical modeling, Hicks used the potential flow theory for a two dimensional case, using an infinitely long cylinder as the target. Using this approximation, Hicks then assumed that the fluid particle velocity surrounding the cylinder was uniform about the cylinder's cross section. This approach was entitled the "distant flow" method because it is based on the assumption that the uniform flow occurred at a distance "several ship diameters away from the charge" [Ref. 7]. Further studies by Hicks revealed that his two dimensional algorithms were indeed accurate for explosions that were "as close as one-fifth of the width of the hull transverse to the direction of vibration" [Ref. 8].

Equations 4 and 5 represent expressions that model a stationary oscillating bubble. In order to include bubble migration, or the bubble's tendency to rise to the surface due to buoyant forces, Hicks added the dipole term to the velocity potential equation, thus becoming:

$$\phi = \frac{e_1}{r_1} + \frac{e_2}{r_1^2} \cdot \cos(\theta_1) \qquad 7$$

where the first term is the simple source term and the second term is the dipole term [Ref. 5].

When Hicks initially allowed for bubble migration, he noticed that his algorithm overpredicted the bubble migration rate. The root of the problem was that Hicks modeled the bubble as a sphere. For a deep explosion, this assumption is quite accurate. However, when an explosion occurs at a more shallow depth, the bubble takes the form of a mushroom cloud, which is denoted in Figure 5. The mushroom cloud shaped bubble rises more slowly than a spherical shaped bubble. In order to correct this problem, Hicks incorporated a high drag coefficient of 2.25 [Ref. 5]. This drag coefficient is larger than

those typically associated with a submerged spherical object. However, it has calibrated for shallow weapon-sized charges which were based on test data from underwater explosions.

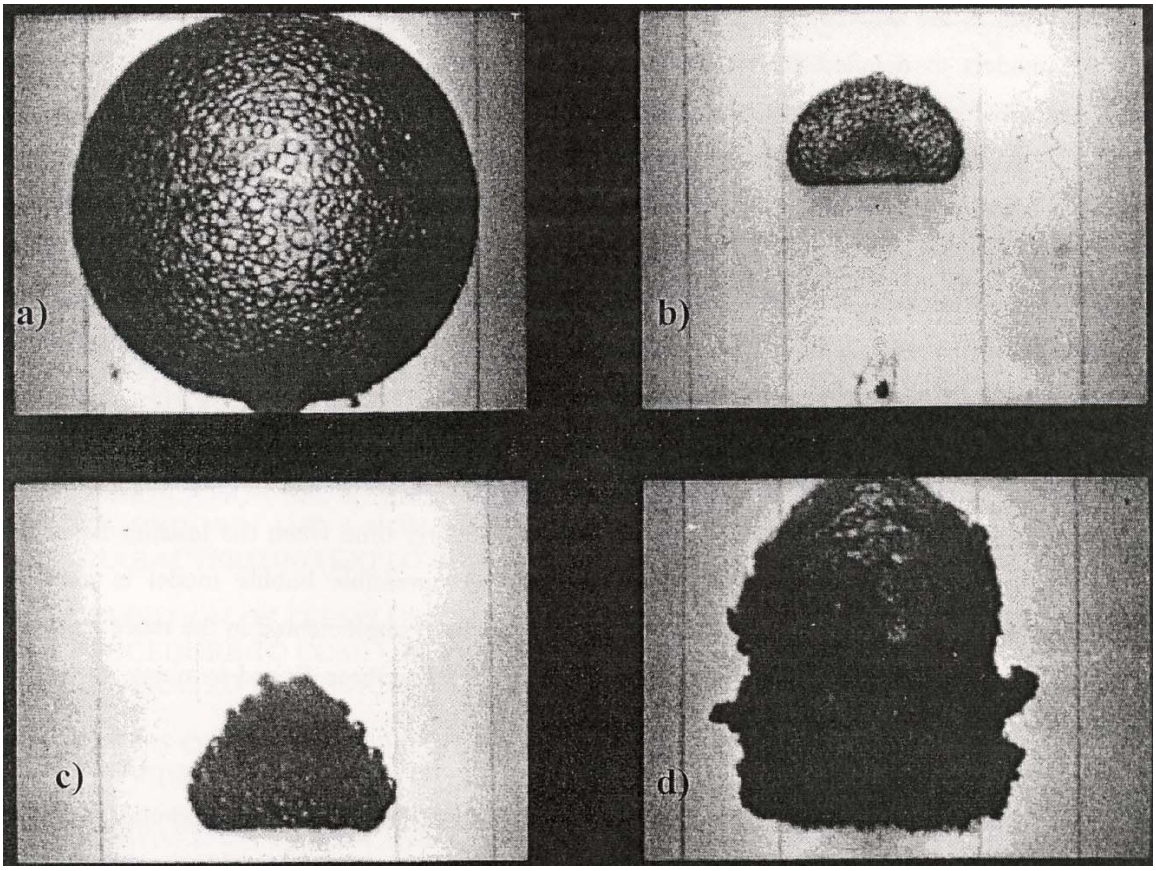

Figure 5. Photograph of Bubble Pulse (From Ref. 3)

In addition, the Hicks Bubble Model does not account for the dissipating amplitude of the bubble pulses. Therefore, the model is only accurate for the first period of bubble oscillations. Hence, the excitation of the hull girder due to bubble oscillations is stopped after 1.5 bubble oscillations, at which time the girder undergoes free vibration [Ref. 9]. Initially, Hicks believed that his modeling technique was inadequate due to the aforementioned approximations. However, after further research, Hicks determined that the effects on a ship due to gas bubble oscillations were well represented by his initial model. He found that his distant flow approximation actually proved to be quite adequate at normal standoff distances. However, when a charge is placed near a target his

approximation loses merit. In Hick's defense, most other approximations also prove inadequate at close range. At a very small standoff distance, the bubble tends to engulf the hull which causes localized damage. This damage will also tend to further distort the flow around the target [Ref. 1].

C. THE PHYSICS OF COLLAPSING WAVES

The implosion phenomenon is also an important part of UNDEX theory. In the past, much work has been completed concerning explosion produced shock waves and subsequent pressure pulses caused by bubble oscillations. However, significant increases in the initial pressure wave can be accomplished by using an implosion creating device. Because the damage producing ability of an underwater detonation is more influenced by the initial shock wave rather than the pressure pulses caused by the bubble oscillation, it is desirable to increase the amount of energy that contributes to the initial shock wave. Of course, this is done at the expense of smaller pressure pulses. One method for producing such an increased initial pressure wave is shown in Figure 6. Notice that the detonation waves are converging on the center of the sphere, rather than diverging as done in a typical underwater explosion [Ref. 10].

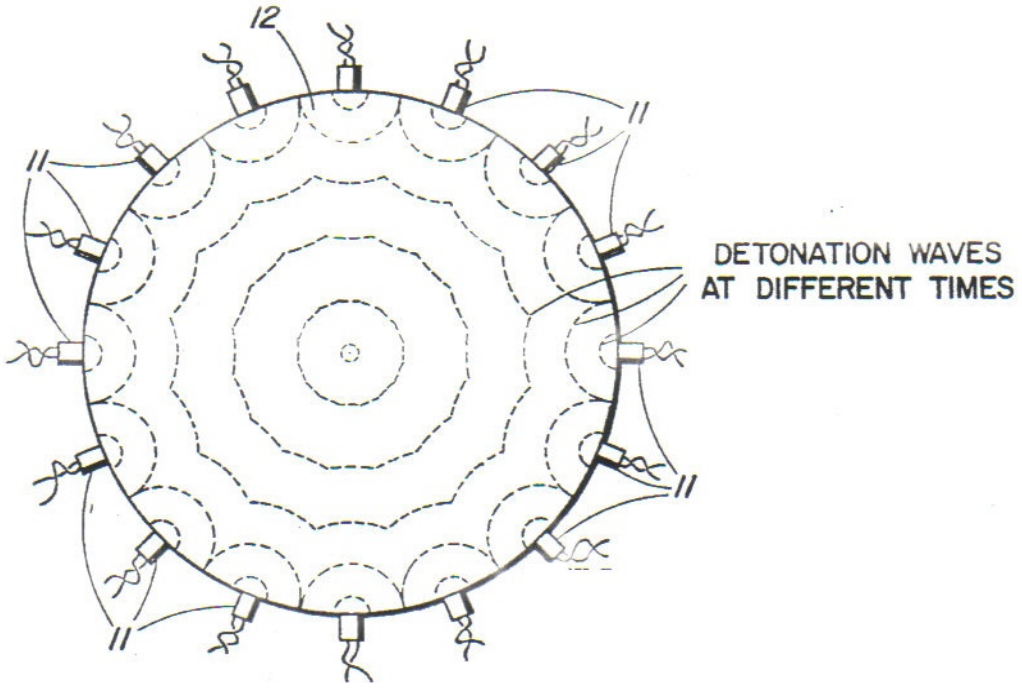

Figure 6. Solid Explosive Charge Surrounded with Plural Detonators (From Ref. 10)

In Figure 6, a solid explosive charge is provided with many detonators attached to the outside surface. At a specified time, divergent waves emerge from the detonators and converge toward the center of the charge. The shock waves form an uninterrupted wave which closes in on a decreasing volume. Thus, the result is a peak implosion pressure within a body of water. Figure 7 displays how the implosion shock wave can be significantly greater than a shock wave induced from a typical underwater explosion [Ref. 10].

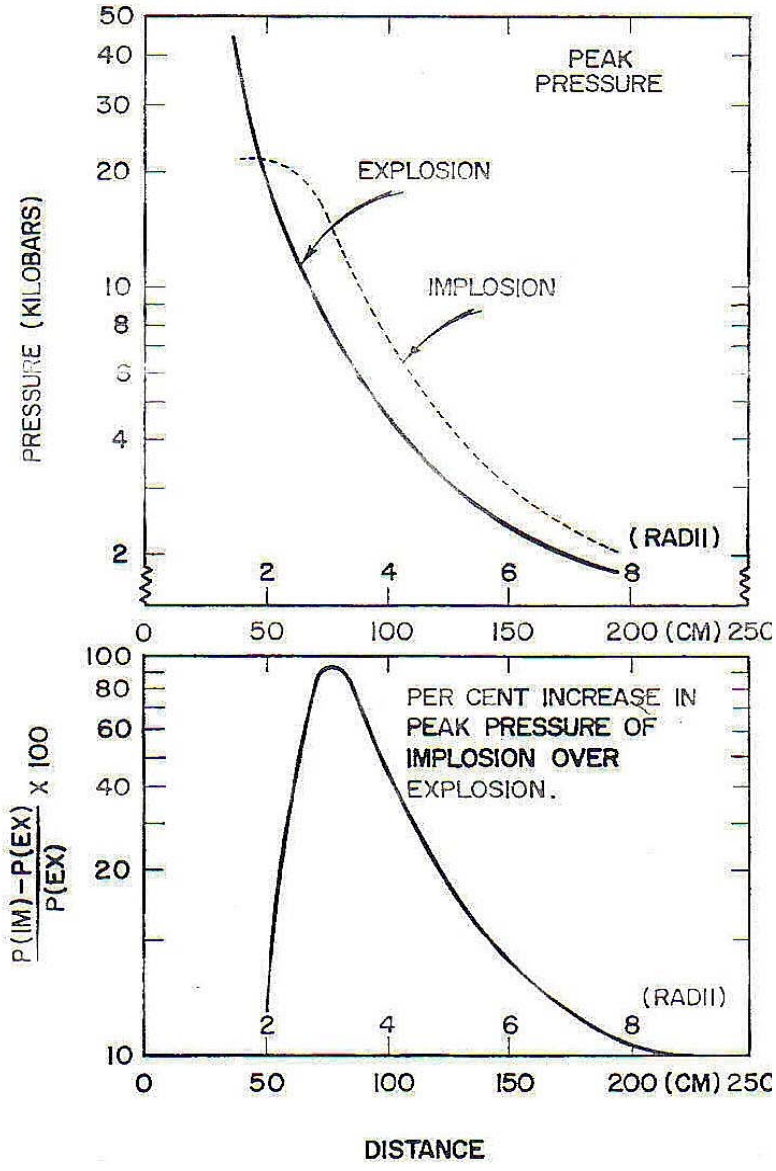

Figure 7. Relation between Implosion and Explosion Peak Pressure Waves (From Ref. 10)

1. The Collapse of a Bubble in a Liquid

In order to understand the physics behind an implosion, it is useful to consider the collapse of an empty spherical cavity in a liquid. Bubbles can form if the pressure at a specific point in a flow field is less than the vapor pressure of the liquid. This phenomenon is especially prevalent when dealing with cavitating propeller blades of a ship or submarine. When these bubbles move at a later time to a region of greater pressure, they collapse. The collapse of these bubbles result in a strong shock wave that causes damage to surfaces, such as the aforementioned propeller blades.

In studying the collapse of a bubble in a liquid, one particular approximation must be made. This approximation deals with the matter inside of the collapsing bubble. In reality, the inside of the bubble is not empty; it contains a vapor. For the calculation of a collapsing bubble, the vapor inside of the bubble is neglected. This assumption is especially valid in the final stages of collapse when the pressure build up near the cavity wall is high. In addition, it is also determined that the bubbles complete their collapse when r = 0 [Ref. 11].

At an initial time of t = 0, a spherical cavity of radius Ro is in an infinite expanse of fluid at a surrounding pressure of Po. The pressure inside the cavity is zero. Thus, the pressure difference is equal to Po. Because of the pressure difference, the bubble begins to shrink. For the initial motion, compressibility effects are neglected because the motion is slow and the pressure rise is low. Hence, the continuity equation for an incompressible fluid yields:

$$\vec{\nabla} \cdot \vec{u} = \rho\left(\frac{\partial u}{\partial r} + \frac{\partial u}{r}\right) = 0 \qquad 8$$

because the flow is spherically symmetric. Solving Equation 8 with the boundary condition that the particle velocity, u, at the cavity wall, R(t), is equal to the velocity of the interface, $\dot{R}$ (t), the velocity distribution follows as:

$$u(r) = \dot{R}(t)\left[\frac{R(t)}{r}\right]^2 \qquad 9$$

From the momentum equation:

$$p = \int -\rho \cdot (\frac{\partial u}{\partial t} + u\frac{\partial u}{\partial r})dr \qquad 10$$

Using Equation 9 to evaluate the derivatives and integrating Equation 10 from the cavity wall, R, to infinity, we see that:

$$p = p_0 + \rho R\frac{\ddot{R}R + 2\dot{R}^2}{r} - \frac{\rho\dot{R}^2}{2}\cdot\frac{R^4}{r^4} \qquad 11$$

Utilizing the boundary condition at the cavity wall where r = R and p(R) = 0, we see that Equation 11 becomes:

$$0 = p_0 + \rho \cdot (\ddot{R}R + \tfrac{3}{2}\cdot\dot{R}^2) \qquad 12$$

Solving Equation 12 using the initial condition of t = 0, $\dot{R}$ = 0, and R = Ro, we obtain the equation for the velocity increase of the collapsing bubble with radius:

$$\dot{R}^2 - \frac{2p_0}{3\rho}\cdot\left[\left(\frac{R_0}{R}\right)^3 - 1\right] \qquad 13$$

Integrating Equation 13 with respect to time yields the trajectory of the collapsing bubble:

$$\left(\frac{2p_0}{3\rho}\right)^{1/2}\cdot\frac{t}{R_0} = \int_{R/Ro}^{1}\frac{z^2dz}{\sqrt{1-z^3}} \qquad 14$$

The total collapse time, τ, may be obtained from Equation 15 by integrating from zero to one. Thus, the total collapse time is:

$$\tau = B(\tfrac{5}{6},\tfrac{1}{2})\cdot R_0\left(\frac{\rho^2}{6p_0}\right)^{1/2} \qquad 15$$

where B is the “Beta Function”, which is defined as:

$$B(\alpha,\beta)=\frac{\Gamma(\alpha)\Gamma(\beta)}{\Gamma(\alpha+\beta)} \qquad 16$$

For the values of α,β =5/6, ½ the collapse time becomes:

$$\tau = 0.915\left(\frac{\rho}{p_0}\right)^{1/2} \qquad 17$$

Using Equation 17, it is possible to find the total time of collapse of a bubble of any given initial size. Realize, however, that this is only an approximate order of magnitude because compressibility effects become significant later on in the collapse and Equation 14 is no longer valid [Ref. 11]. The pressure distribution can be found from Equation 11 using Equation 12, which is expressed as:

$$\frac{p}{p_0}=\frac{1}{2}\left(\frac{\rho\dot{R}}{p_0}\right)\cdot\left(\frac{1}{\xi}-\frac{1}{\xi^4}\right)+\left(1-\frac{1}{\xi}\right) : \text{where } \xi=\frac{r}{R(t)} \qquad 18$$

2. Converging Shock Waves

Recalling the improved warhead design that was presented in Reference10, mathematical modeling can also be accomplished for converging shock waves. Previously, the collapse of bubbles in liquid was studied. Although the collapse of a bubble in a fluid medium does create a significant initial pressure wave, a greater initial pressure can be obtained by using a detonation device that focuses converging shock waves to a focal point that subsequently causes a rapid expansion. The asymptotic self similar solution was originally obtained by Guderley and later replicated by Butler. A detailed derivation of the solution to the problem of converging shock waves may be found in Reference 11 of this thesis.

III. PREVIOUS EXPERIMENTS AND SIMULATIONS CONCERNING IMPLOSION PHENOMENA

A. IMPLOSION EXPERIMENTS REGARDING STEEL CYLINDERS

Long before copious computing power was readily available for educational and research oriented pursuits, experiments were completed in order to better understand the implosion phenomenon. During the early 1970s, a series of tests were completed by the Naval Ordnance Lab at White Oak, Maryland. During that time period, the implosion sounds of air-filled structures during collapse due to hydrostatic pressure had drawn the interest of the underwater acoustics community. For instance, implosions provided a safe and efficient way to study sound propagation in water [Ref. 13]. Also, studies conducted in this era by Reader and Chertock had shown that the pressure wave emitted by an imploding structure is negative while the interface is moving away from the water while the pressure wave is positive while it is accelerating toward the water. This principle is true whether the structure in question is glass walled, steel walled, or simply a cavity of air [Ref. 14].

1. Experimental Procedure

The Naval Research Laboratory conducted implosion tests using steel cylindrical structures that were lowered or dropped into the ocean. The Naval Ordnance Laboratory recorded the acoustic signals produced as the steel tanks collapsed. The purpose of the experiment was to link the acoustic signals with the mode of collapse of the cylindrical structure.

The test consisted of twenty-four tanks that contained air at atmospheric pressure. Each tank consisted of three compartments which were separated by rigid bulkheads. The center compartment was longer than the two outer compartments, which were of equal length. Thirteen tanks were controllably lowered into the ocean. After some type of collapse had been recorded, the tanks were raised back to the surface for inspection. For these tanks, external gages were mounted to record external pressures while an additional pressure gage was mounted internally at the center of the center compartment.

As previously mentioned, some tanks were allowed to sink freely instead of being controllably lowered. Although this ruled out the possibility of recovery in most cases,

this type of testing allowed for more of the compartments to implode. One of these free sinking tanks had an internal pressure gage connected to a recorder by an expendable wire. In addition to the pressure gages, hydrophones were also used to collect acoustic signals emitted from the collapsing cylinders. Of note, the recording system performance was verified by recording signals from known explosive sources [Ref. 13].

2. Experimental Summary

Inspection of implosion waveforms and the recovered tanks indicate that tanks of a similar material and geometry were damaged similarly and also created similar pressure waves. Generally speaking, the damage was uniform and the method of collapse was reproducible. An assumption was made that all cylinders collapsed because of hydrostatic loading by first forming an inward buckle. Further damage seemed to be a function of material properties, length to diameter ratio, wall thickness ratio, and the properties associated with the end cap structures.

The steel tank implosion characteristics were compared against the glass bottle implosion characteristics which were studied in depth by Urick [Ref. 15]. In Urick's experiments, the air-filled glass bottles propagated an initial negative pulse followed by diminishing pulsations. These later pulses were due to the gas bubble oscillation and are much like the gas bubble oscillations associated with underwater explosions. However, the initial pressure wave created by the implosion of the glass bottle is negative, while an initial pressure wave emitted from an explosion is positive. The following figure compares the pressure signals from one of Urick's glass bottles to that emitted from an explosion.

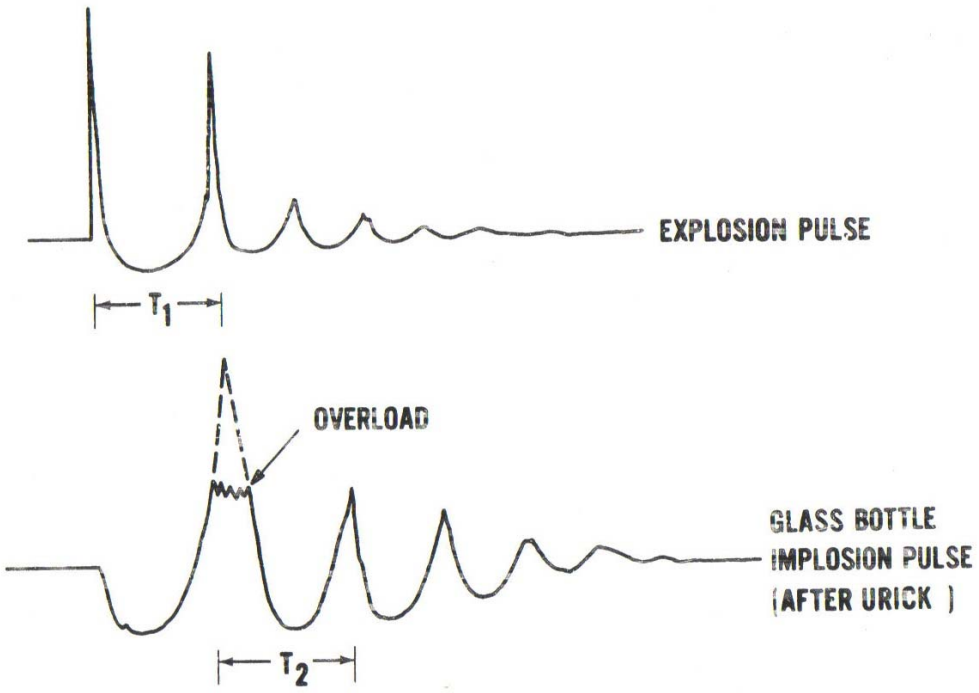

Figure 8. Comparison of Explosion Pulse with Glass Bottle Implosion Pulse (From Ref.13)

In comparison of the cylinder implosion signature with the glass bottle signatures, as well as comparisons against explosion wave forms, different waveforms were observed. The negative initial pulse of the glass bottle is due to implosion, while the oscillatory response is due to the gas bubble. The gas bubble induced response is much like the gas bubble oscillations in an explosion caused event. As for the steel cylinders, the negative initial pressure wave is attributed to the formation of an inward buckle. After the initial pressure wave, the response is largely dictated by the number and size of the buckles that form. The final collapse of the structure is indicated by a relatively large positive pressure pulse [Ref. 13]. Figure 9 displays the pressure time history at locations outside and inside of a steel cylinder.

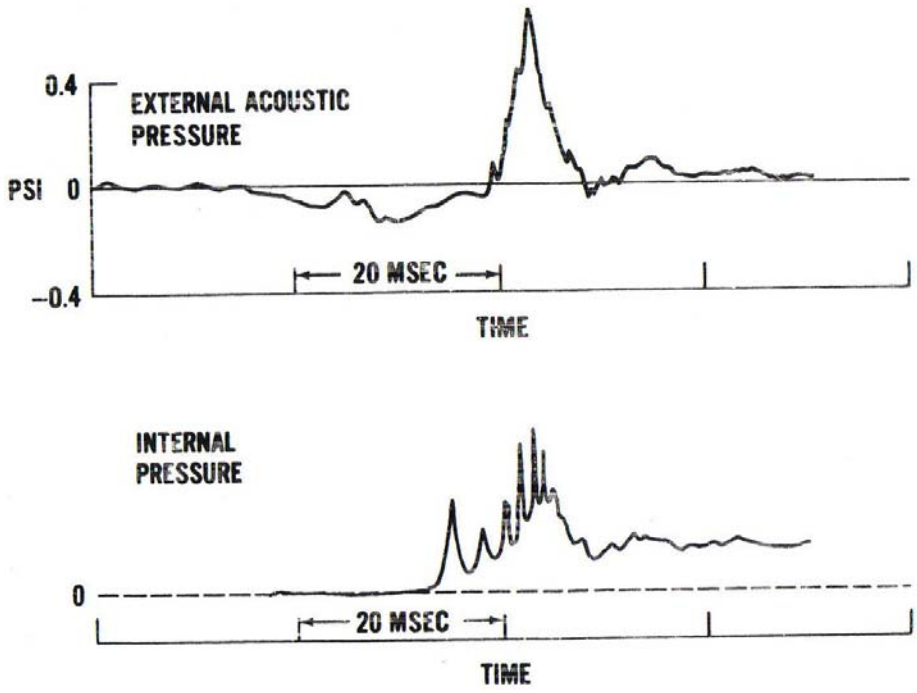

Figure 9. Implosion of 26 Inch Steel Tank (From Ref. 13)

B. SMALL-SCALE IMPLOSION TESTING OF GLASS AND ALUMINUM CYLINDERS

Recently, implosion tests were conducted at Naval Undersea Warfare Center Division Newport. Four implosion experiments were conducted that consisted of cylindrical test samples made of aluminum (2) and borosilicate glass (2). The purpose of the experiment was to determine the effect of material properties on the rate of the implosion event. NAVSEA's current method for assessing peak pressure created by an implosion event is a one dimensional, spherical bubble collapse model [Ref. 16]. NAVSEA's model does not account for the structure that separates the air and water.

The conclusions of the NUWC-NPT technical memo offer some insight into the events that occur during an implosion event. When an implosion occurs, the pressure wave is of the same magnitude at a constant radius from the event while varying the angle around the circumference of the cylinder. This effect was also true for an aluminum test sample, which does not collapse symmetrically. In addition, the rate and duration of the collapse is very much dependent on the material properties of the

structure. Also of interest, the experiments showed signs of irreversibility. Thus, losses or irreversibility is a characteristic of implosion phenomena [Ref. 16].

C. SIMULATIONS OF FLUID, GLASS, AND ALUMINUM MODELS

Further research into the implosion phenomena has been completed at NUWC-NPT. In a more recent technical memo, personnel at NUWC-NPT document the development of a computational model that simulates the implosion of glass cylinders and spheres. Two models were constructed to analyze an implosion event. One model was a fluids-only model that simulated a low pressure gas surrounded by a high pressure water volume. The assumption was that at the initial time of t=0, the surrounding structure around the gas would uniformly disappear. The second model incorporated rigid body elements that at an initial time would begin to fail at a specified location and continue to fail at a specified "crack propagation rate." For the second type of model, predictions were made for a sphere and four cylinders, each cylinder with a varying length to diameter ratio [Ref. 17].

Results from the simulations reveal variations due to length to diameter ratio and pressure probe location. Due to the distribution statement associated with Ref. 17, specifics can not be discussed in this thesis.

THIS PAGE INTENTIONALLY LEFT BLANK

IV. STUDY OF IMPLOSION EVENT THROUGH MODELING AND SIMULATION

A. INTRODUCTION TO DYSMAS

Post World War II, the Navy completed many live fire UNDEX experiments on surface ships and submarines. Those tests provided useful data that helped create the basis for the empirical and semi-empirical equations used today in evaluation of peak pressures, decay rates, impulse, and other useful quantifications of UNDEX events. In addition to providing these useful tools, these live fire tests tested a vessel's overall ability to withstand an attack.

Even in modern times, similar experiments to those completed in the 1940s and 1950s are done to test the combat survivability of modern war fighting ships. These tests are not only extremely expensive, but pose serious threats to the ship, the ship's crew, and to the underwater environment. Recent tests included shock trials for the USS JOHN PAUL JONES and the USS WINSTON S. CHURCHILL and future shock trials are scheduled for the new LPD-17 class ship.

Fortunately, a viable alternative to full scale shock trials is available. With modern advances in computing power, simulations of shock trials can be completed using the finite element method (FEM). At Naval Postgraduate School, data taken from the shock trials of both DDG-53 and DDG-81 was compared to simulations that were completed using LS-DYNA/USA, a finite element code. Close correlation to the actual shock trial was found. Further research into the simulation of these UNDEX events has provided strong evidence that finite element simulations are accurate approximations to ship response recorded during the ship shock trials. Figure 10 is a plot comparing the simulation results to the data taken from the live fire shock trials of DDG-81.

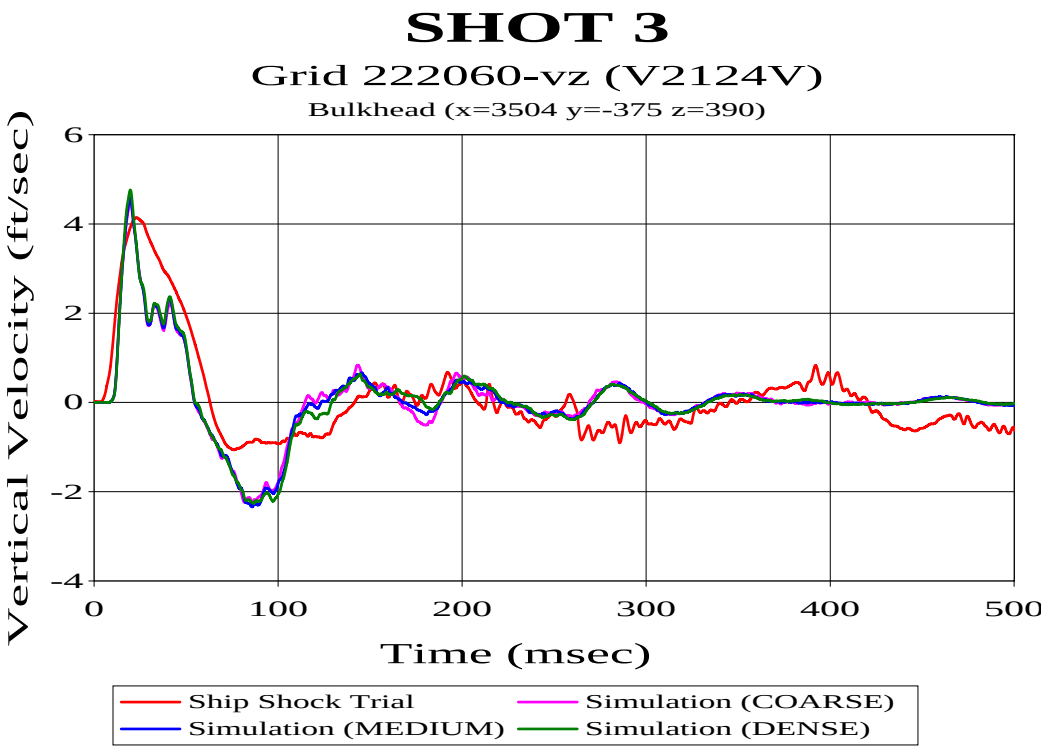

Figure 10. Midship Region Velocity Plot Comparison (DDG-81)

Previously, LS-DYNA was used to simulate UNDEX events. However, a powerful Navy based alternative code, DYSMAS, has been released that offers advantages over the commercial LS-DYNA code. DYSMAS (Dynamic System Mechanics Advanced Simulation) is a coupled Eulerian-Lagrangian hydrocode that has been developed by Naval Surface Warfare Center, Indian Head Division. The code couples the GEMINI hydrocode with a version of DYNA-N. DYSMAS is especially useful for simulating the response of surface and subsurface structures to UNDEX events.

GEMINI is a set of codes that is used to model the environment surrounding an UNDEX event. The environment can include the explosive, a liquid, or a gas that surrounds a ship, submarine, or other marine structure (however, DYSMAS is not limited to UNDEX events; it can also perform calculations for air blasts). The structural calculations are completed by a code such as DYNA-N. The Euler and structure codes are coupled using interface elements which exchange information after each computational step. Gemini supports both single processor and multiple processor computing [Ref. 12]. Figure 11 shows the relationship of the basic GEMINI components.

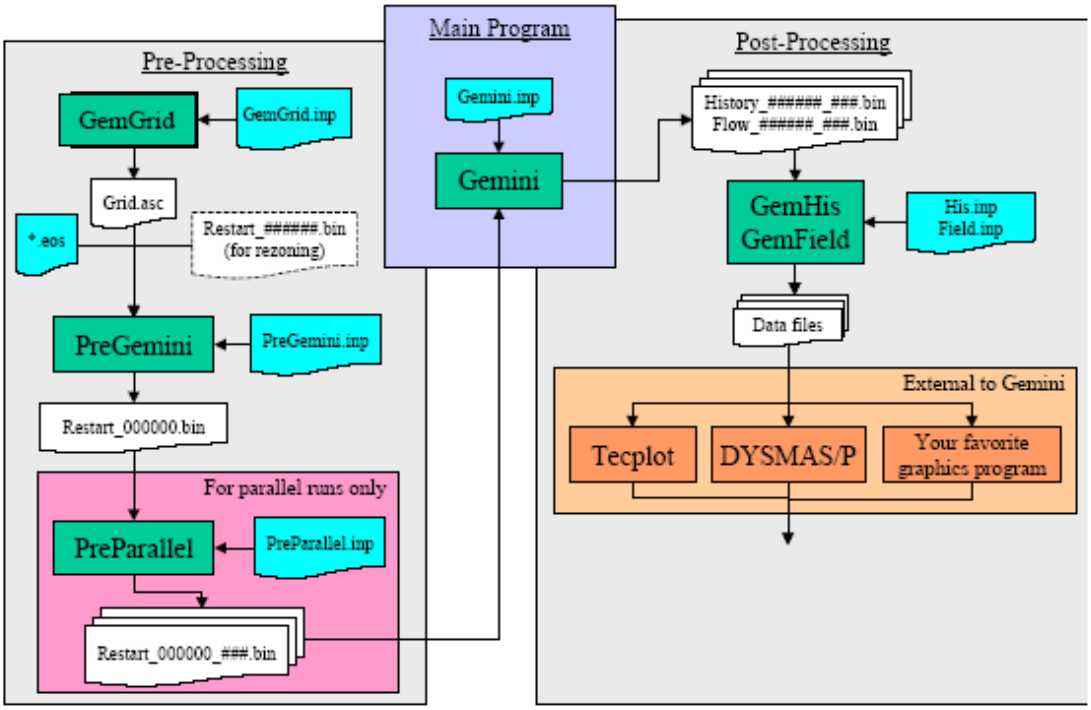

Figure 11. Basic Gemini Components (From Ref. 12)

The process of using GEMINI is similar to most other FEM programs. Pre-processing and post-processing programs are needed before and after the calculation, respectively. In order to gain an understanding of the programs used in the GEMINI suite, a brief overview of the process is given below. A full input deck will be provided in Appendix C of this report.

1. Pre-Processing Components of GEMINI

In order to begin a calculation using DYSMAS, the environment must be established. This is done in the pre-processing portion of the GEMINI program. Setting up the surrounding environment for a calculation consists of setting up a coordinate grid, establishing an environment (water, air, explosive, etc.), and preparing for any parallel processing that is going to be done.

The first step to setting up a simulation is to determine the coordinate system that will be used. GEMINI is capable of one, two, and three dimensional processing using spherical, cylindrical, or Cartesian coordinates. In addition the being able to use these three systems of coordinates, the field can later be rezoned in order to a higher dimension or different coordinate system. Once a coordinate system is chosen, the user can create a

unique flow field using GEMGRID. Using GEMGRID, the user can specify the size of the cells used in the calculation. Using GEMGRID is optional, if it is not used all cells in the calculation will have the same size. It allows the generation of the grid to be independent in each direction. GEMGRID is useful in cutting down simulation time, as cells away from the structure being studied can have an increased size (thus allowing for faster computation).

Once GEMGRID has been run (if desired), the user then utilizes PREGEMINI in order to model the physical environment. In PREGEMINI, the user defines the water or air environment. In addition, the charge type, weight, and location are input in PREGEMINI. PREGEMINI is also used to 'rezone' previous flow fields (i.e., model a cylindrical 2-D calculation into a 3-D Cartesian calculation) or divide the computational domain into 'subgrids' that will allow for multiple processing.

2. Computational Component of GEMINI

Once the computational domain has been modeled using PREGEMINI, the main processing program can be used. GEMINI begins its calculation by referring back to the output files created by PREGEMINI. In addition to the PREGEMINI output files, the GEMINI program also reads its own user specified input deck. This user defined deck tells GEMINI is the simulation is a fluids only calculation or a coupled calculation (amongst other inputs). In addition to the type of calculation to be performed, other GEMINI inputs include cell, node, and element histories, termination parameters, restart parameters, and integration parameters. If a coupled calculation is being performed, the DYNA deck is also initialized with the execution of the GEMINI program.

3. Post-Processing Components of GEMINI

Once GEMINI (and DYNA if coupled calculation) has completed running, post-processing of the data can be performed. The GEMINI post-processing programs take the data that is output from GEMINI in binary form and translates that data into plot files that can be used in various visualization programs. There are two programs that are currently used to post-process the data: GEMHIS and GEMFIELD. GEMHIS is used to create a time history of points that were selected in the GEMINI input deck. These points can include structural nodes or elements or can be a point specified in the flow field.

There are a number of parameters that can be recorded, such as pressure, velocities, displacements, accelerations, density, forces, etc.

In order to visualize the flow field, the GEMFIELD program is used. In GEMFIELD, the user specifies the subdomain of the simulation that is of interest. Then, GEMFIELD creates a time series of data records for the specified variables within that subdomain. GEMFIELD is useful when illustrations and animation are desired.

Both GEMHIS and GEMFIELD are useful tools in visualizing the output data from GEMINI. The output from these two programs can currently be used in TecPlot and DysmasP applications. The output can also be put into plain ASCII if desired. In addition to specifying the variables to be plotted, GEMHIS and GEMFIELD also allow for the scaling of these variables. For example, this is helpful if the pressure output from GEMINI would want to be converted from dyne per square centimeter to kilopascals.

B. SPHERICAL MODEL IMPLOSION SIMULATIONS

As previously discussed, implosion models that have been previously studied include a fluids only model, a glass model, and a steel or aluminum cylinder model. The results from these tests indicate that a fluids only model will produce the greatest initial pressure wave. Intuitively, this is due to the uninterrupted inward flow of water creating what is similar to a converging shock wave. In the glass model, a crack propagation velocity and origin needed to be specified. In Steve Turner's report, a velocity of 400m/s was chosen. Although this is a reasonable approximation, the velocity does vary and leads to the possibility of different magnitude shock waves being emitted from similar glass specimens. As shown in aforementioned experiments, the collapse of aluminum and steel cylinders are somewhat predictable, but also tend to give varying results between identical specimens in experimental tests.

For the aforementioned reasons, a fluids only implosion modeling approach was utilized. Using a fluids only model, the pressure wave will be symmetric (in the case of an imploding spherical cavity) and will not depend on a crack propagation rate or location of initial damage. A fluids only model will also clearly depict bubble oscillations due to an implosion event.

In order to study the pressure wave due to an implosion, a spherical "air cavity" was created at a specified depth of water. At time t=0, the air cavity collapses upon itself due to the surrounding hydrostatic pressure. While the volume of the spherical cavity varied, the pressure probe locations were fixed relative to the radius of the cavity. Table 1 indicates where the pressure probes were located in the simulation.

Table 1. Location of Pressure Probes with Respect to Cavity Radius

Pressure Probe #	X Distance (m)	Z Distance (m)	Radial Distance (m)
1	0.01	0.01	0.0141
2	R	R	1.414 R
3	2.5 R	2.5 R	3.536 R
4	5 R	5 R	7.071 R
5	10 R	10 R	14.142 R

The probe locations are graphically illustrated in Figure 12. Again, notice that the locations of the probes are associated with constants based upon the air cavity initial radius.

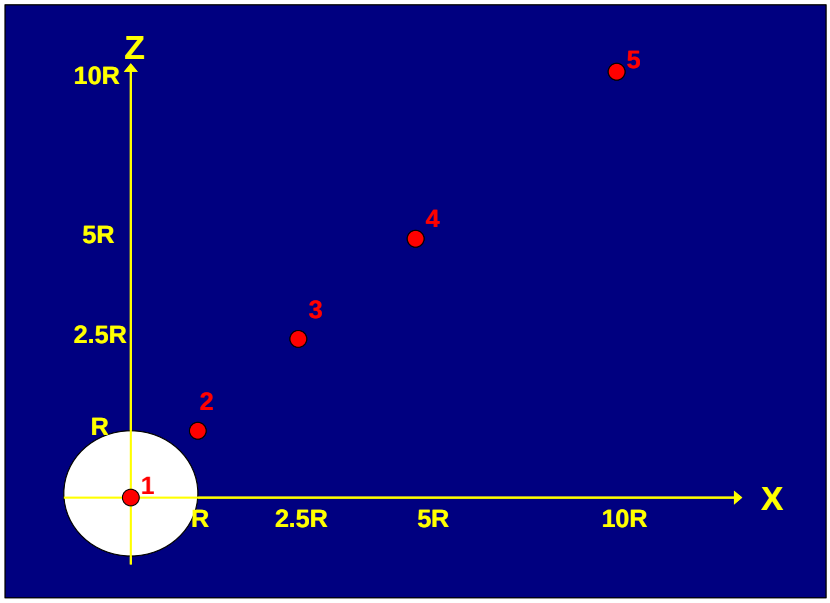

Figure 12. Pressure Probe Locations for Spherical Air Cavity Model

1. DYSMAS Simulations of Spherical Cavity Implosion

As illustrated in Figure 13, the pressure decreased as the radial distance from the center of the implosion increased. Additionally, subsequent bubble oscillations create additional pressure pulses to a diminishing degree. This type of behavior is similar to that of an explosion event. The flow field due to a spherical implosion is illustrated in Appendix A.

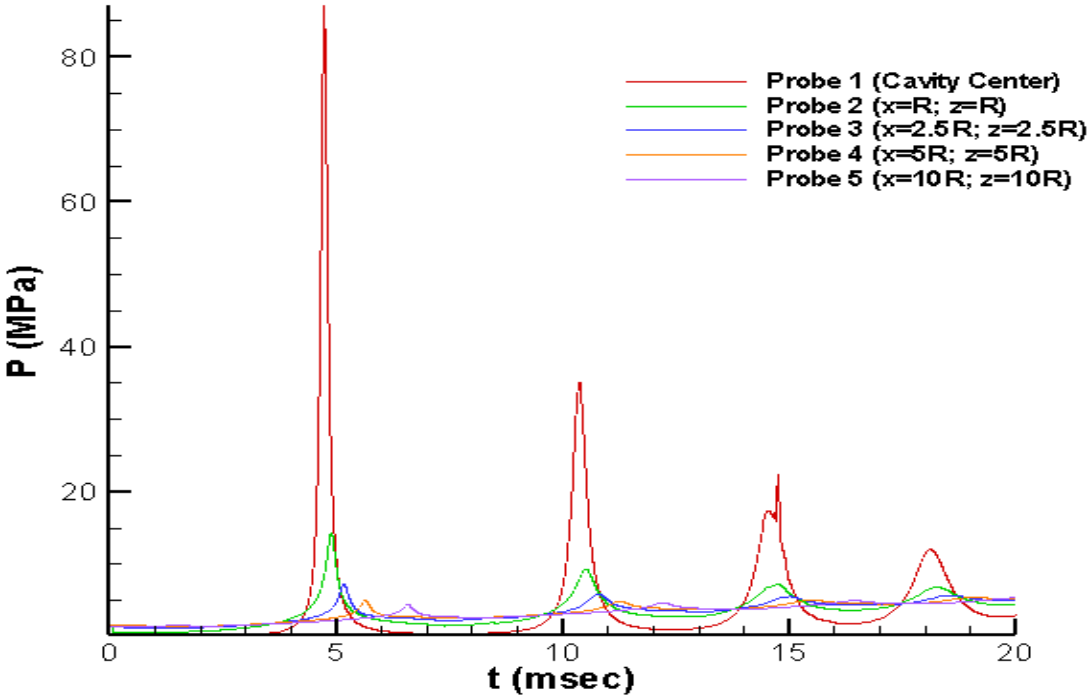

Figure 13. Spherical Cavity Implosion of 2 Meter Radius Pressure History

From the above figure, it seems apparent that the pressure wave created by the implosion acts very much like that of an explosion. The bubble pulses are similar and decrease as time progresses. Also, the pressure pulses that occur have less magnitude than the initial pressure wave. Also notice that as the distance from the center of the imploded volume is increased, the pressure wave magnitude is decreased. Indeed, from the above figure, it is apparent that the pressure wave created from an imploded spherical shape is influenced by the initial volume of the implosion and dissipates as the distance from the implosion is increased.

The following figures are pressure history plots of implosion events. The volume of the implosion is varied. Recall that the probe locations are normalized by the distance

from the implosion center divided by the initial radius of the imploded gaseous sphere. The figures are scaled such that the initial pressure wave is exemplified.

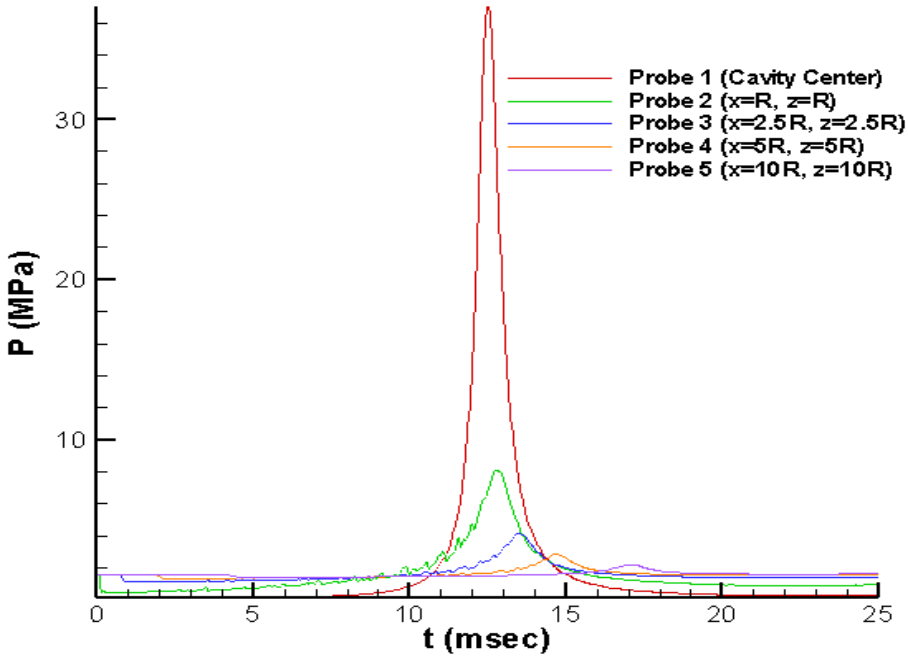

Figure 14. Initial Pressure Wave Due to Spherical Cavity Implosion of 0.5 Meter Radius

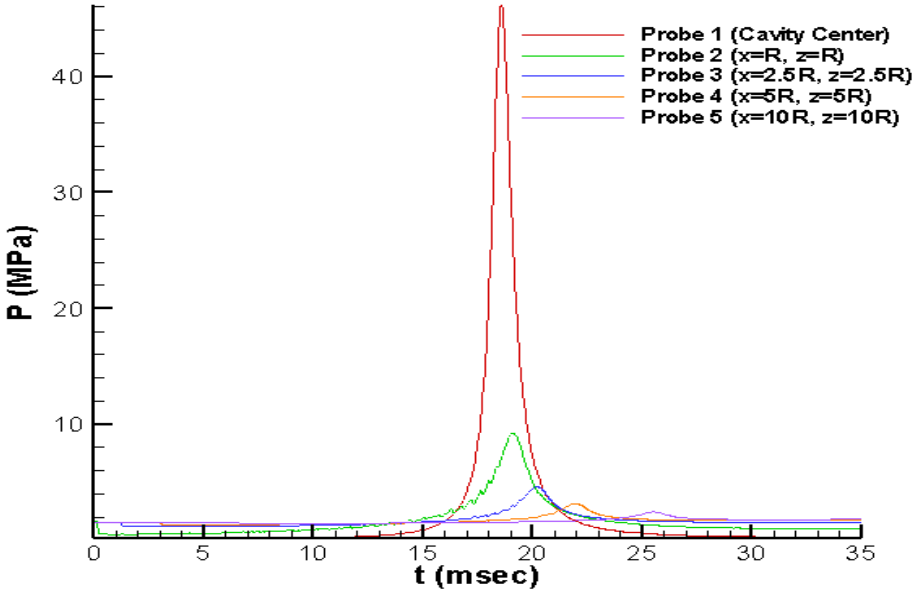

Figure 15. Initial Pressure Wave Due to Spherical Cavity Implosion of 0.75 Meter Radius

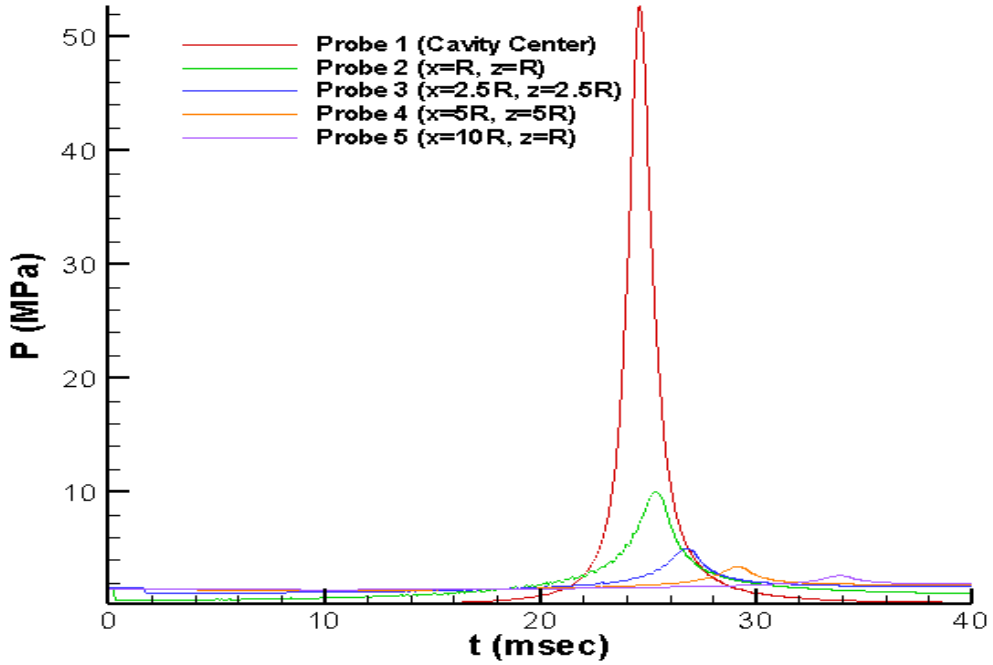

Figure 16. Initial Pressure Wave Due to Spherical Cavity Implosion of 1.0 Meter Radius

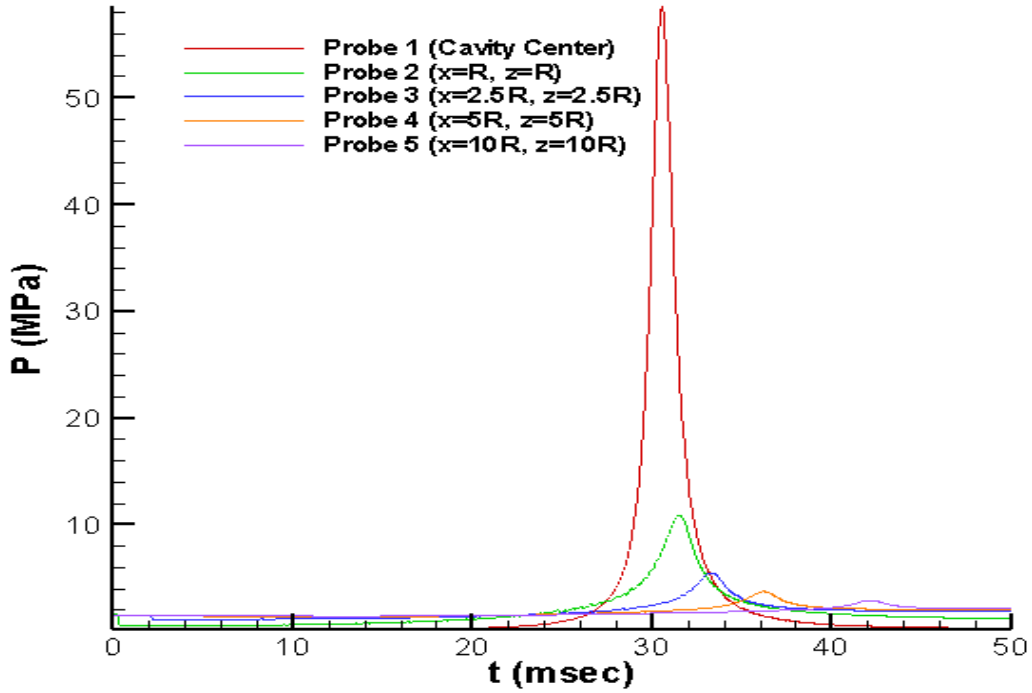

Figure 17. Initial Pressure Wave Due to Spherical Cavity Implosion of 1.25 Meter Radius

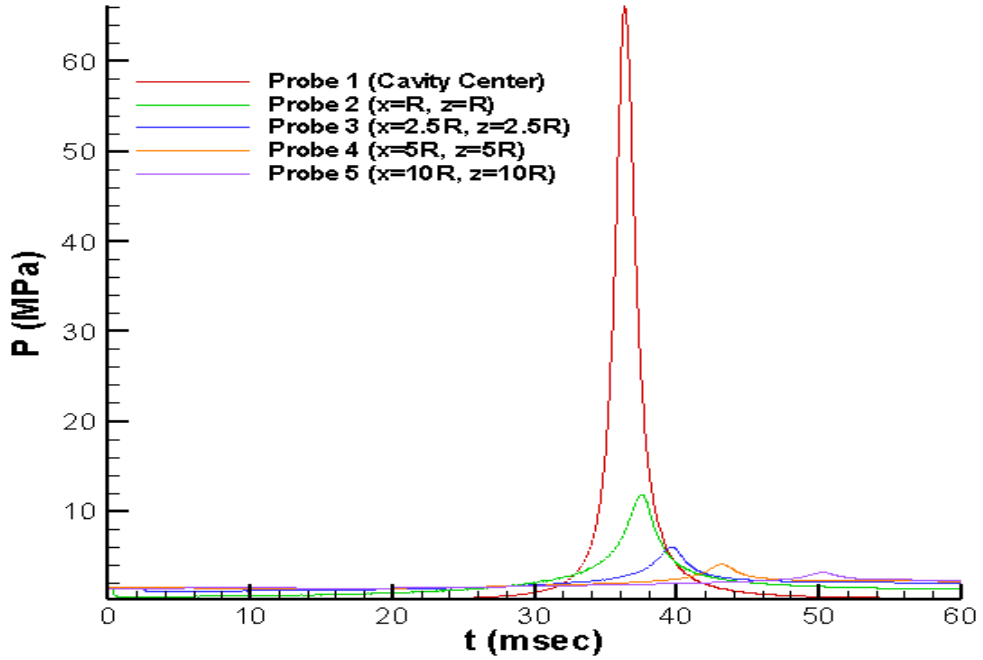

Figure 18. Initial Pressure Wave Due to Spherical Cavity Implosion of 1.5 Meter Radius

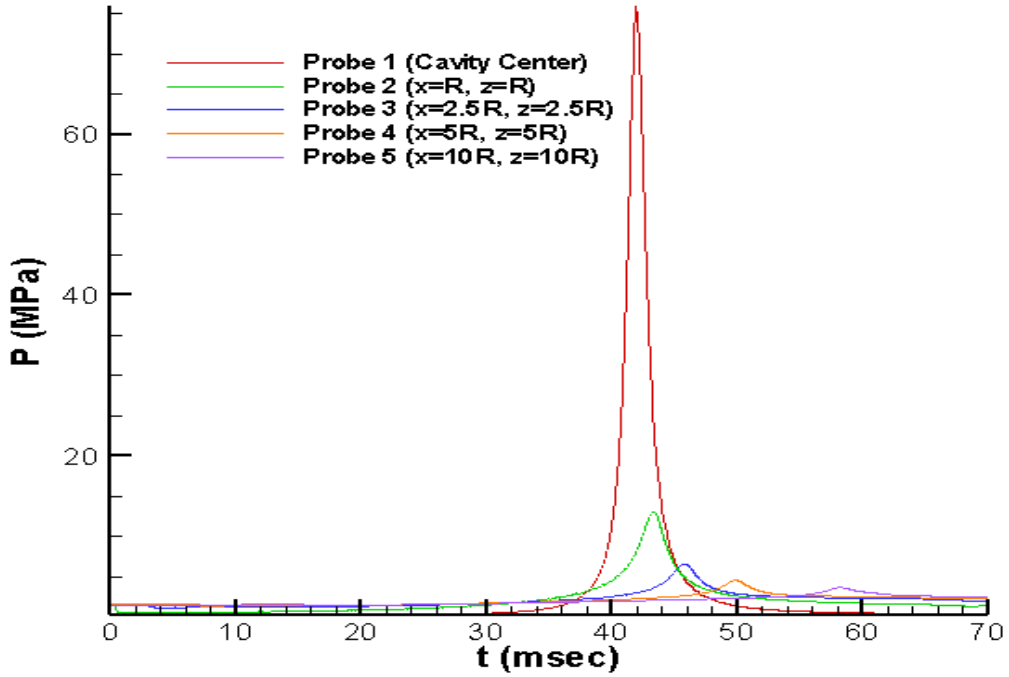

Figure 19. Initial Pressure Wave Due to Spherical Cavity Implosion of 1.75 Meter Radius

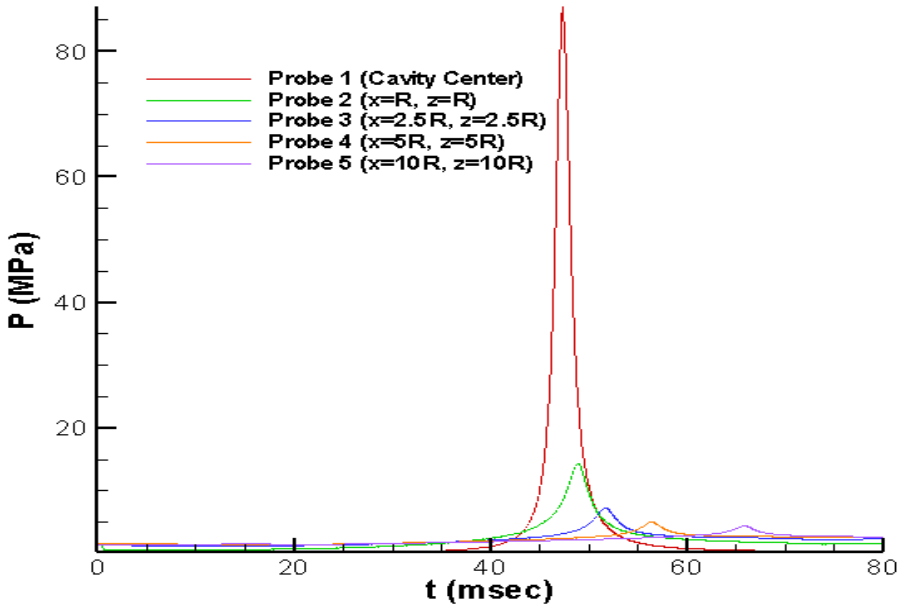

Figure 20. Initial Pressure Wave Due to Spherical Cavity Implosion of 2.0 Meter Radius

Figures14-20 have a similar pattern. Notice that as the volume of the imploding cavity increased, the time to the initial peak increased. This is intuitive, reasoning that more time would lapse before the larger volume would collapse upon itself. In addition to the time to initial peak increasing, the magnitude of the initial pressure wave also increases as the volume is increased. Of interest, the pressure recordings at the probes maintain the same relative trend regardless of initial volume. For example, notice the pressure history of probes one and three. In each of the simulations, the pressure time history of probe one generally cuts through the initial pressure wave peak of pressure probe three.

2. Relation of Peak Pressure at Probe Locations and Implosion Volume

As shown in the above data plots, the implosion pressure wave is influenced by the initial volume of the implosion. In order to determine how heavily the volume of the implosion influences the pressure wave, the pressure histories were plotted by individual probe. The data was then given a trend line that best described the data. The following figures display those data points and associated trend lines. Notice the good correlation between the data and the fit curve, as indicated by the R^2 value.

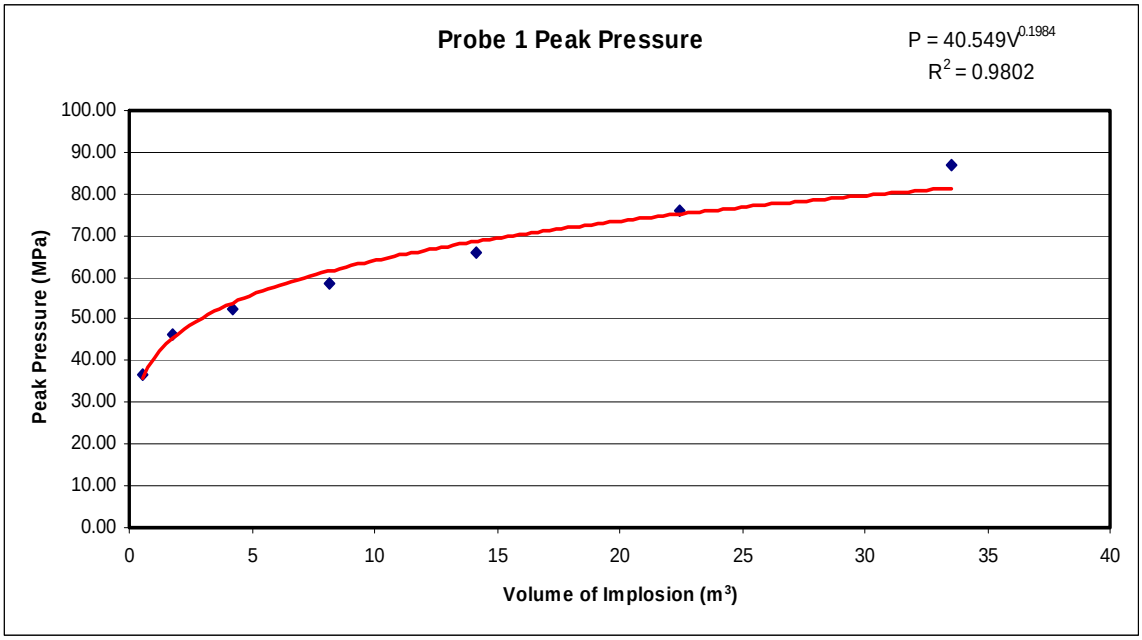

Figure 21. Peak Pressure Wave at Probe 1 as Function of Volume: Spherical Cavity

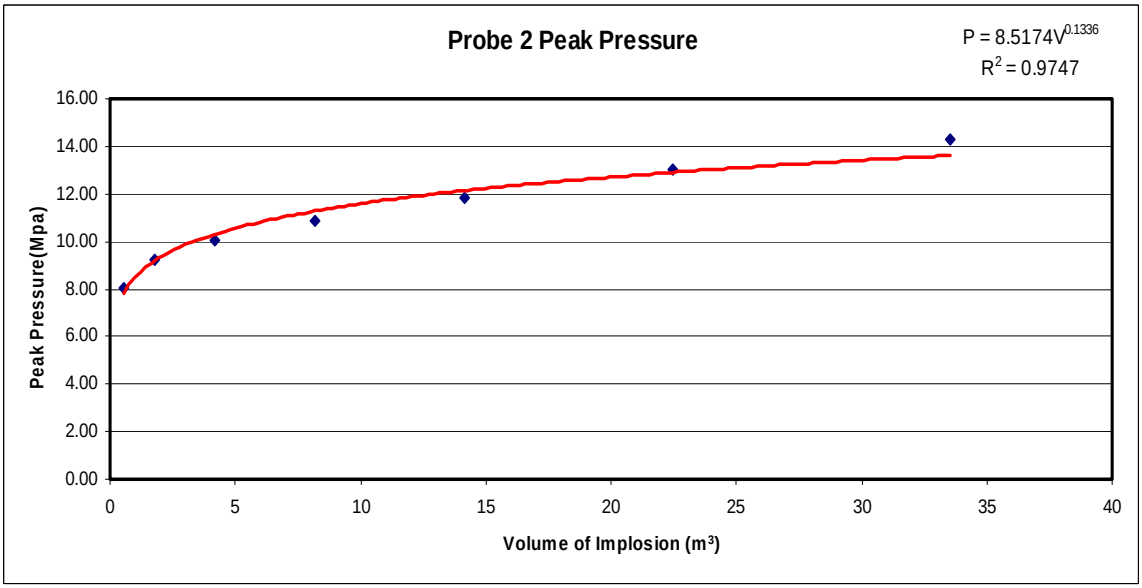

Figure 22. Peak Pressure Wave at Probe 2 as Function of Volume: Spherical Cavity

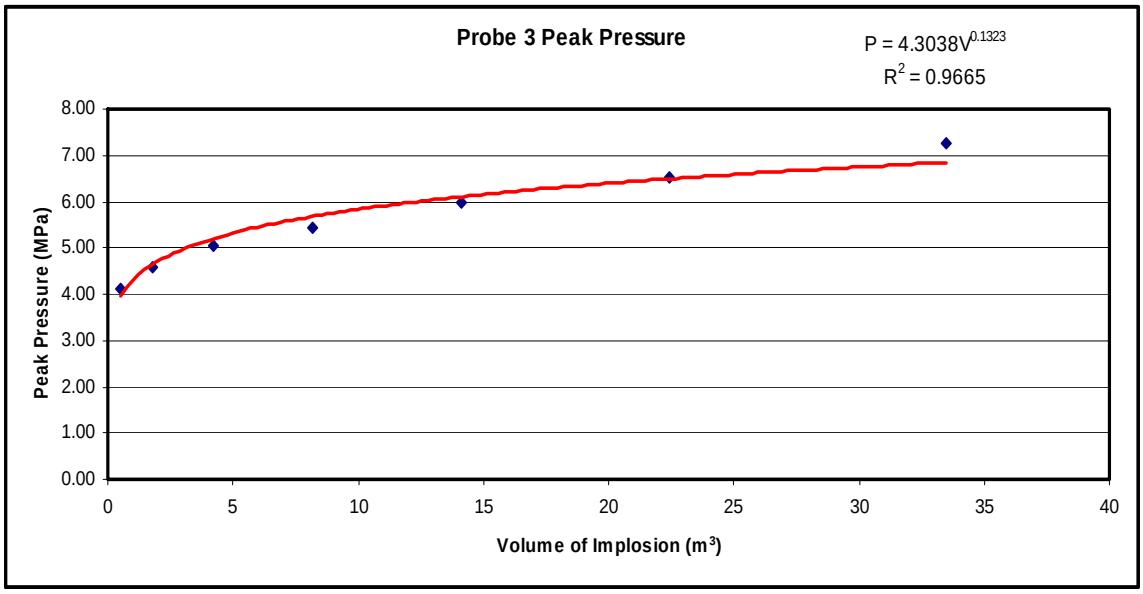

Figure 23. Peak Pressure Wave at Probe 3 as Function of Volume: Spherical Cavity

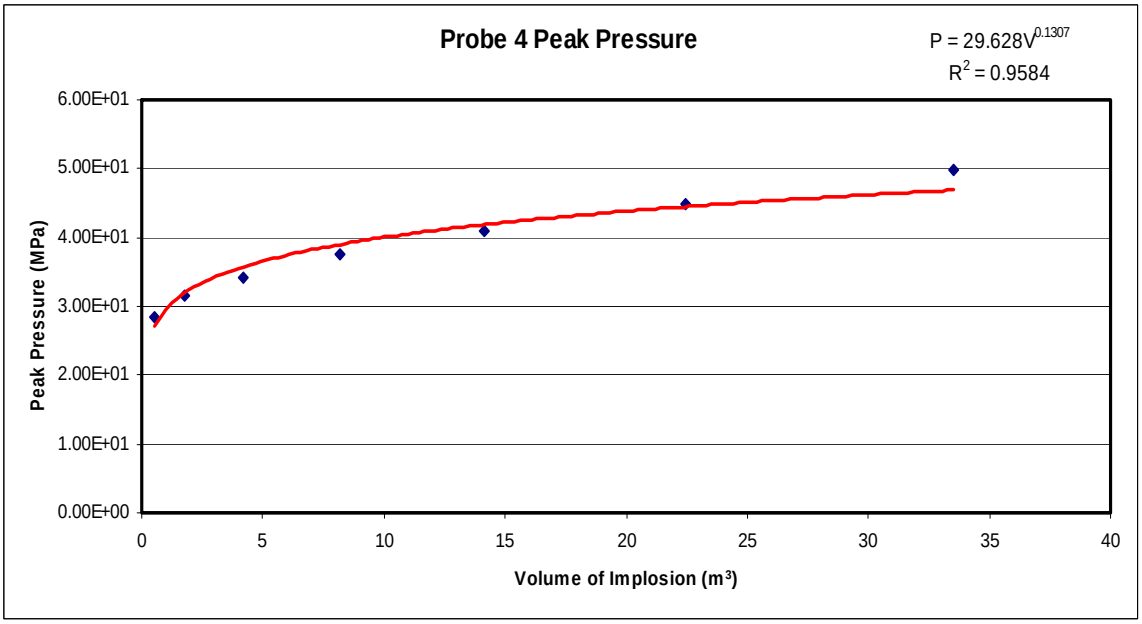

Figure 24. Peak Pressure Wave at Probe 4 as Function of Volume: Spherical Cavity

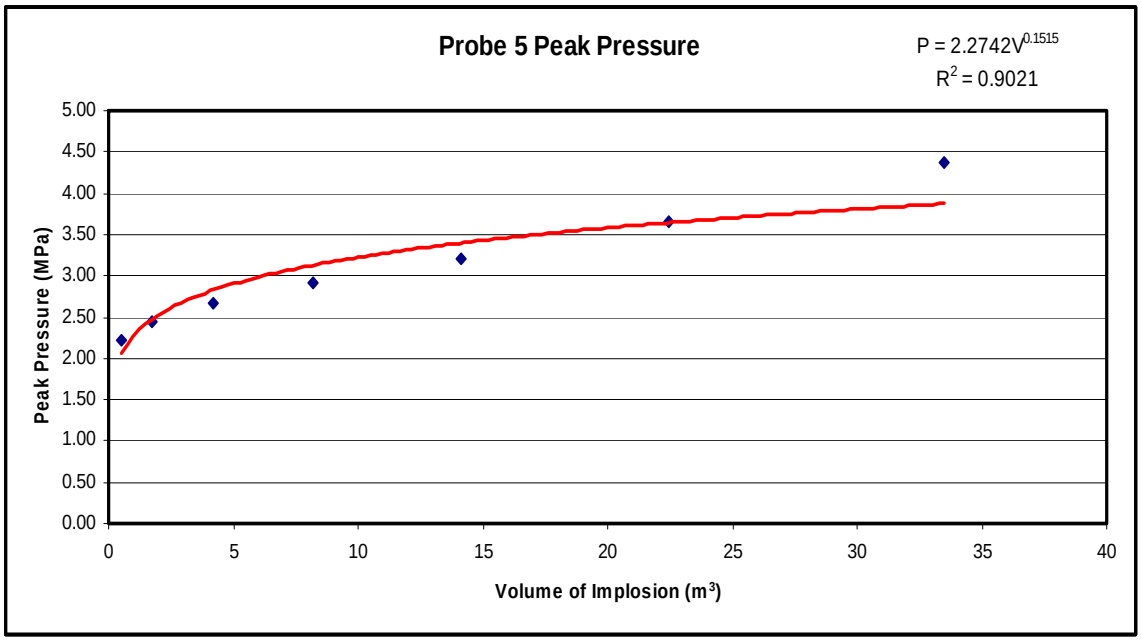

Figure 25. Peak Pressure Wave at Probe 5 as Function of Volume: Spherical Cavity

There are similarities between the probe histories. Notice the equations that best fit the data. Each of the equations is a function of volume to a power, preceded by a coefficient. Two assumptions should be noted. Acknowledging the fact that the pressure at probe one may be regarded as high in this comparison due to the short radial distance from the center of the implosion and, on the same token, the pressure history at probe five may be construed as low due to its relative further distance from the center of the implosion, these points (and their respective data fit trend lines) should weigh less heavily in the general formulation of the impact of volume to pressure. Thus, the influence of the volume seems to be that of $V^{0.132}$. The constant ahead of the volume term is a function of the radial distance of that probe from the center of the implosion.

3. Relation of Peak Pressure and Distance from Center of Implosion

As mentioned above, the radial distance from the center of the implosion also impacts the peak pressure wave. In Figure 26, the peak pressure is plotted against normalized distance while the volume of the imploding cylinder and depth are held constant. Cleary shown is a dependence on radial distance, defined as $(R/r)^{0.57}$. Again, in this case the varying coefficients are due to the initial volumes of the imploding spherical cavities.

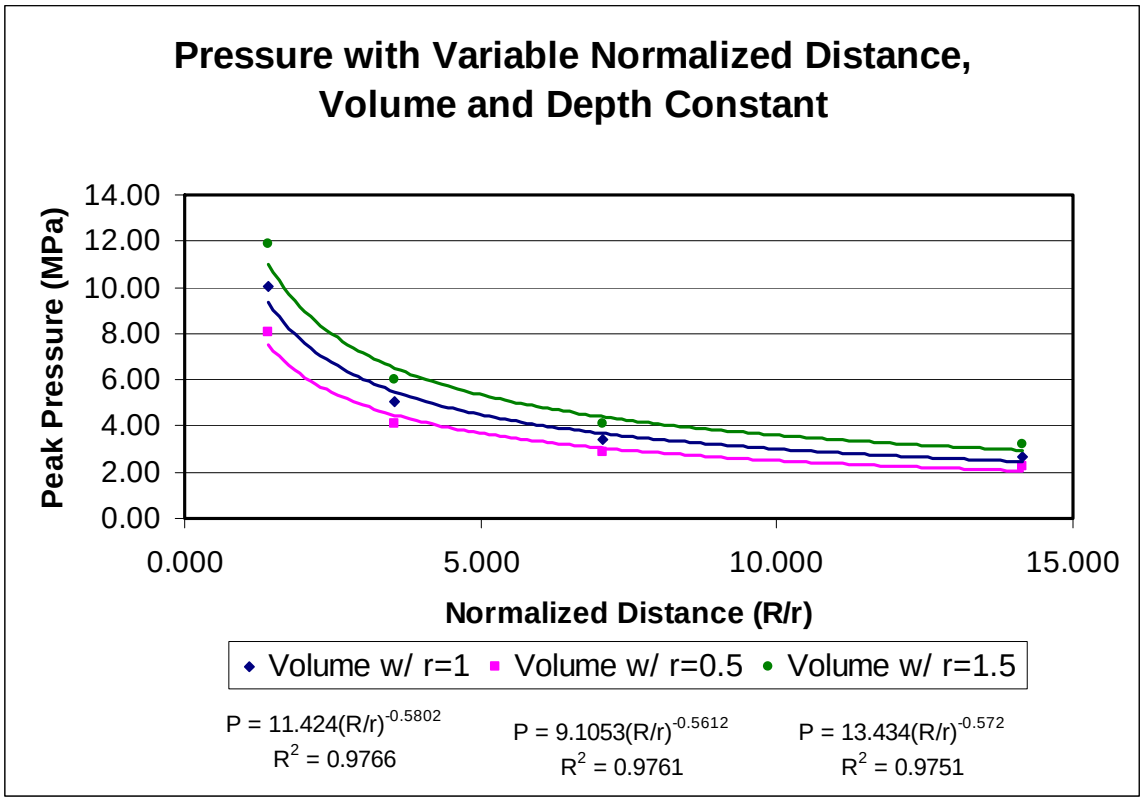

Figure 26. Peak Pressure as Function of Normalized Radial Distance

4. Relation of Peak Pressure and Depth of Implosion

Intuitively, as depth is increased the pressure wave created by an implosion will increase. This is due to the pressure difference between the pressure of atmospheric air inside the spherical cavity and the hydrostatic pressure of water outside of the cavity. Thus, not only should the peak pressure created by an implosion increase with increasing depth, it should increase linearly. In order to test this hypothesis, simulations were conducted that placed an equal volume sphere at depths of 38.1, 76.2, 152.4, and 304.8 meters. Figure 27 displays the results of these simulations. Indeed, the increase of peak pressure is linear with respect to depth. However, of note is the trend that as the distance from the center of the implosion is increased (denoted by increasing probe numbers) the less of an effect depth has on the magnitude of the peak pressure.

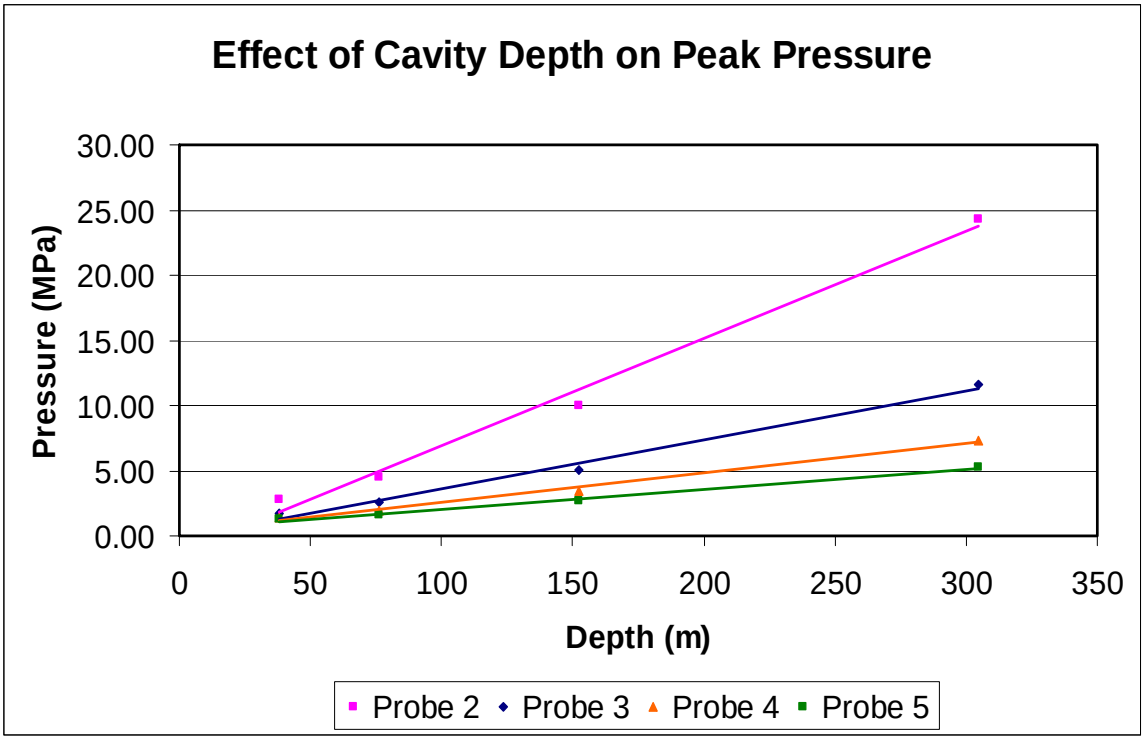

Figure 27. Effect of Depth at Which Implosion Occurs on Peak Pressure

5. Determining an Approximation to the Pressure Wave Created by an Imploding Spherical Cavity

DYSMAS is a powerful modeling tool that has the capability to accurately predict responses due to UNDEX events. The results from the preceding tests demonstrated relations between the cavity's volume and depth, the distance from the center of the implosion, and the subsequent pressure wave that was created by the imploding spherical air cavity. Using these similarities and relations, equations were derived that predict the peak pressure at a point due to an imploding spherical air cavity. Of course, the peak pressure is a function of depth, volume, and radial distance from the center of the implosion. In addition to presenting these equations, the error between the approximation and DYSMAS provided data is provided.

First, the peak pressure will be determined by holding the depth constant (this is due to the fact that the power of the implosion is driven by a difference is pressure, which is constant for our hydrostatic case) while showing the influence of distance and volume. The equation should be of the following form:

$$P_{\max} = CV^m R^n \tag{19}$$

where in this case, *C* is a constant that will later be associated with the depth of the implosion. From the data collected from the DYSMAS simulations, it has been determined that the radial exponent, *n*, is a constant value of *n* = -0.43 at a depth of 152.4 meters. From Figure 27, it is shown that as the radial distance from the center of the implosion is increased, the rate at which pressure changes with respect to depth is decreased. Thus, the exponent of the radial distance term, *n*, is not a constant and varies with respect to depth. The exponent *n* is of the form:

$$n = \frac{17d}{11430} + \frac{61}{300} \tag{20}$$

where *d* is the depth in meters.

In addition to the varying value of n with respect to depth, the exponent of the volume, *m*, is not constant. From the collected data, it seems that as the volume of the implosion is increased, the amount that the volume influences the magnitude of the peak pressure wave increases. Thus, the exponent of the volume, *m*, is of the form:

$$for \qquad r \le 1.25 \qquad m = 0.23 \tag{21}$$

$$r > 1.25 \qquad m = \frac{r}{15} + \frac{11}{75} \tag{22}$$

Lastly, the constant value must be determined. The constant is a function of depth. However, it is not linearly dependent on depth. The constant, *C*, is of the form:

$$C = 8.33E^{-5}d^2 + 0.025674d + 0.087759 \tag{23}$$

where again *d* is depth in meters.

With the terms being defined, the approximation of the peak pressure created by an imploding spherical air cavity is defined as:

$$P_{\max} = (8.33E^{-5}d^2 + 0.025674d + 0.087759) \cdot \frac{V^m}{R^{17d/11430 + 61/300}} \qquad 24$$

where P_{max} is in MPa. The depth and volume should be entered in *meters* and *meters*^{3}, respectively.

This approximating equation is based on the data provided from DYSMAS simulations. The approximating equation provides good correlation to the data outside of the initial radius of the imploding spherical cavity. For example, if the spherical air cavity has an original radius of 1.0 meter, the approximation provides good correlation (under 10% error) outside of 2.0 meters away from the center of the implosion. Near the initial radius of the imploding sphere, the approximation under predicts the peak pressure by about 27%. With this in mind, the appropriate adjustment can be made for calculations at this range. Although the approximating equation does not correlate well within the original radius of the sphere, the damage done by an implosion event will likely occur outside of that radius. For example, a parent submarine hull would not be within the radius of the spherical air cavity, but it would be located close by. The approximating equation would predict the pressure wave that would impact that parent hull with relative certainty.

While the approximating equation correlates well outside of the original spherical radius, it also does an adequate job at predicting the peak pressure at the center of the imploding volume. Most error is seen at the original radius of the spherical cavity. Figure 28 displays the correlating data for spherical implosion of 1.0 meter radius.

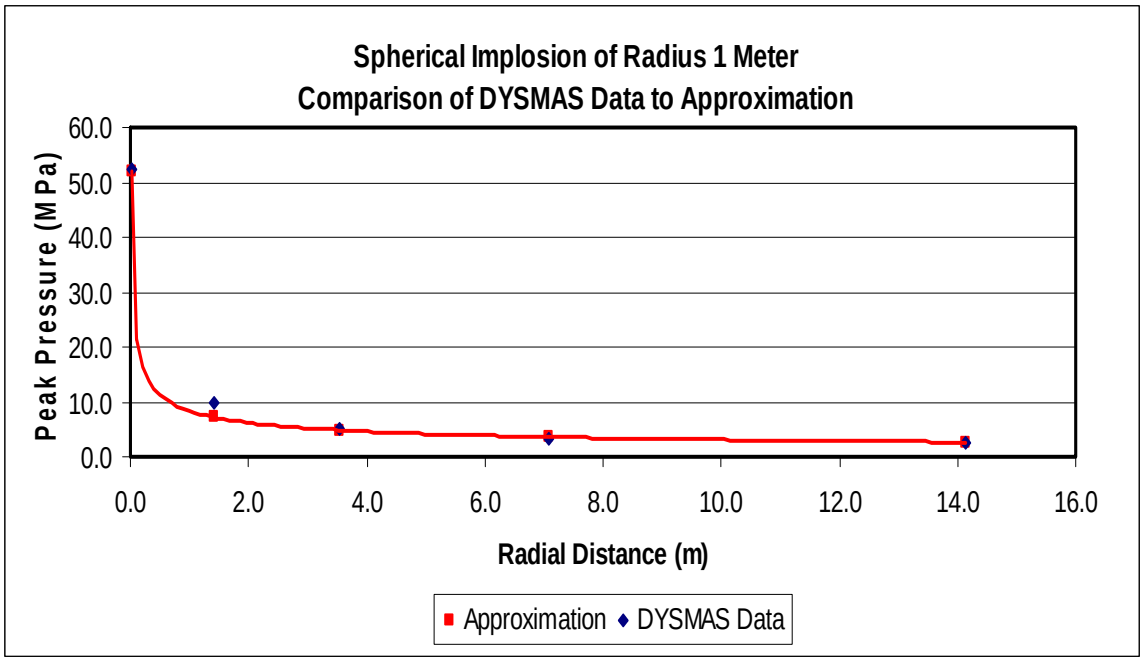

Figure 28. DYSMAS Data and Approximate Correlation: Spherical Cavity of 1.0 Meter Radius

The following table displays the approximated peak pressure as well as the error compared to the DYSMAS data. Notice that the percent error is at the most near the initial radius of the spherical air cavity.

Table 2. Approximated Values of Peak Pressure and Associated Percent Error: Spherical Cavity of 1.0 Meter Radius

R (m)	Approximated Pmax (MPa)	Error
0.014	52.06	0.7%
1.414	7.19	28.1%
3.536	4.85	4.1%
7.071	3.60	5.0%
14.142	2.67	0.1%

Additional figures displaying the correlation between the DYSMAS data and approximated values are shown on the following pages.

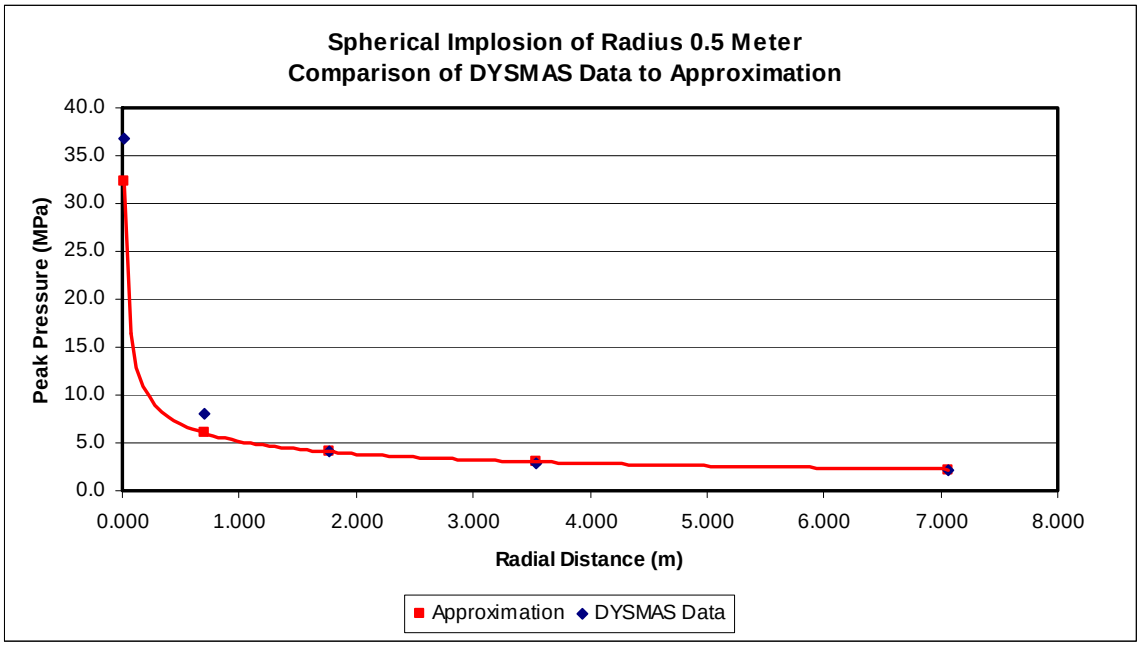

Figure 29. DYSMAS Data and Approximate Correlation: Spherical Cavity of 0.5 Meter Radius

Table 3. Approximated Values of Peak Pressure and Associated Percent Error: Spherical Cavity of 0.5 Meter Radius

R (m)	Approximated Pmax (MPa)	Error
0.014	32.27	12.1%
0.707	6.00	25.4%
1.768	4.05	1.8%
3.536	3.00	5.4%
7.071	2.23	0.0%

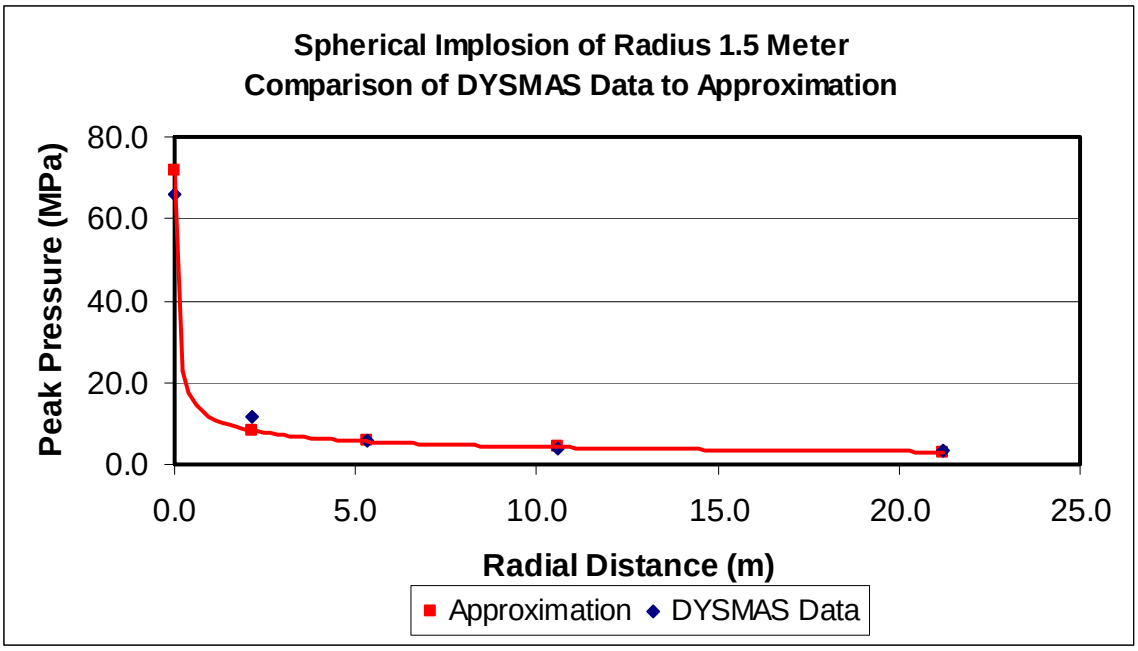

Figure 30. DYSMAS Data and Approximate Correlation: Spherical Cavity of 1.5 Meter Radius

Table 4. Approximated Values of Peak Pressure and Associated Percent Error: Spherical Cavity of 1.5 Meter Radius

R (m)	Approximated Pmax (MPa)	Error
0.014	71.85	8.8%
2.121	8.33	29.7%
5.303	5.62	6.1%
10.607	4.17	1.7%
21.213	3.10	3.4%

This approximate equation is based on data from DYSMAS simulations. It is limited to the peak pressure calculation of spherical air cavities (at atmospheric pressure) placed in a hydrostatic field (water) with no structure. As the volume of the imploding sphere increases, the implosion becomes more unpredictable. Thus, this approximation should be limited to spherical air cavities with an initial radius of 2.0 meters or less.

C. IMPLOSION OF CYLINDRICAL FLUID MODEL

In addition to testing spherical air filled cavities, cylindrical air cavities were also modeled. Comparisons between spherical and cylindrical cavities of identical volume were studied. The probe locations for the cylindrical air cavity models are described in the table below and visually depicted in the following figure. Notice that the length to diameter ratio of the cylinders is, L/D = 2.

Table 5. Location of Probes for Cylindrical Air Cavity Tests

H = 2 R			
Pressure Probe #	X Distance (m)	Z Distance (m)	Radial Distance (m)
1	0.01	0.01	0.0141
2	R	0.5 H	1.414 R
3	2 R	H	2.828 R
4	2 R	1	2 R
5	10 R	2.5 H	11.18 R
6	10 R	1	10 R

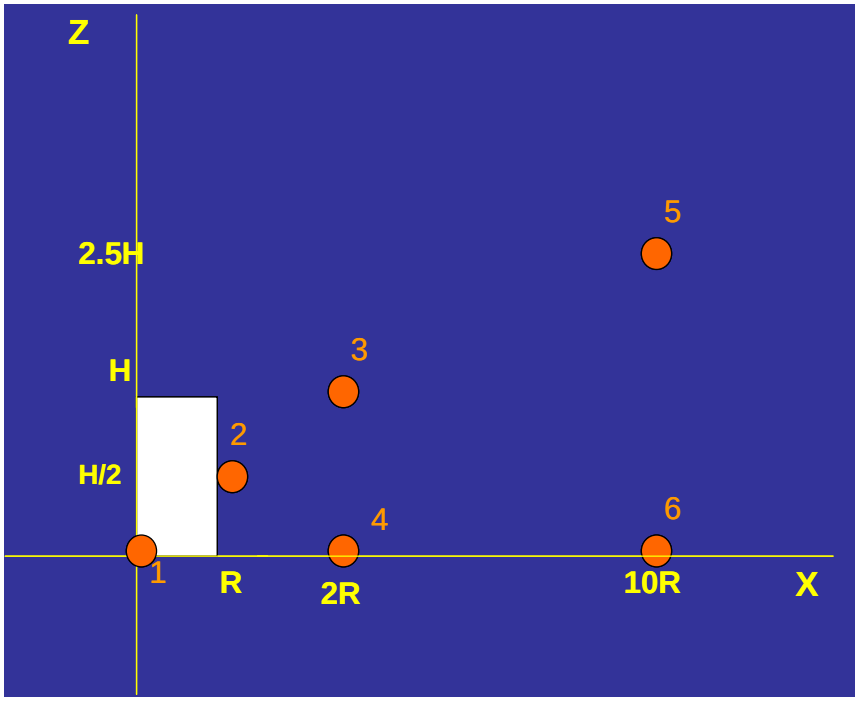

Figure 31. Probe Locations of Cylindrical Air Cavity Tests, Quarter Model Utilizing Symmetry

Using DYSMAS, two scenarios were modeled and simulated. In the first scenario, an air filled cylindrical cavity with L/D = 2 was modeled with the equivalent volume of a sphere of radius 0.5 meters. The second scenario consisted of an air filled cylindrical cavity of L/D = 2 with the equivalent volume of a sphere of 0.75 meter radius. The results were compared to the air filled spherical cavity results that were previously obtained in order to determine the difference in peak pressure magnitudes. Similar volumes were compared at equal distances from the center of the implosion.

First, a comparison study considering the first scenario will be presented. Recall that the volume of the imploding sphere and cylinder are the same (volume equivalent to

a sphere of 0.5 meter radius). Figure 32 shows the pressure history of Probe 1, the probe at the center of both the cylindrically and spherically shaped implosion cavities.

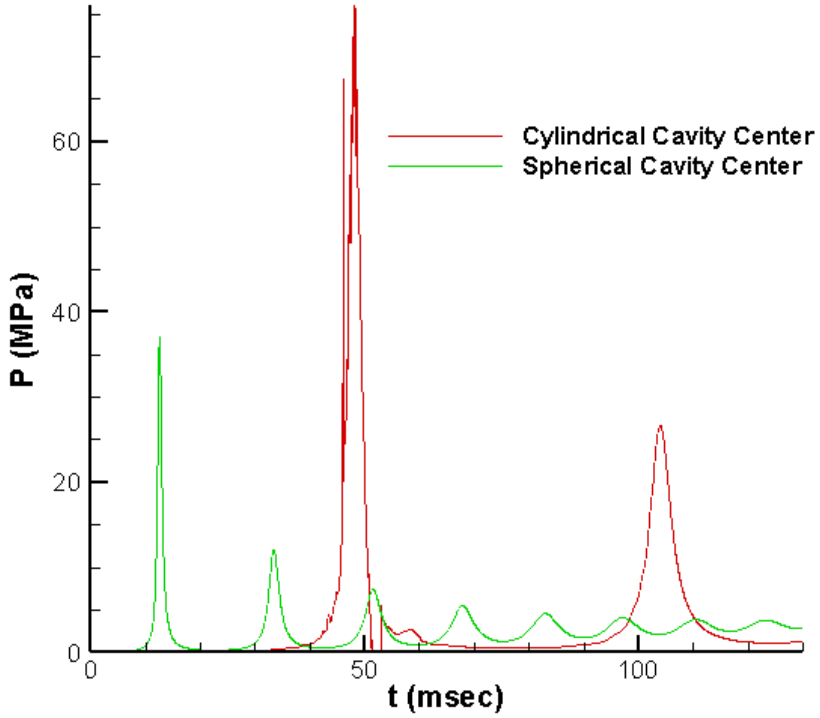

Figure 32. Probe 1 Pressure History Comparison of Spherical and Cylindrical Implosions

From the pressure history, it is evident that the implosion of the cylinder takes a longer period of time than the implosion of the spherical cavity. In addition, the peak pressure at this distance for the cylinder is nearly twice that of the peak pressure caused by the spherical implosion. The period of the bubble oscillation is also much greater in the case of the cylindrical implosion. Below is a table that compares the peak pressures caused by a cylindrical and spherical implosion. These implosions have the same volume and occur at the same depth.

Table 6. Comparison of Peak Pressure Caused by Cylindrical and Spherical Implosions

Distance from Implosion Center (m)	Pmax Cylinder (MPa)	Pmax Sphere (MPa)	Greater Pressure	Pressure Ratio
0.0141	75.90	32.31	Cylinder	2.3
2.04	16.07	3.81	Cylinder	4.2
2.88	12.05	3.28	Cylinder	3.7
4.07	9.35	2.83	Cylinder	3.3
14.4	4.63	1.64	Cylinder	2.8
16.1	4.46	1.57	Cylinder	2.8

Figure 33 displays the data from the table above. It is apparent that the peak pressure caused by the cylindrical implosion does not decline as quickly as the peak pressure caused by the spherical implosion. The pressure wave caused by the cylindrical implosion is approximately three times the magnitude of the pressure wave caused by the spherical implosion.

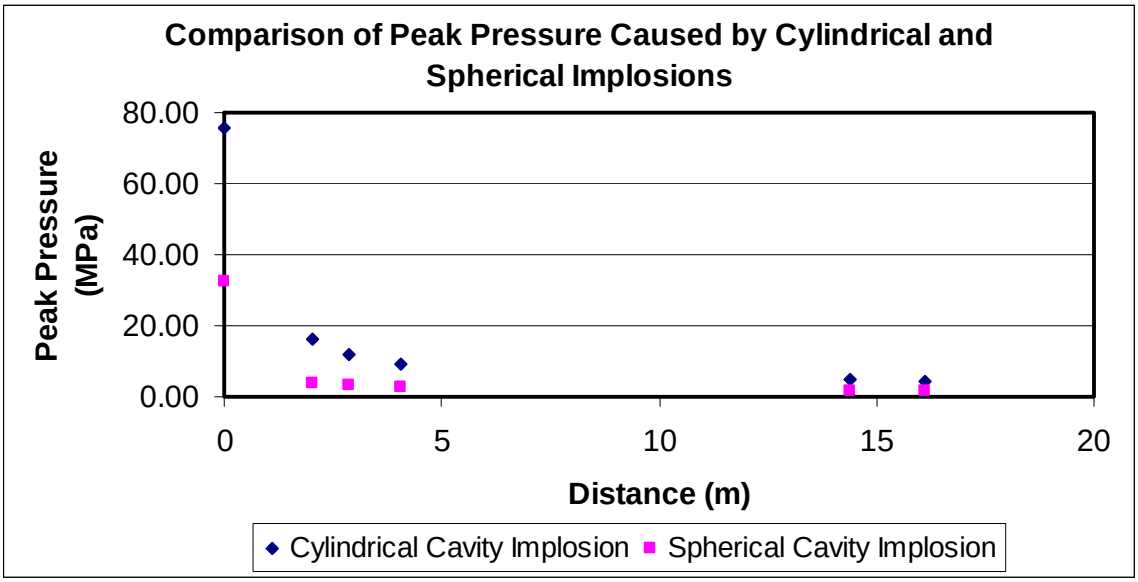

Figure 33. Comparison of Peak Pressure Caused by Cylindrical and Spherical Implosions

Consider the second scenario, where the volume of both the sphere and cylinder are equal to that of a sphere with radius 0.75 meter. Again, the implosions occur at the same depth. The following table provides the peak pressure data for comparison.

Table 7. Comparison of Peak Pressure Caused by Cylindrical and Spherical Implosions

Distance from Implosion Center (m)	Pmax Cylinder (MPa)	Pmax Sphere (MPa)	Greater Pressure	Pressure Ratio
0.0141	209.00	42.74	Cylinder	4.9
3.75	53.01	3.87	Cylinder	13.7
5.3	63.05	3.34	Cylinder	18.9
7.49	28.98	2.88	Cylinder	10.1
26.5	21.22	1.67	Cylinder	12.7
29.63	12.39	1.59	Cylinder	7.8

Figure 34 displays the data from the above table. Notice that in two cases, distances of 5.3 and 26.5 meters, that the peak pressure is slightly elevated. This is due to the location of the probes. These probes are located perpendicular to the center of the cylinder, whereas the other probes (excluding probe 1) are located at an angle from the center of the imploding cylinder. As the cylindrical cavity implodes, the pressure wave is greatest along its axis and dissipates as the angle from the axis increases (of course, this is not the case with a spherical implosion due to symmetry). This phenomenon did not occur with the lesser volume cylinder.

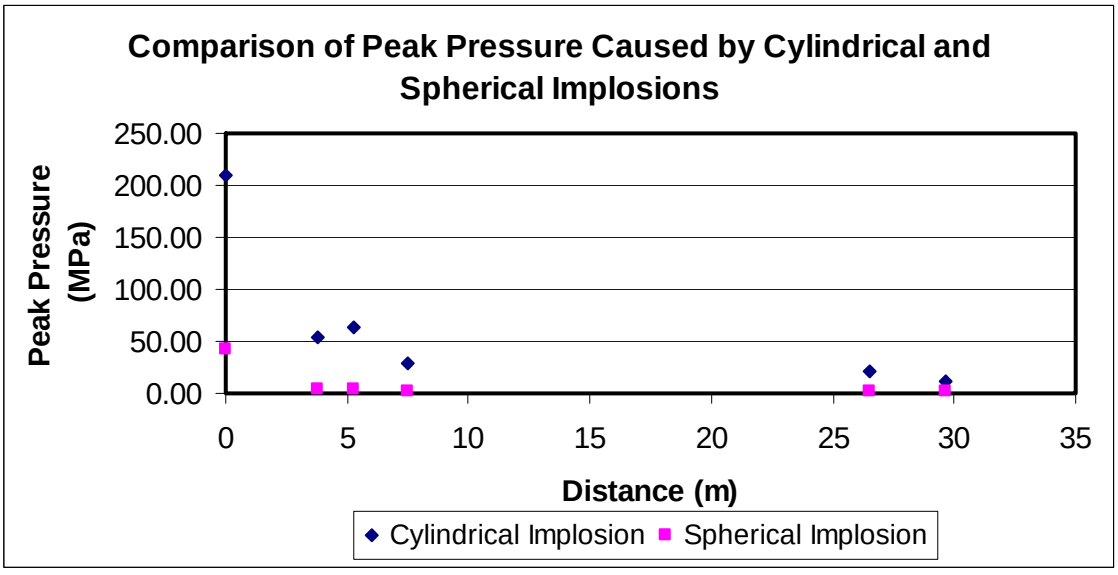

Figure 34. Comparison of Peak Pressure Caused by Cylindrical and Spherical Implosions

As shown in the modeled scenarios, cylindrical shaped implosions create a larger magnitude pressure wave than their respective equal volume spherical implosion

counterparts. The shape of the pressure wave is also dictated by the shape of the implosion. Clearly, the spherical implosion forms a symmetric pressure wave, while the cylindrically shaped implosion creates a pressure wave that is greatest along its axis of symmetry and decreases in magnitude as the angle from that axis increases.

D. IMPLOSION OF ALUMINUM CYLINDER

1. Test Series

Previously discussed was the data collected from fluids only models consisting of only water and air. Although those simulations offered insight into the behavior of an implosion event, a simulation is needed that would predict the pressure wave caused by the implosion of a structure. Experimental tests were completed in nearly forty years ago to determine the acoustical properties of implosion shock waves. More recently, simulations were conducted at NUWC-NPT to test the influence of length to diameter ratio of the cylinder, material construction, and initiation location on the magnitude of the implosion pressure wave. In those simulations, an initiating device was utilized that would create an initial deformation in the cylinder that would cause the cylinder to buckle and cause a pressure wave due to an implosion.

Of interest is, instead of using an initiator to begin the implosion process, placing a small explosive charge near the cylinder and letting the pressure wave from the charge initiate the implosion of the cylinder. For these tests, the model will remain the same, allowing for a constant volume and identical material properties. However, the depth at which the cylinder is located (thus influencing the hydrostatic pressure surrounding the cylinder) will be varied. In addition, pressure probes will be located at specific locations to capture the effect that the cylindrical model has on the formation of the implosion pressure wave. Also, the charge weight will be varied to determine if decreasing the magnitude of the initiating pressure wave subsequently influences the pressure wave due to the implosion. The distance from the center of the charge to the outer hull of the cylinder will be held constant at 15.24 cm.

A test matrix is given below that describes the types of tests that will be conducted in the simulations.

Table 8. Matrix for Structural Cylinder Implosion Simulations

Test	Charge Weight (grams)	Depth (meters)
1	50	1091
2	50	1635
3	50	2073
4	25	1091
5	12.5	1091
6	12.5	2073 +
7	12.5	2073 -

The depths were calculated based on a percentage of critical buckling pressure. Tests one, two, and three are conducted at 50%, 75%, and 95% of buckling depth. The critical buckling pressure was calculated using the following:

$$P' = \frac{t}{R} \cdot \frac{\sigma_y}{1 + \left(\frac{4\sigma_y}{E}\right) \cdot \left(\frac{R}{t}\right)^2} \qquad 25$$

where t is wall thickness, r is mean radius, E is Young's Modulus, and σ_y is the yield stress [Ref.18].

2. Computational and Structural Modeling

The structural model was created using DYSMAS-P, a pre- and post-processing tool that complements the DYSMAS suite. The model dimensions are listed in the table below.

Table 9. Dimensions of Aluminum Cylinder

Length	91.44	cm
Diameter	45.72	cm
Wall Thickness	1.27	cm

The structural model is made of 4224 shell elements. The cylinder's material property model includes an elastic/plastic behavior with strain rate dependence. Each shell element has three integration points through its thickness. The material model for AL6061-T6 was provided by NSWC-IH. Failure criteria were input to allow the deletion of failed elements. Figure 35 displays the cylindrical structural model. The endcap is

shown in red, while the body of the cylinder is shown in blue (for viewing clarity). Both structures are made of the same material. Notice that two planes of symmetry are used; half the longitudinal length and half of the circumferential distance are modeled.

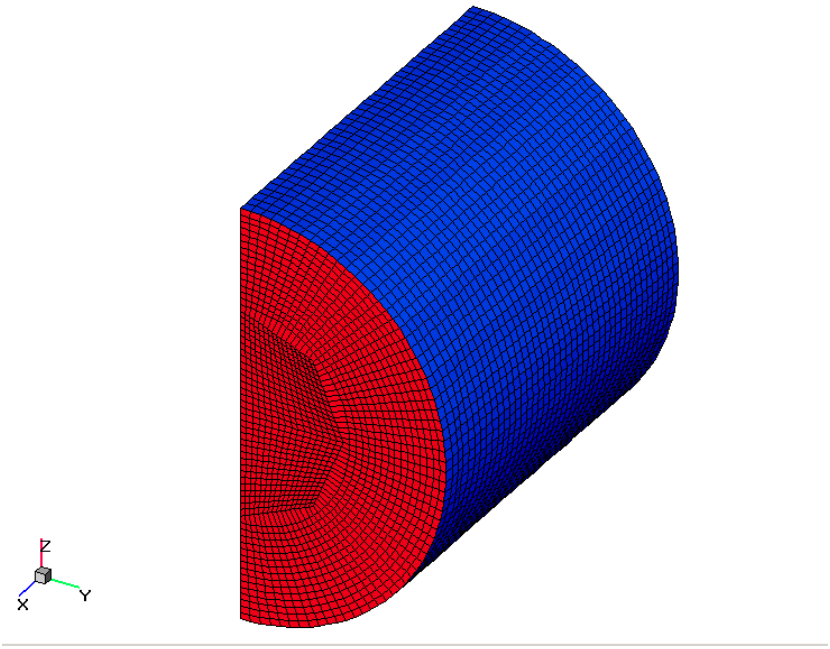

Figure 35. Cylinder Structural Model

The cylinder is placed at the predetermined depth and an explosive charge is placed 15.24 cm above the upper hull of the cylinder. In Figure 37, the charge would be placed at x=0, y=0, z=15.24+r (considering the shown endcap as L/2). A hydrostatic flowfield is placed around the model and the internal pressure of the cylinder is set to atmospheric.

In order to decrease the computational time needed to complete the simulation, the initial pressure wave propagation was captured using a 2-D fluid pre-calc using GEMINI. Trap conditions were specified to halt the calculation once pressure or the flow field velocity change by a certain amount. Once the pre-calc completed, a rezone was performed in order to allow calculation in three dimensions. Figure 36 displays the trapped fluid flow condition for the 50% crush depth simulation. Again, the charge is a 50 gram TNT explosive.

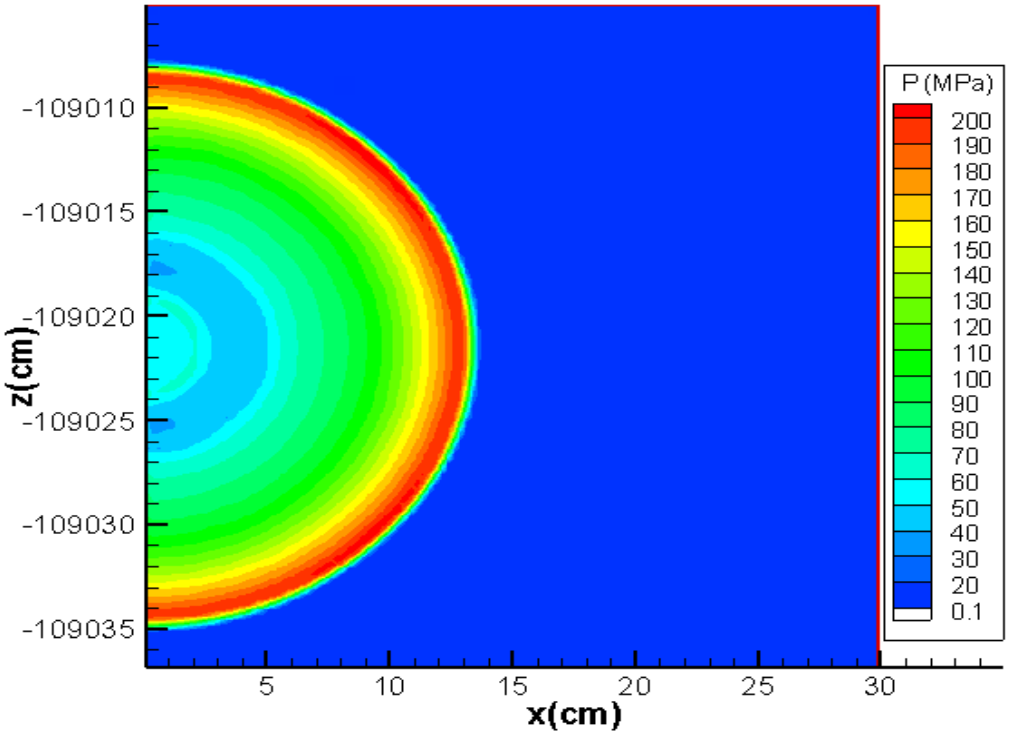

Figure 36. Fluid Pre-Calc for the 50% Crush Depth Cylinder Model: 50 g Charge

Once the trap condition is achieved, the problem domain is rezoned into a three dimensional domain and the structure is added. Figure 37 shows the problem now rezoned into the three dimensional domain. Notice that the internal pressure of the cylinder is at atmospheric pressure.

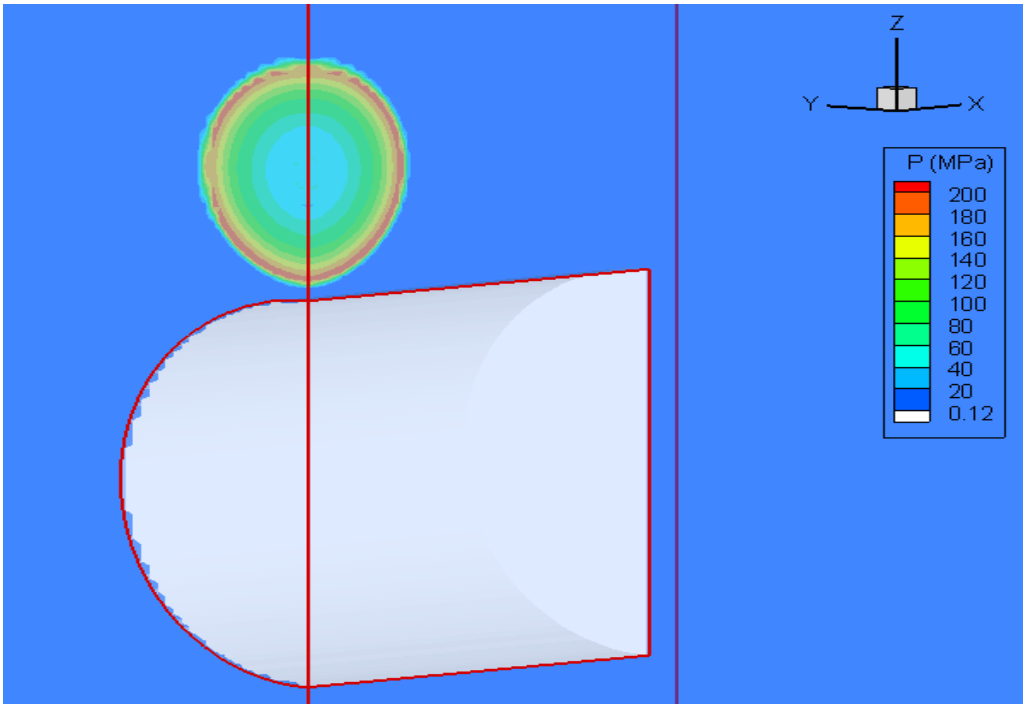

Figure 37. Three Dimensional Rezone: Completed in PREGEMINI

Once the re-zone has been completed in 3-D using PREGEMINI, GEMINI and DYNA_3D are used to calculate the responses of the structure and surrounding fluid. These simulations were only carried out to 8 milliseconds to capture the initial shock wave due to the implosion. A flow field displaying the pressure contour plots and structural response are shown in Appendix B. The response in Appendix B is for test four indicated in the test matrix, Table 8. Appendix C is an annotated input deck to run this simulation.

In order to capture the effects of the pressure wave, cells have been denoted to record pressure histories throughout the simulation. The locations of these “pressure probes” are denoted in the following table.

Table 10. Location of Pressure Probes; Coordinate Origin Considered at x = L/2, y = z = 0

Probe	X Coordinate	Y Coordinate	Z Coordinate	Physical Description
1	0	0	r + 25	25 cm above; center
2	0	0	r + 50	50 cm above; center
3	0	0	r + 100	100 cm above; center
4	0	r + 25	0	25 cm athwart; center
5	0	r + 50	0	50 cm athwart; center
6	0	r + 100	0	100 cm athwart; center
7	0	0	-(r + 25)	25 cm below; center
8	0	0	-(r +50)	50 cm below; center
9	0	0	-(r + 100)	100 cm below; center
10	L / 4	0	r + 25	25 cm above; quarter length
11	L / 4	0	r + 50	50 cm above; quarter length
12	L / 4	0	r + 100	100 cm above; quarter length
13	L / 4	r + 25	0	25 cm athwart; quarter length
14	L / 4	r + 50	0	50 cm athwart; quarter length
15	L / 4	r + 100	0	100 cm athwart, quarter length
16	L / 4	0	-(r + 25)	25 cm below; quarter length
17	L / 4	0	-(r +50)	50 cm below; quarter length
18	L / 4	0	-(r + 100)	100 cm below; quarter length
19	0	0	0	internal; center cylinder
20	L / 4	0	0	internal; quarter length

On the following page, a figure depicting the probe locations in accordance with the locations listed in Table 10 is displayed. Take note of the symmetry condition in this view.

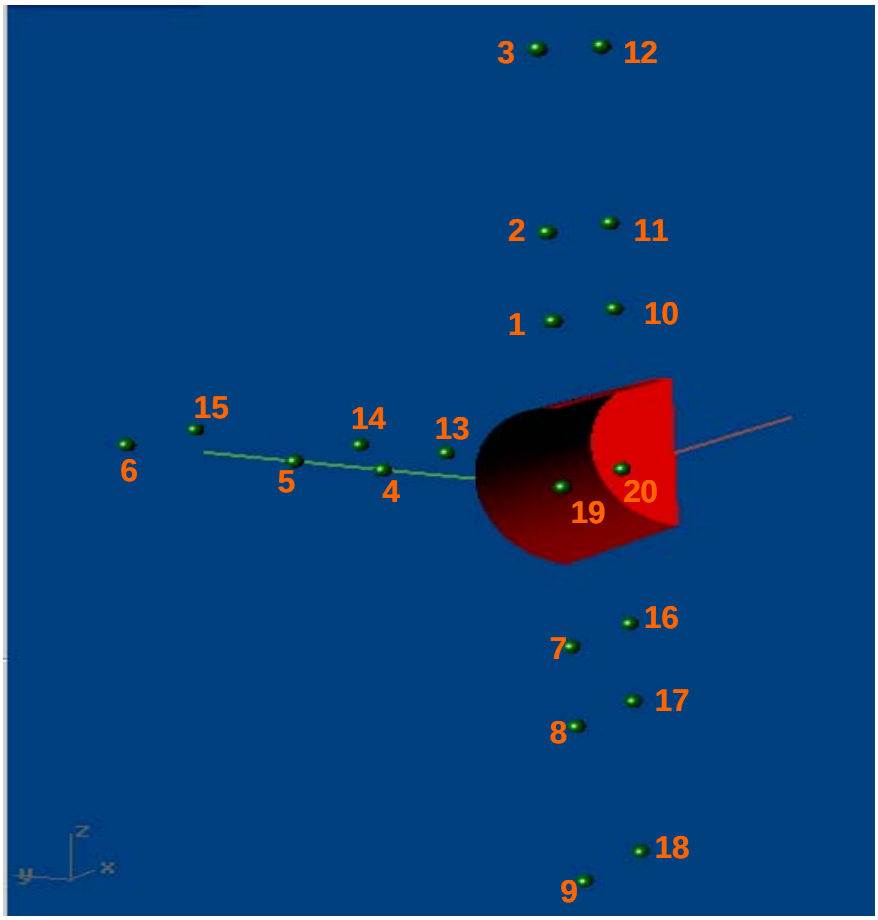

Figure 38. Visual Depiction of Pressure Probe Placement Around Aluminum Cylinder

3. Pressure Wave Behavior Around Cylinder

In order to understand the behavior of the implosion shock wave at locations around the cylinder, the scenario of a 50 gram TNT charge with the model at 95% crush depth. The pressure probes used can be referenced in Table 10.

First, pressure probe data will be examined from below the center of the cylinder. Recall that the small charge is placed above the cylinder, thus the fluid below the cylinder should not be influenced by the explosive's pressure wave. Probes 7, 8, and 9 are displayed in the Figure 39.

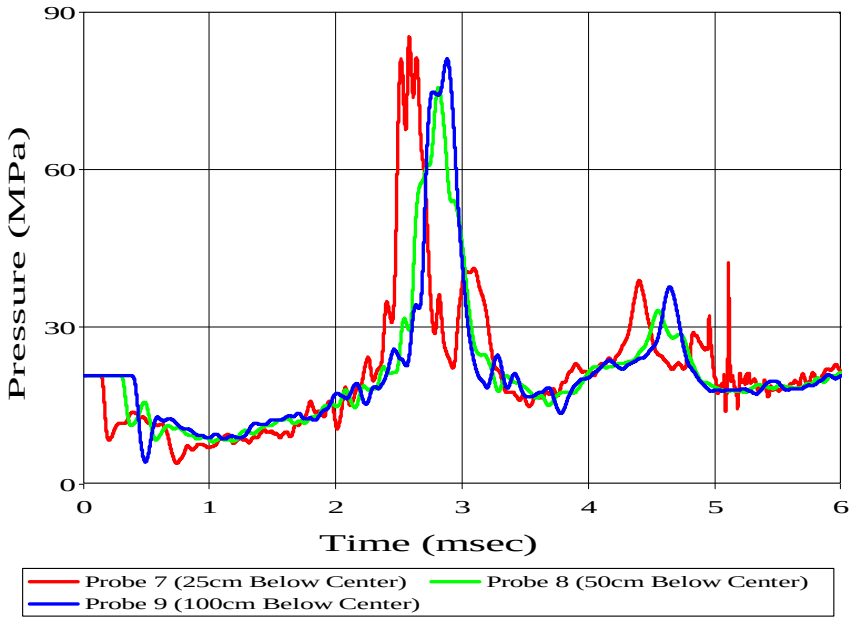

Figure 39. Pressure History Below Center of Cylinder: Probes 7, 8, and 9

Notice at early time (about 0.5 msec) that the ambient hydrostatic pressure is disturbed and pressure suddenly drops. This is due to the imploding cylinder; the fluid is rushing inward to fill the lower pressure volume. Then, an implosion occurs, creating a pressure wave that is four times that of hydrostatic pressure.

Next, probes 4, 5, and 6 will be examined. These probes will display the pressure wave as it moves laterally from the imploding cylinder. Figure 40 displays the pressure histories of these probes.

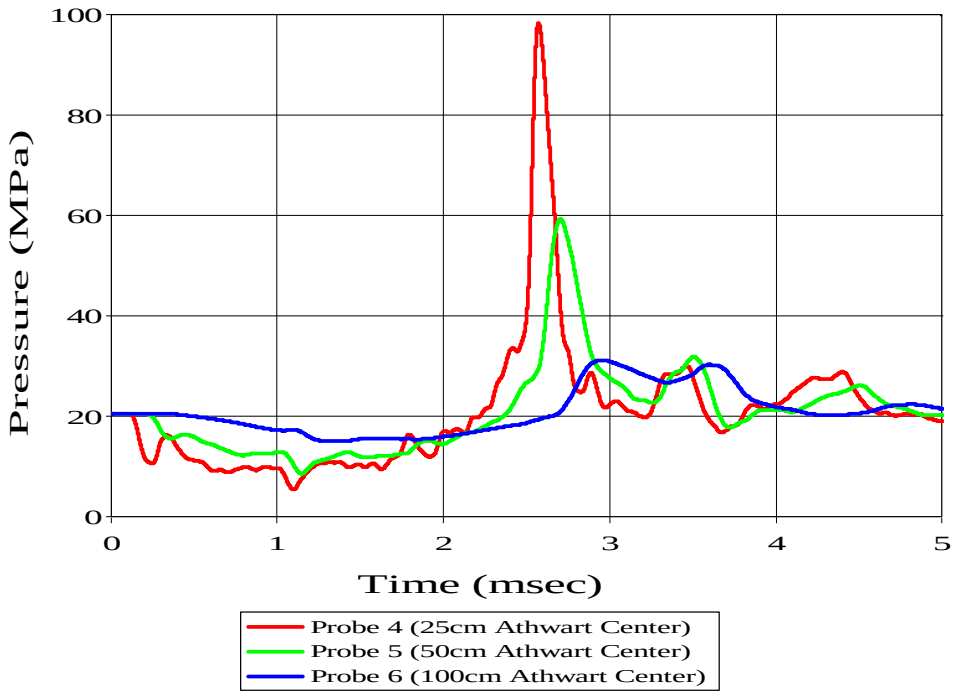

Figure 40. Pressure History Athwart Center of the Cylinder: Probes 4, 5, and 6

Notice the marked decrease as the distance from the implosion is increased. Because of the charge location (above the cylinder), the brunt of the implosion pressure wave travels in directions above and below the cylinder, while quickly diminishing laterally from the cylinder.

Figure 41 displays the pressure history 50 cm around the cylinder at three positions; above, below, and athwart. Note that the pressure wave athwart of the cylinder is less. In addition, the initial peak of probe two (at time less than 1 msec) is attributed to the explosive pressure wave. The pressure wave caused by the implosion of the cylinder is also greatest in the direction toward the explosive charge (above the cylinder).

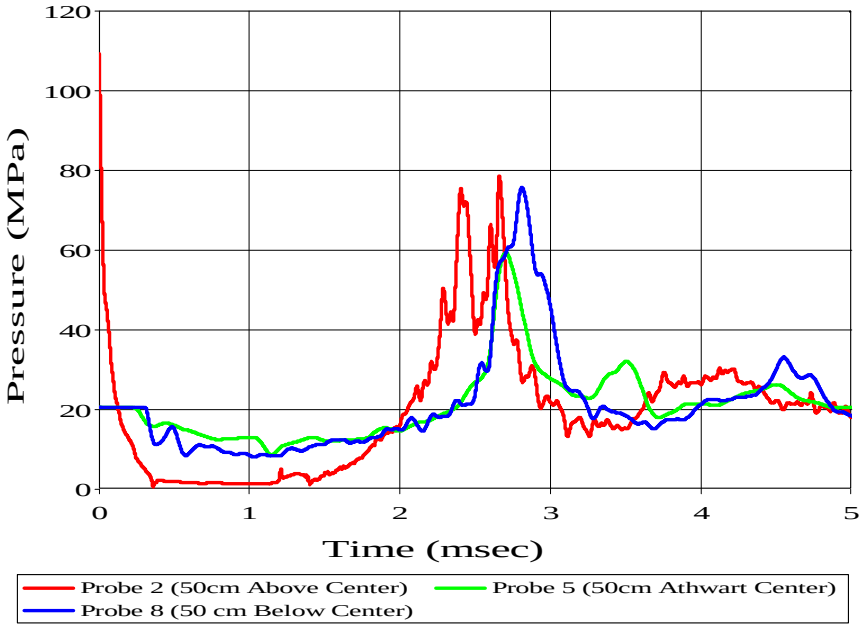

Figure 41. Pressure History Around the Center of Cylinder at Various Angles: 95% Crush Depth: Probes 2, 5, and 8

Figure 42 displays the pressure history of probes also located 50cm from the cylinder at three positions, but the probes are located at a quarter of the cylinder's length (not the center).

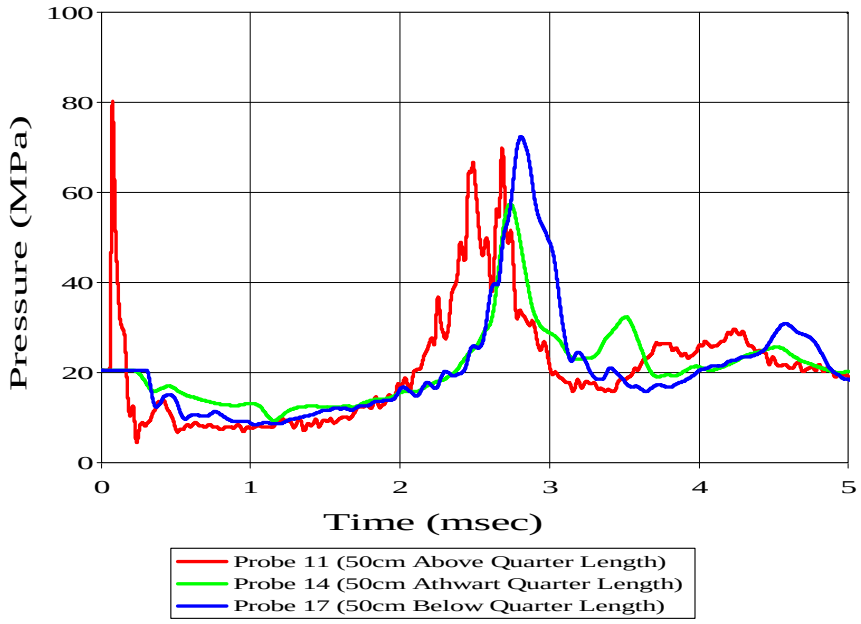

Figure 42. Pressure History 50cm from Cylinder at Quarter Length: 95% Crush Depth: Probes 11, 14, 17

The difference in longitudinal position is not as influential as the angle from the cylinder. As shown in Figures 41 and 42 the pressure wave caused by the implosion is smaller at a position lateral to the cylinder. In addition, as the distance from the center of the cylinder increased, the magnitude of the pressure wave caused by the implosion also decreased slightly.

Of interest is the pressure history for points that were initially inside of the cylinder. Probes 19 and 20 recorded the pressure history of this scenario. Probe 19 is located in the center of the cylinder while probe 20 is at the quarter length of the cylinder. Pressure histories for these two points are shown in Figure 43.

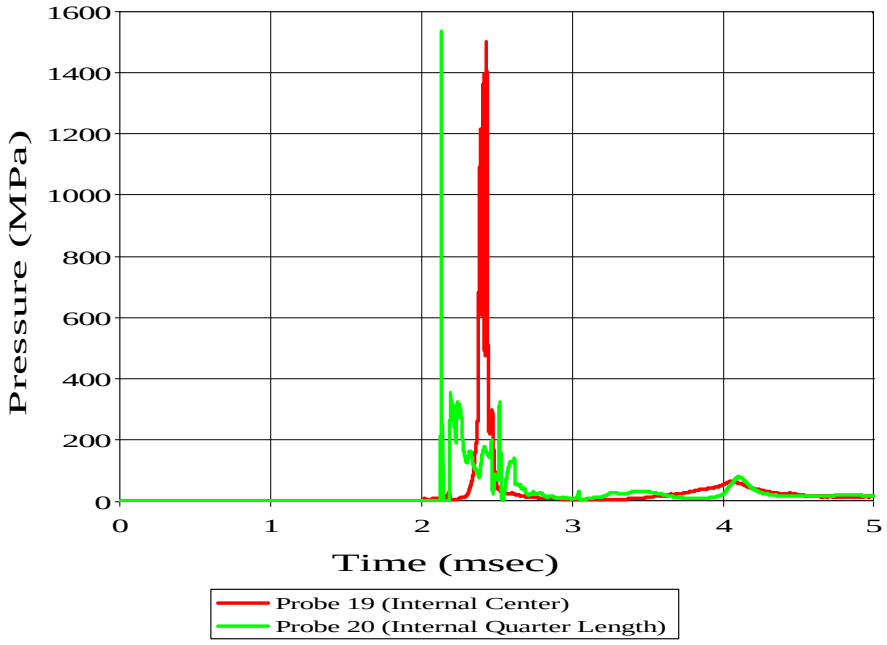

Figure 43. Pressure History of Probe Inside of Cylinder: 95% Crush Depth

Notice that the pressure peaks at different times for the probes separated by 22.86cm longitudinally. In addition, the peak pressure at the center of the cylinder has a slightly lower magnitude than the peak pressure at the quarter length of the cylinder.

4. Comparison of Implosion Pressure Wave at Various Depths

In order to determine the influence of depth on the implosion pressure wave, three simulations were conducted that varied the depth of the cylinder. The cylinder was placed in a hydrostatic field at 50%, 75% and 95% of hull crush depth. The charge size remained constant (a 50 gram TNT charge). Pressure histories were again collected at pressure probe locations, again as indicated in Table 12.

Figure 44 displays the pressure wave 25 cm below the cylinder at various depths.

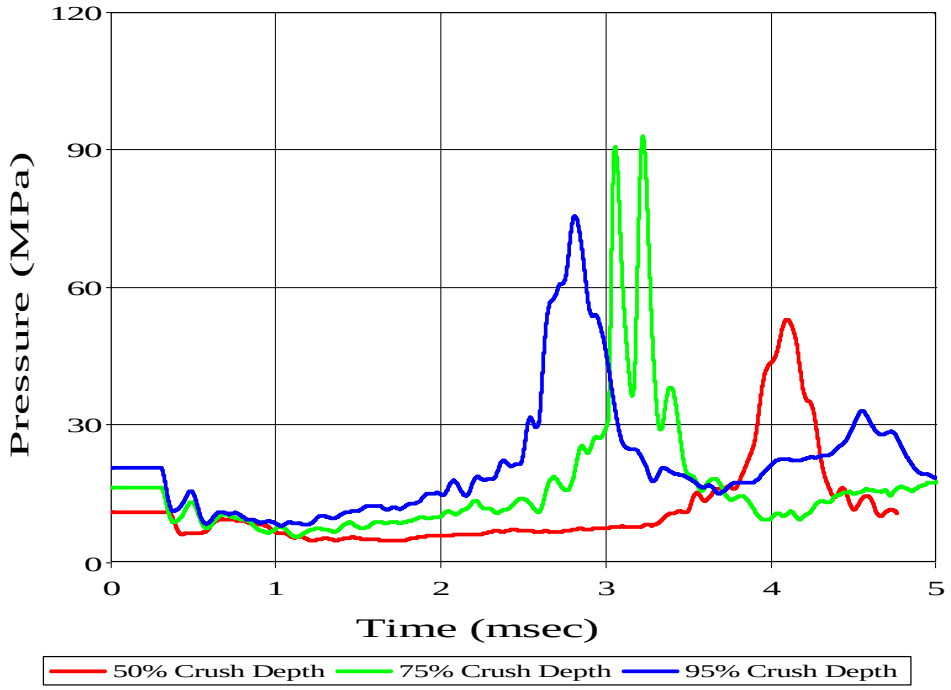

Figure 44. Probe 8 Pressure History at Various Depths

Notice that as the depth is increased, the time until the implosion is accomplished is decreased. This is due to the increase of hydrostatic pressure outside of the cylinder. Of interest in this case is that the magnitude of the implosion pressure wave at 75% crush depth is greater than the 95% crush depth case.

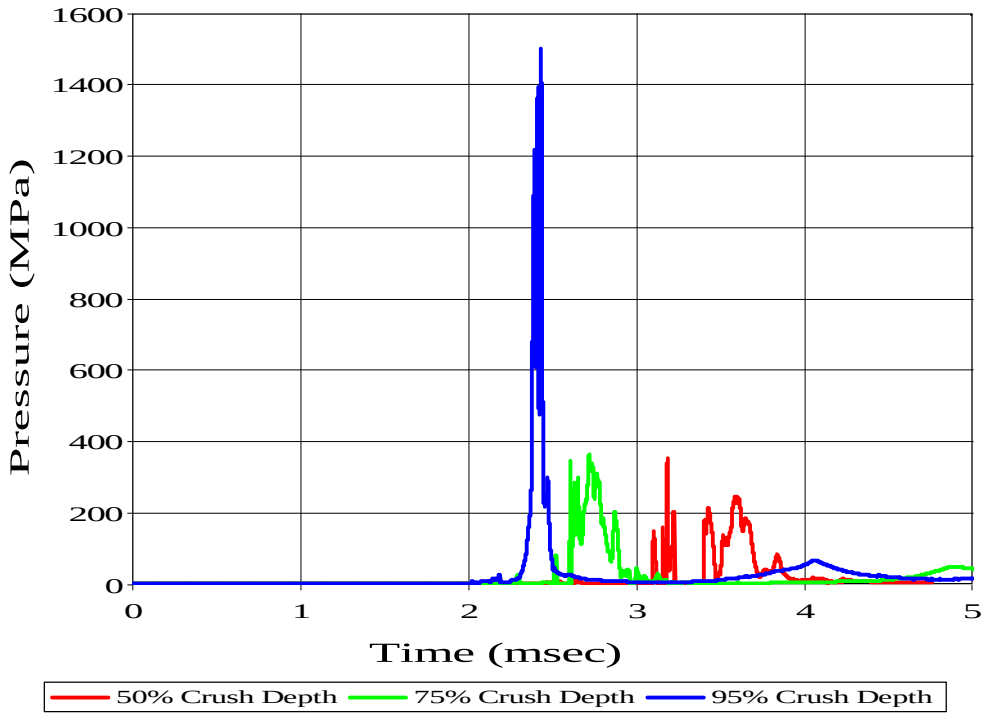

Figure 45. Probe 19 Pressure History at Various Depths

Figure 45 displays the pressure history at probe 19, which is positioned inside of the cylinder. Again, as the depth of the cylinder is increased the time elapsed until the implosion occurs is decreased. At this pressure probe, the magnitude of the implosion pressure wave increases as the depth is increased.

Figure 46 displays the pressure history at Probe 3 at various depths. At this location, the time elapsed until the implosion occurs is decreased as the depth of the cylinder is increased. However, the magnitude of the pressure wave does not increase at the depth is increased.

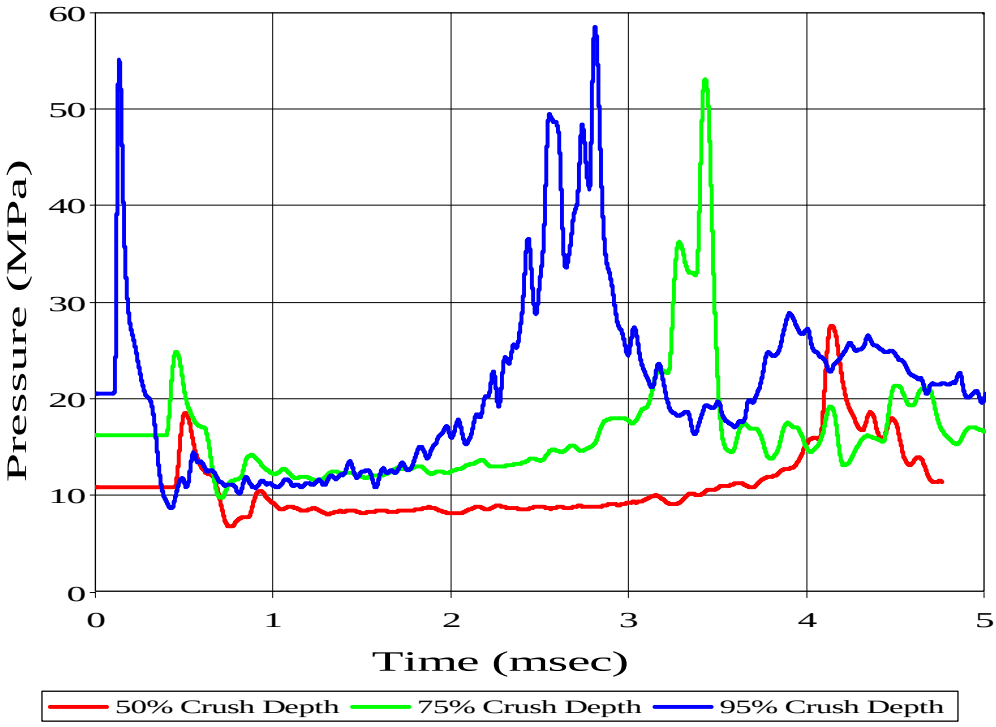

Figure 46. Probe 3 Pressure History at Various Depths

These simulations suggest that as the depth of the cylinder is increased, the time at which the cylinder implodes is decreased. There does appear to be a correlation between the depth of the cylinder and the magnitude of the pressure wave due to the implosion of the cylinder for the probes located at the center of the cylinder and above the cylinder. It is noted, however, that the magnitude and direction of the pressure waves are influenced by the implosion of the structure, which is not a process that occurs identically each time.

5. Variance of Charge Mass and Influence on Implosion of Cylinder

The mass of the charge influences the pressure wave emitted from an explosion event. Thus, by changing the mass of the charge, the pressure wave that will initiate the implosion of the cylinder will be affected. In order to study the effect of the mass of the explosive charge, three scenarios were modeled that placed a 12.5, 25, and 50 gram charge of TNT 15.24 cm above the center the cylinder. The pressure histories were again recorded using the probes located in accordance with Table 10. All the simulations were

conducted at 50% crush depth in order to mitigate any effects that depth may have on the implosion of the cylinder.

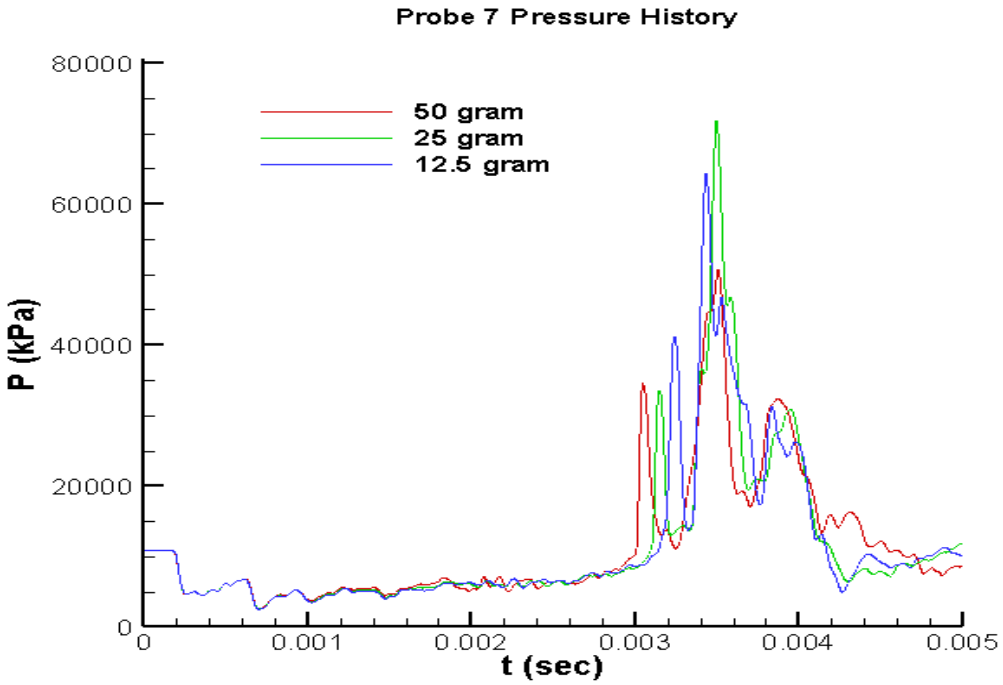

Figure 47. Probe 7 Pressure History: Effect of Varied Charge Mass

Figure 47 displays the pressure history 25 cm below the center of the cylinder. At this location, the size of the charge does not seem to influence the time at which the implosion of the cylinder occurs. The effect of the charge size is inconclusive from this location's data.

Figure 48 displays the pressure history at the center of the cylinder. Again, there is no difference of time of implosion due to a variance in charge size. However, notice that the 50 gram charge does produce a lower implosion pressure wave at the center of the cylinder.

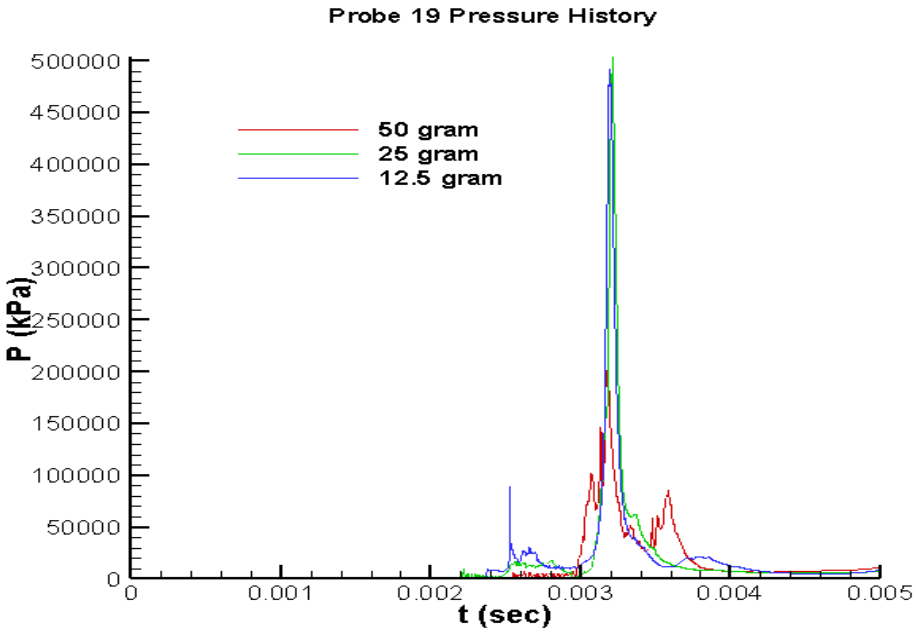

Figure 48. Probe 19 Pressure History: Effect of Varied Charge Mass

Figure 49 displays the pressure history one meter above the cylinder. The initial peak is due to the explosive's pressure wave (at about 0.5 msec).

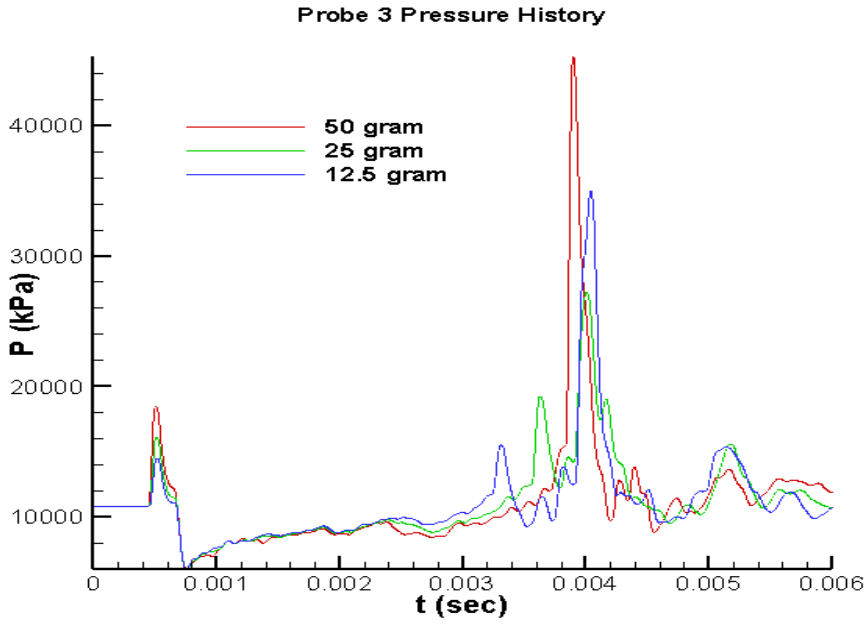

Figure 49. Probe 3 Pressure History: Effect of Varied Charge Mass

From this set of three simulations, it is apparent that the charge size does not influence how quickly the implosion will occur. In these figures, time zero (t = 0) is the instant that the pressure wave has nearly reached the cylinder. From this point, the 3D simulation begins: the pressure wave interacts with the structure and the implosion occurs. The charge mass does not seem to have some impact on the magnitude of the pressure wave created by the implosion. Above the cylinder, the larger charge stimulates a larger implosion pressure wave response. However, that is not the case at the center and below the cylinder. Clearly shown in the data figures in this section, the larger charge weight did not necessarily produce a larger implosion pressure wave at all locations. However, in order to mitigate the influence of the explosive pressure wave, the smallest possible charge should be used to instigate the implosion of the cylinder.

6. Effect of Charge Placement on the Implosion of a Cylinder

In the previously modeled scenarios, the placement of the charge has been 15.24cm above the cylinder. In the following modeled scenario, a 12.5 gram TNT charge will be placed 15.24 cm below the cylinder. The depth at which this implosion occurs is the same for the cases of the charge above and below the cylinder.

The following figure displays the pressure histories of probes 100 cm above the cylinder.

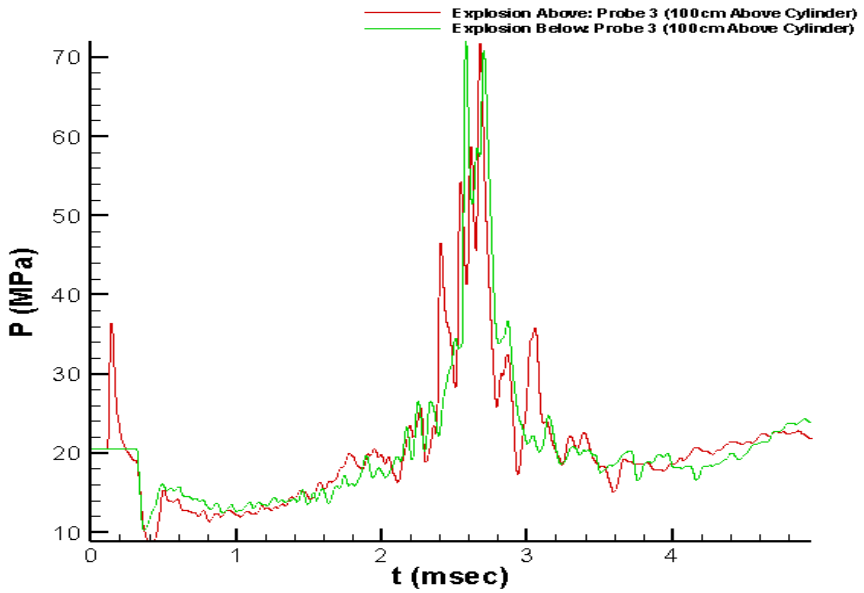

Figure 50. Charge Placement Comparison: Pressure History of Probe 3 for Charge Placed Below and Above Charge

From Figure 50, it seems that the placement of the charge did not greatly alter the magnitude of the peak pressure wave. In addition, the general trend of the pressure histories is similar for both cases. The following figure displays the pressure history of probe 8, which is located 50cm below the cylinder.

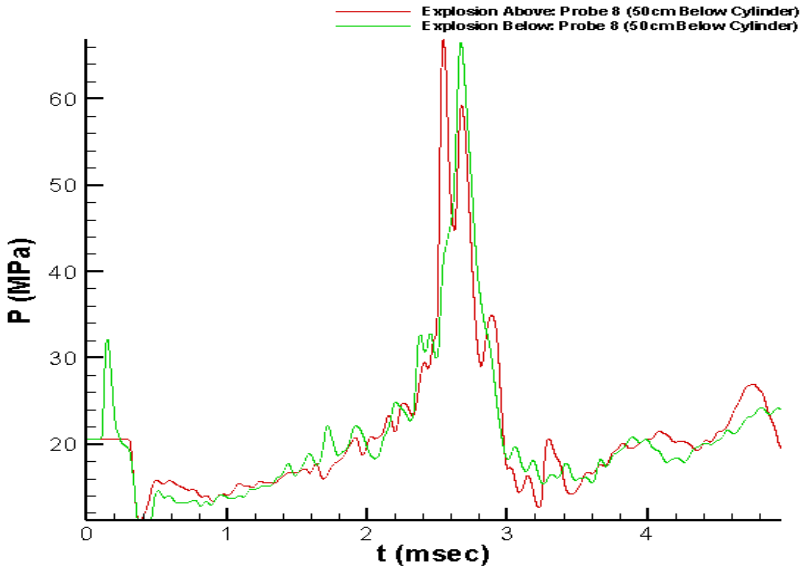

Figure 51. Charge Placement Comparison: Pressure History of Probe 8

Figure 51 shows that the peak pressure magnitude is not greatly influence by the placement of the charge. Again, as shown in both Figures 50 and 51, the trend of the pressure history is comparable between the two charge placements.

The following figure shows the pressure history of probe 4, which is located 25cm athwart of the cylinder. Notice that the magnitudes of the pressure waves are similar and that the trend, as in the previous two figures, is similar between the cases with varied charge placement.

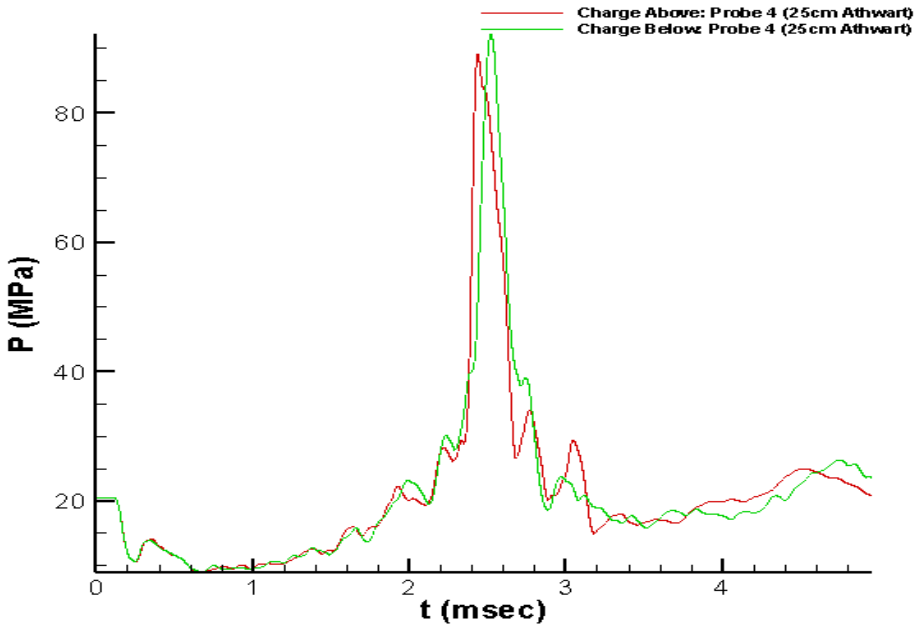

Figure 52. Charge Placement Comparison: Pressure History of Probe 4

The placement of the charge does not seem to have an effect on the pressure wave emitted from the imploding cylinder. As shown in Figures 50-52, the magnitude and general trend of the pressure wave are not impacted by the placement of the charge, whether the charge is above or below the cylinder.

E. COMPARISON OF PRESSURE WAVES CREATED BY EXLOSION AND IMPLOSION

Thus far, the pressure wave created by an implosion of a spherical cavity has been studied and an approximation method for calculating the peak pressure caused by the implosion has been accomplished. Of interest is the comparison of the pressure wave created by the implosion and the pressure wave created by a typical underwater explosion. Previously, the background and physics of UNDEX phenomena has been explained. Recall that the peak pressure at a distance, *R*, from a charge of a given type (TNT, HBX, etc) and weight can be calculated by using Equation 2:

$$P_{\max} = K_1 \cdot \left(\frac{W^{1/3}}{R} \right)^{A_1} \qquad 2$$

where K_1 and A_1 are properties of the charge type, W is the charge weight (lbs), and R is the distance from the center of the charge (ft). P_{max} is then determined (psi). Referring back to Figures 6 and 7, it is shown that the pressure wave created from an implosion can be greater than that of a similar explosion. This is accomplished by directing multiple detonators toward a central focal point (similar to a fluids only model in which the fluid begins moving toward the center of the cavity at the same rate from all directions).

The following figure compares the peak pressure wave created by an explosive charge, a spherical fluids model implosion, and an imploding aluminum cylinder. The explosive is a 1.36 kg TNT charge. The spherical implosion pressure wave is based upon the approximation method discussed earlier. The parameters for the spherical implosion are a depth of 2073 meters and a diameter of 5 cm. The imploding cylinder occurs at 2073 meters as well and the pressure readings are taken above the cylinder.

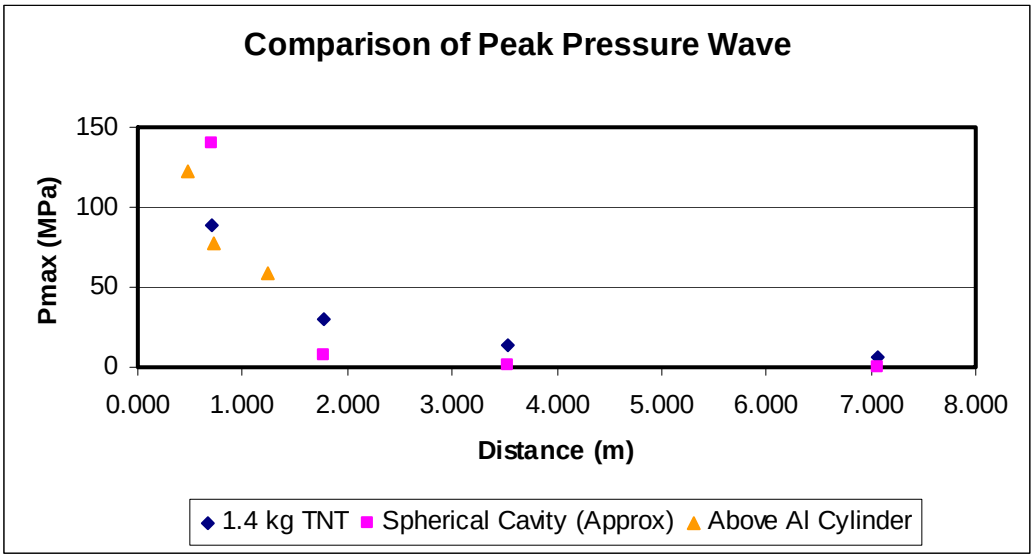

Figure 53. Comparison of Peak Pressure Wave Caused by Various UNDEX Events

From Figure 53, it is apparent that the peak pressure wave created by an explosion and two modeled implosion scenarios are similar. Of note, however, is the relative small size of the charge and the extreme depth at which the implosions occur. The pressure wave from the implosion is a function of pressure difference (pressure outside of

imploding volume vs. the pressure inside the imploding volume). The pressure difference needs to be immense in order to develop the same peak pressure wave created by the small explosive charge.

THIS PAGE INTENTIONALLY LEFT BLANK

V. FINAL REMARKS

A. CONCLUSIONS

It has been demonstrated through modeling and simulation that an implosion event does cause a peak pressure wave followed by subsequent pressure pulses similar to that of an underwater explosion. Previous research has proven that collapsing waves impinging on a central focal point can create a pressure wave that is greater than that of a typical explosion. This shaped charge weapon displayed in Figure 6 is an example of this principle.

The shaped charge weapon initiates collapsing detonation waves that have a large pressure and velocity associated with them. In the models in this thesis, the driving force behind the collapsing wave was hydrostatic pressure. The difference between the internal pressure of the structure and the external hydrostatic pressure caused the implosion pressure wave. As shown through modeling and simulation, the magnitude of the pressure wave caused by an implosion of a small pressure vessel (with the driving force behind the initial collapsing pressure wave being hydrostatic pressure) creates a pressure wave that is comparable to that of a small underwater explosion. However, it seems that multiple detonators directing pressure waves inward toward a converging point are needed if an "implosion" pressure wave is to have a greater magnitude than a typical underwater explosive pressure wave.

During experiments conducted by Naval Ordnance Laboratory, the collapse and implosion of cylinders under hydrostatic loading is shown to be somewhat repeatable. The depth at which implosion occurs is generally the same, but the shape of the imploded cylinder and the pressure pulse emitted from the implosion vary between occurrences. In the simulations conducted in this thesis, a cylinder was placed at a depth that was less than the crush depth of the cylinder. Then, a small charge was placed nearby the cylinder in order to initiate the implosion of the cylinder. Previous simulations have been conducted at Naval Undersea Warfare Center-Newport that initiated the implosion by placing a cylinder at subcritical hydrostatic pressure and initiating an implosion by giving the cylinder an initial deformation at a point. The pressure wave emitted from a "tapped"

cylinder implosion was symmetric about the entire model. However, when a small charge is used to initiate the implosion event, the pressure wave from the small charge interferes with the pressure wave caused by the subsequent implosion. This is shown by a non-symmetric pressure wave being emitted from the imploding cylinder as well as the general shape of the imploding cylinder. While a tapping of the cylinder initiates a controlled buckling process, the small charge creates buckling that collapses the entire cylinder upon itself. Also note, because of the interference caused by the explosive pressure wave, it is suggested that the smallest possible charge size be used in order to mitigate the influence of the explosive's pressure wave. However, the placement of that small charge (whether below or above) does not have an effect on the pressure wave emitted from the implosion event. The use of a small charge to initiate the implosion process is recommended as a more realistic approach to modeling pressure vessel implosions.

B. FURTHER STUDIES

There is much work yet to be accomplished in the study of implosion phenomena. While this thesis has touched on the implosion of an unstiffened cylinder due to a small charge placed in close proximity to the cylinder, further work should be done on the implosion of stiffened cylinders. The implosion of a stiffened cylinder will be more complex, especially if the implosion is due to a placement of a small charge. The charge type and weight will be dependent upon the structure of the cylinder, and thus will be different for each structure studied.

In addition, further studies should include simulations of shaped charge explosive devices. As documented in this thesis, a solid explosive charge outfitted with plural detonators that send multiple explosive pressure waves converging to a focus point can provide a marked increase in the magnitude of the pressure wave that is emitted from the weapon. The simulation of such an event should be accomplished. The future of mine warfare may include this type of warhead, and the effects of such a weapon should be studied.

APPENDIX A: SPHERICAL IMPLOSION FLOW FIELD

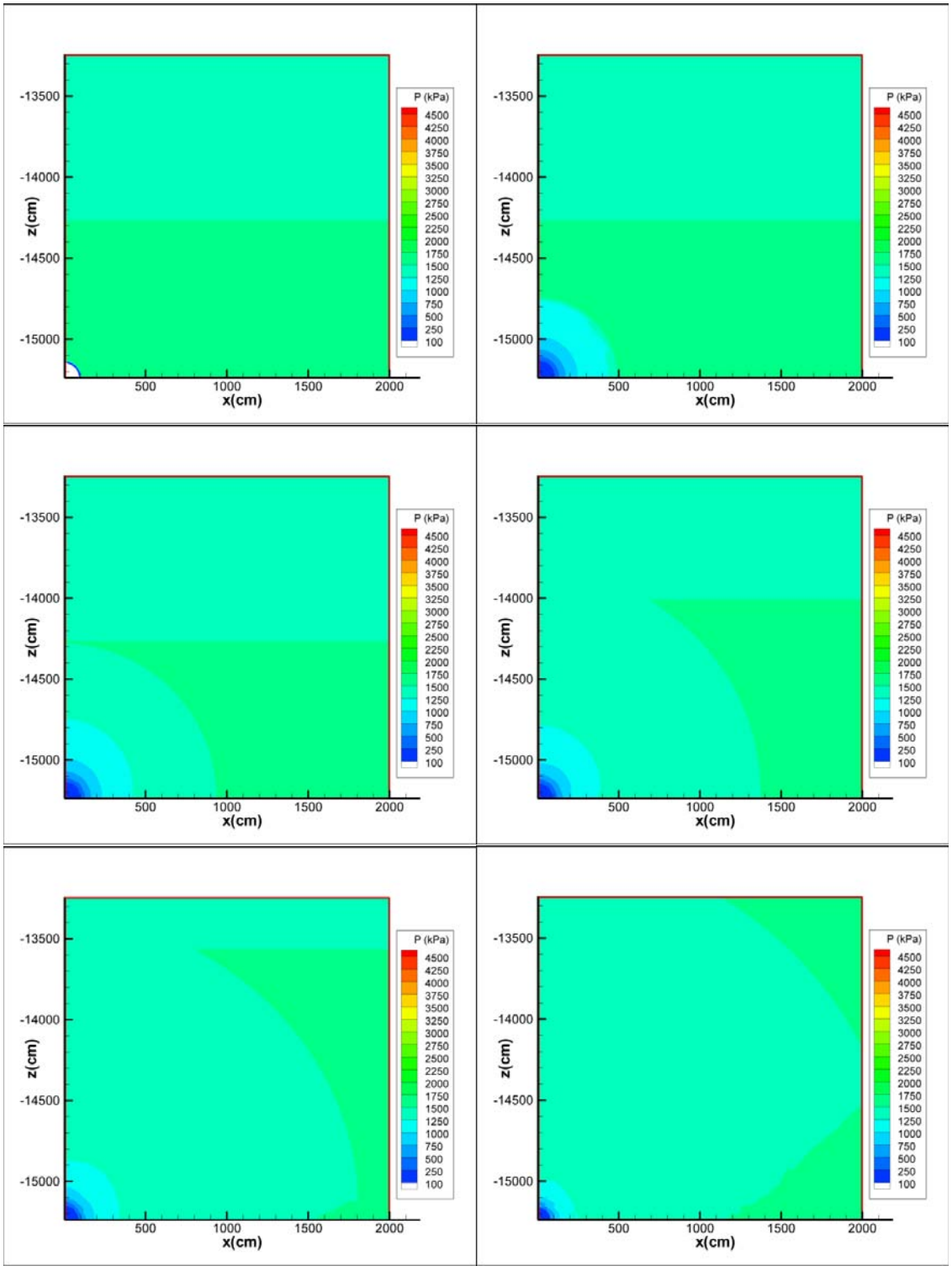

Figure 54. Spherical Implosion Flow Field: Frames 1-6

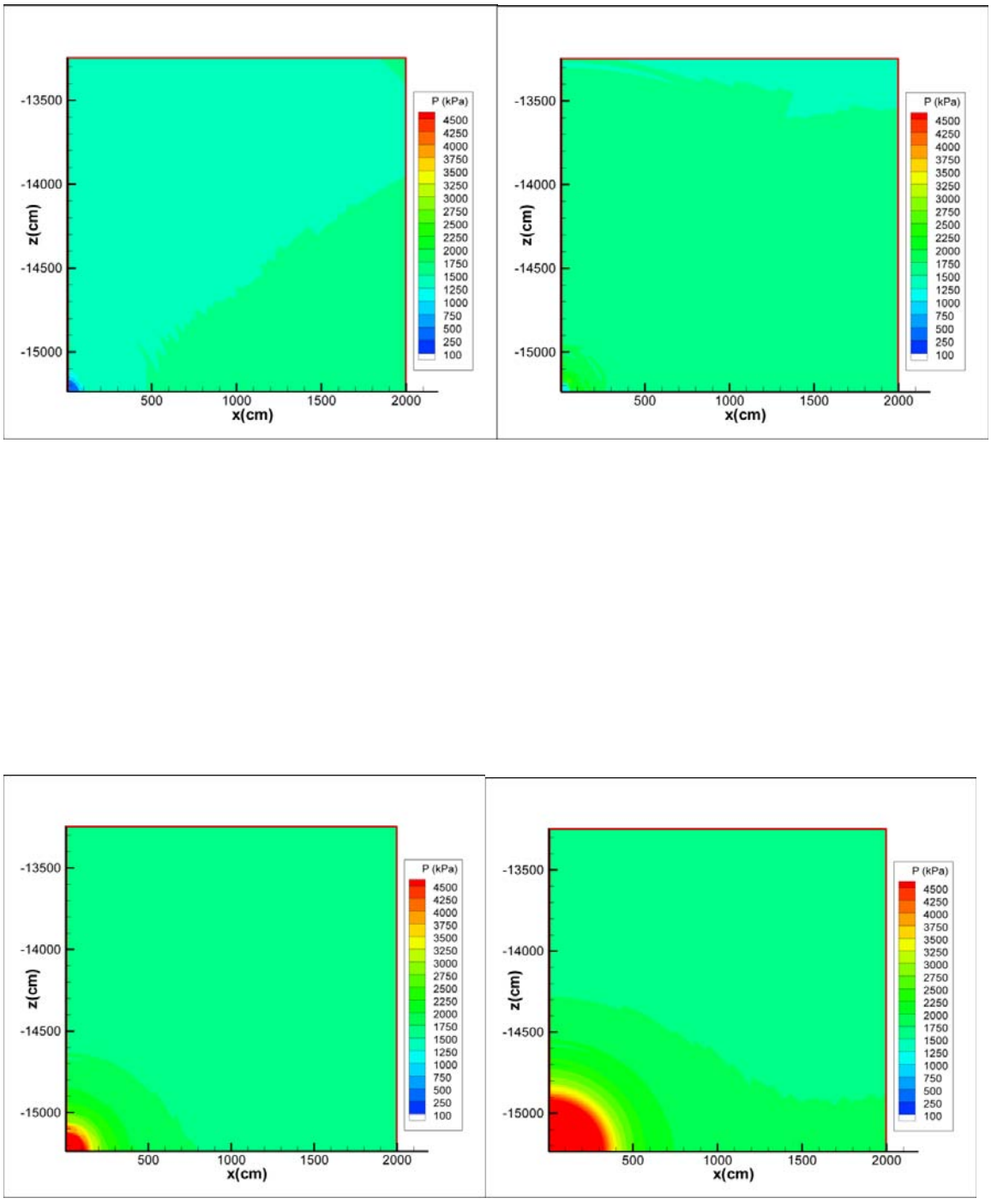

Figure 55. Spherical Implosion Flow Field: Frames 7-10

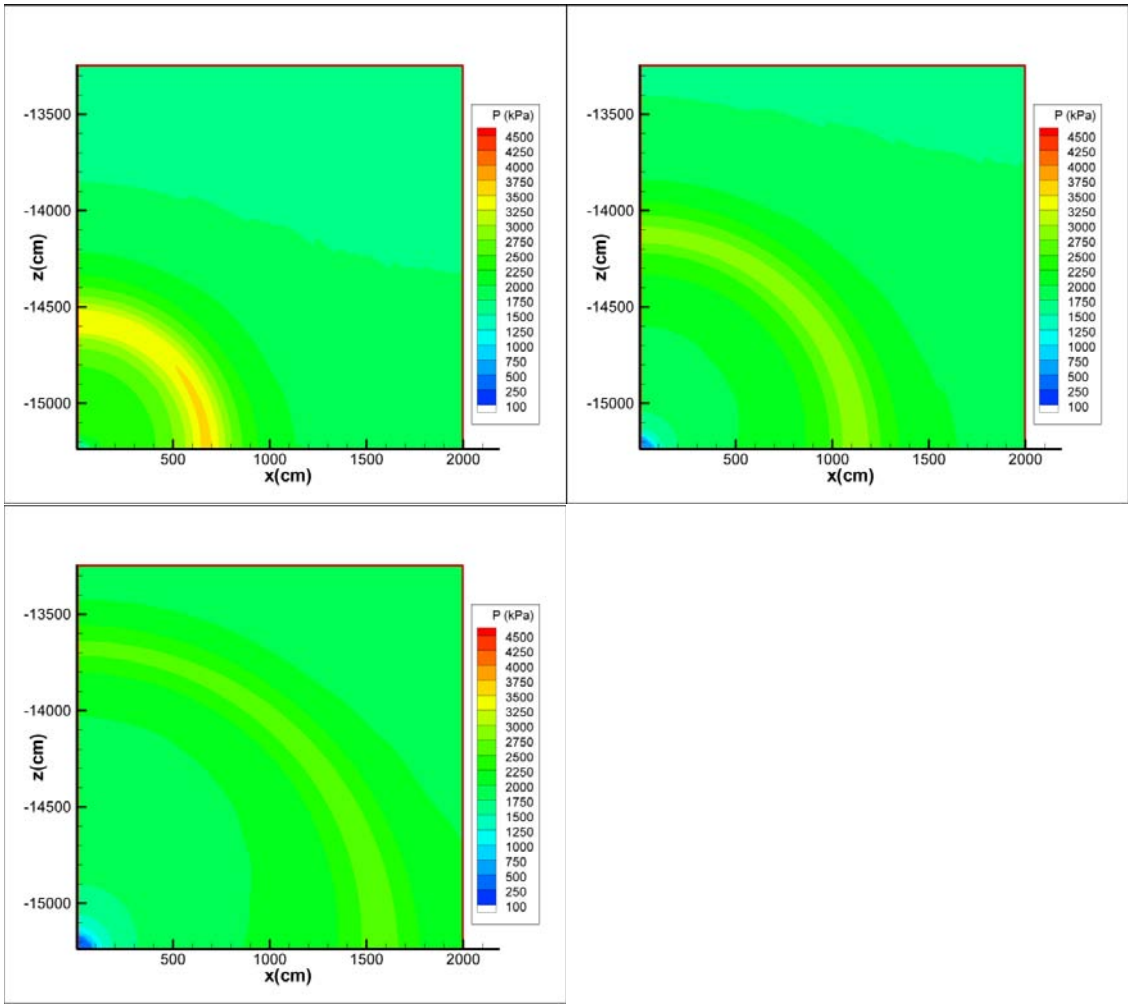

Figure 56. Spherical Implosion Flow Field: Frames 11-13

THIS PAGE INTENTIONALLY LEFT BLANK

APPENDIX B: IMPLOSION OF ALUMINUM CYLINDER

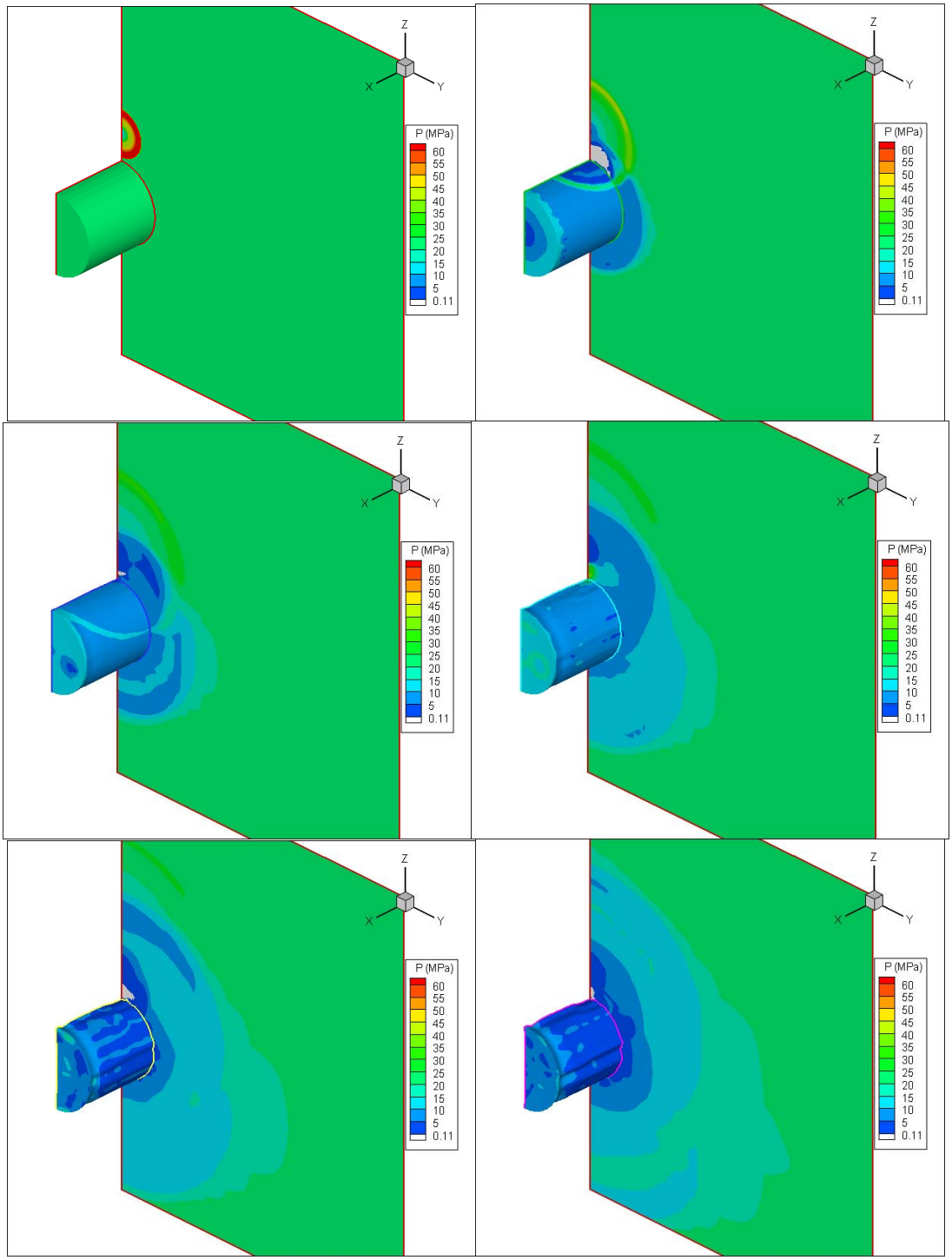

Figure 57. Implosion of Aluminum Cylinder: Frames 1-6

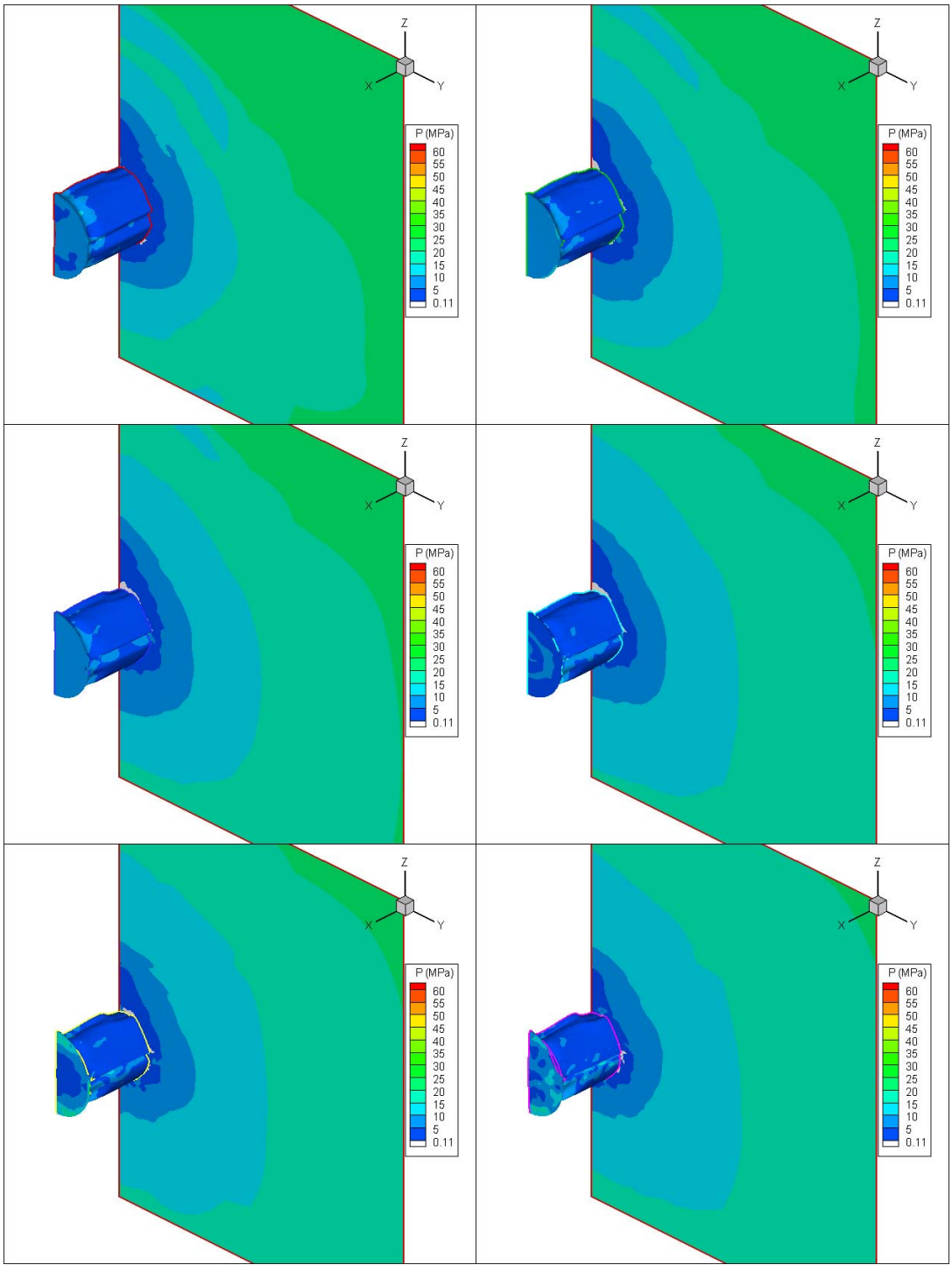

Figure 58. Implosion of Aluminum Cylinder: Frames 7-12

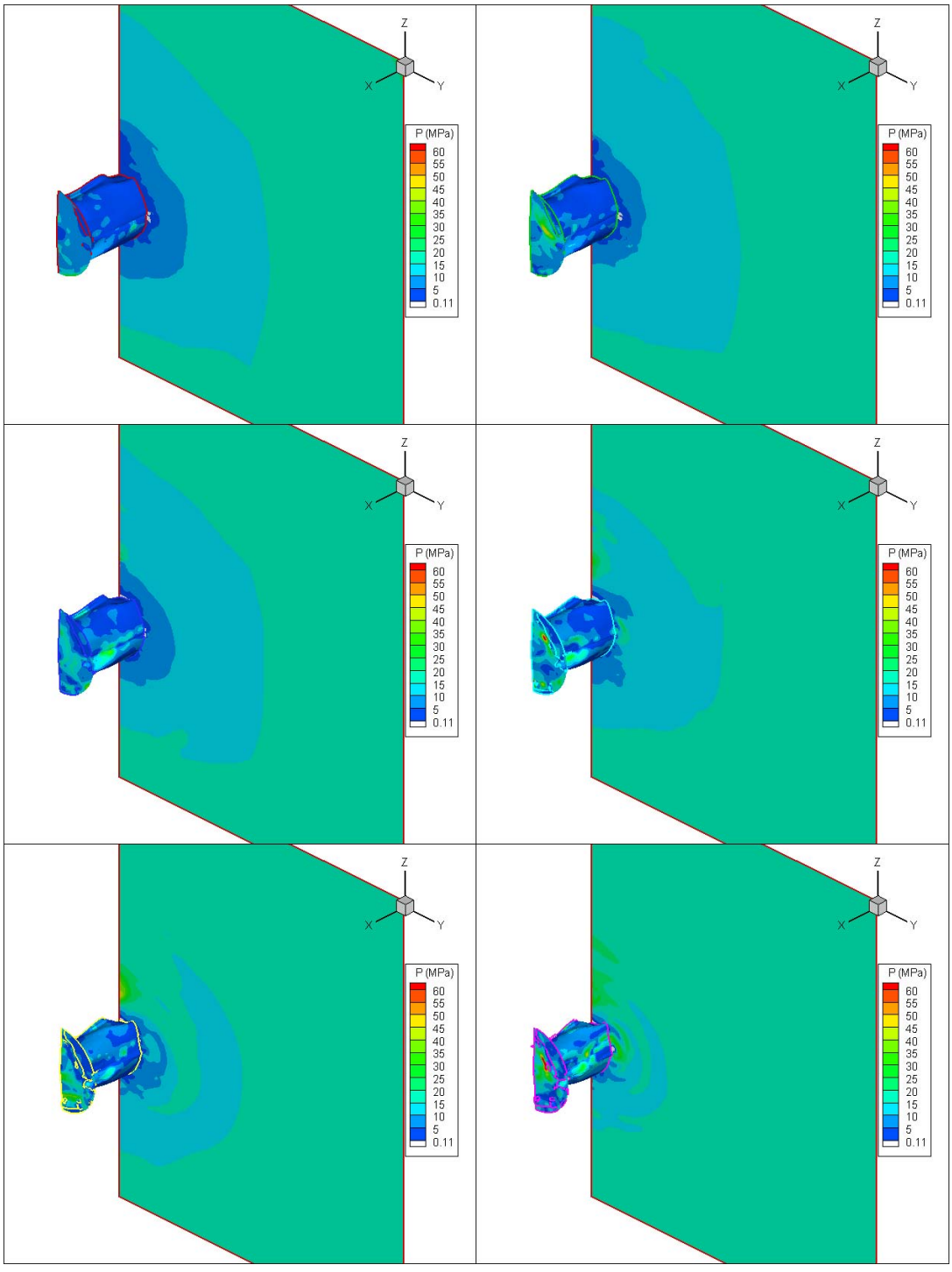

Figure 59. Implosion of Aluminum Cylinder: Frames 13-18

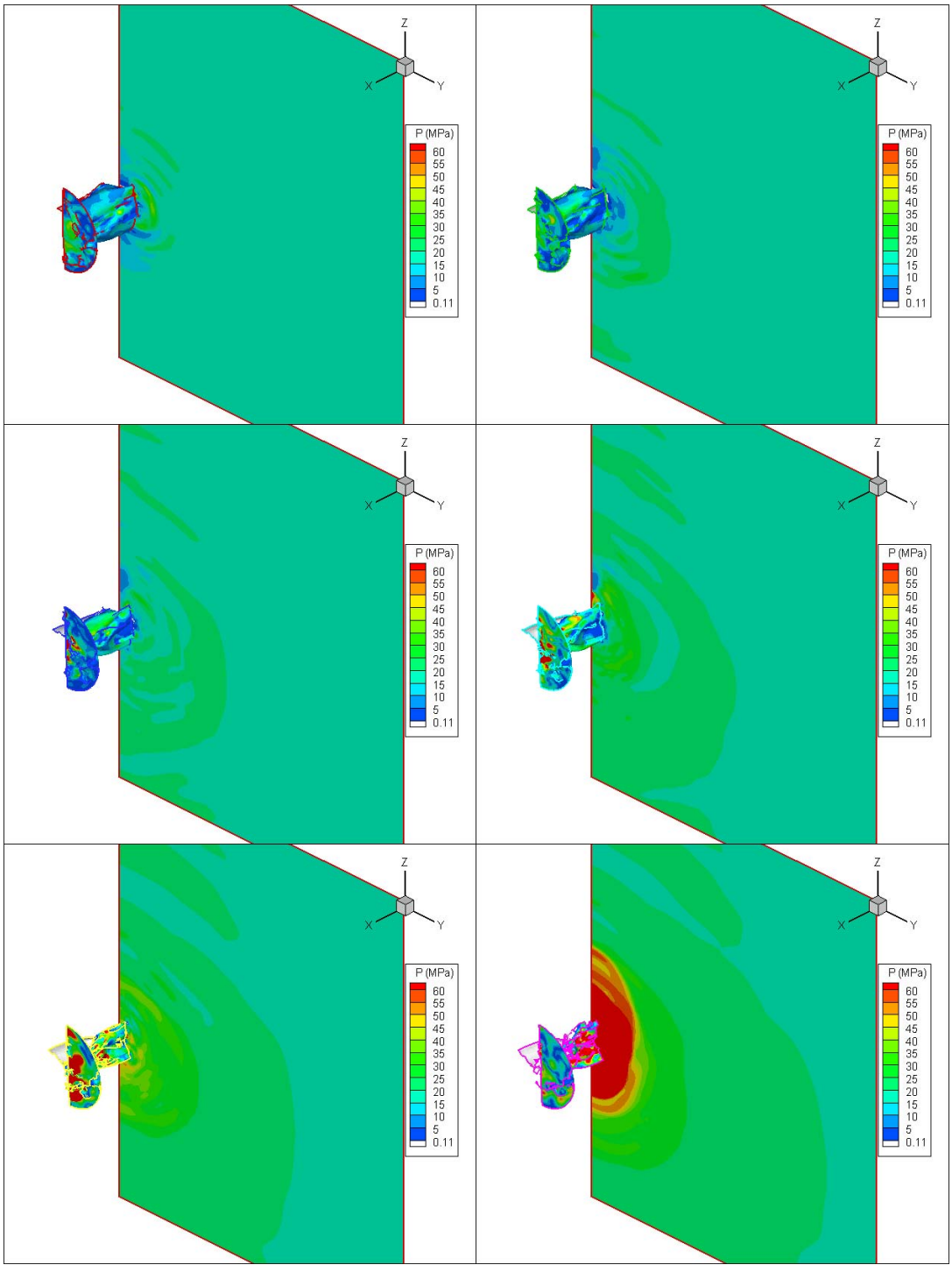

Figure 60. Implosion of Aluminum Cylinder: Frames 19-24

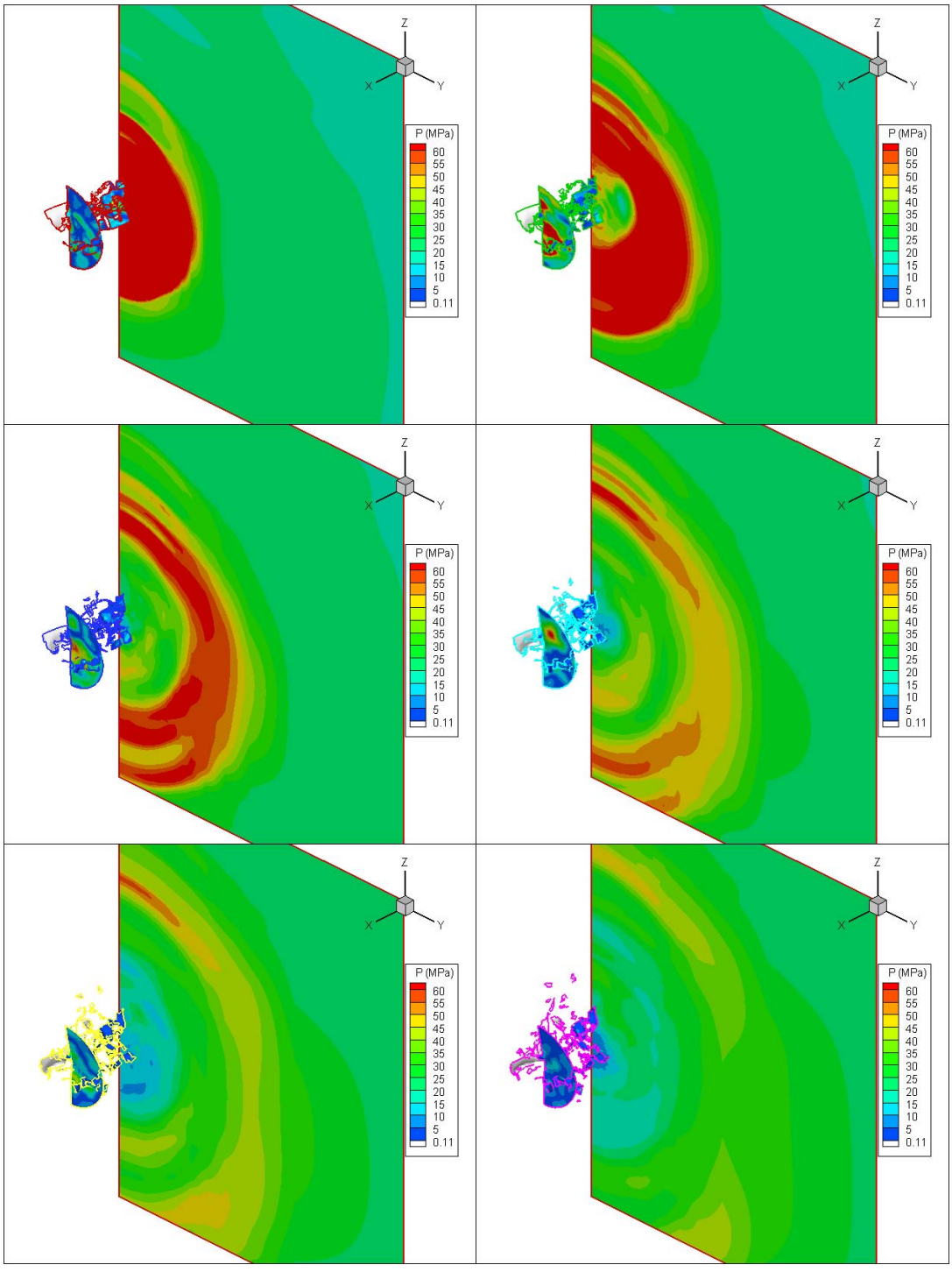

Figure 61. Implosion of Aluminum Cylinder: Frames 25-30

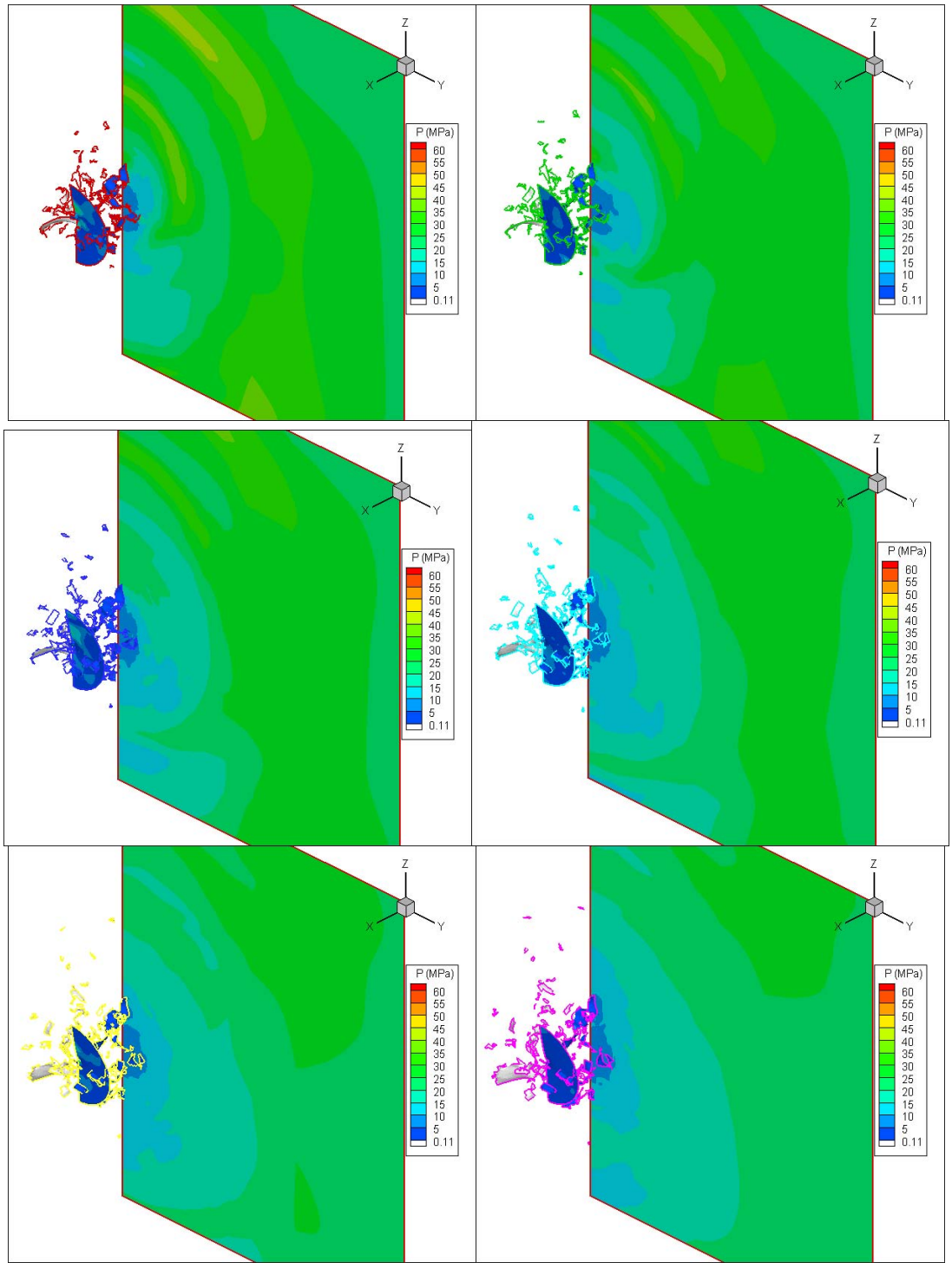

Figure 62. Implosion of Aluminum Cylinder: Frames 31-36

APPENDIX C: GEMINI SUITE INPUT DECKS

The following input deck comes from the implosion of an aluminum cylinder at 95% crush depth using a 50 gram TNT charge. The following figure displays the flow path of this simulation.

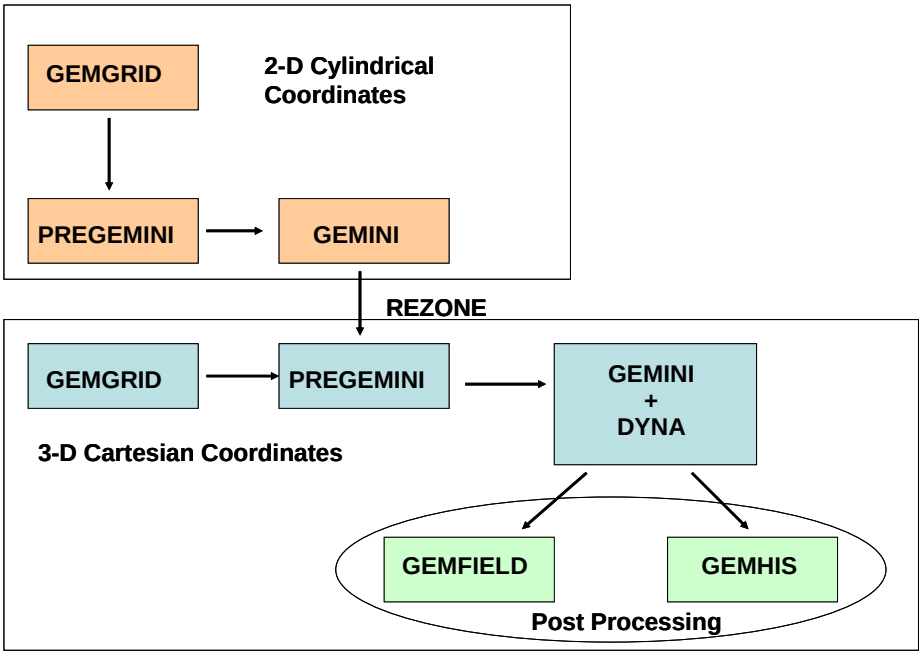

Figure 63. Program Flow Path for Cylinder Implosion

A. 2-DIMENSIONAL COORDINATE SYSTEM

1. GEMGRID

```
# In this grid, the cells will be uniform in the X
# direction.  The cells will be 0.25 cm in length.
# There will be 120 cells in this direction.
                    <X BLOCK>
#             +++++ r,x    mesh +++++
1                      idatum
0.                     xdatum
#number  xs       xe        ratio        width
NA      0.25       NA          1.           30
                    <END X BLOCK>
```

```
#The Y BLOCK does not need to be input (only 2-D case).
                      <Y BLOCK>
#             ++++++ y   mesh ++++++
1                       idatum
0.                      ydatum
#number  xs       xe        ratio        width
1         1.      NA         1.            NA
                   <END Y BLOCK>


# In this grid, the cells will be uniform in the Z
# direction.  The cells will be 0.25 cm in height.
# There will be 128 cells in this direction.
                     <Z BLOCK>
#              +++++++ z   mesh  +++++++
1                       idatum
-207356                      zdatum
#number  xs       xe        ratio        width
NA      0.25      0.25       NA           32
                   <END Z BLOCK>

                        <POST>
Standard       # Half, Standard or double
                    <END POST>
```

2. PREGEMINI

```
<OPTIONS>
 START
 None             # Modifications
     0.           # initial time (<0 then use value in restart file)
-980.665          # gravity constant(e.g. -981cm/sec**2 ; z-direction)
<END OPTIONS>

<REZONE>              # section necessary for rezone runs only
0                 # cell subdivision in each direction
0                 # subdivision refine in mixed cells
0.                # new flow field conservation scaling factor
0.  0.  0.        # location of old grid origin in new grid
<END REZONE>

<GRID>
CYLINDRICAL        # coordinates: CARTESIAN, CYLINDRICAL or SPHERICAL
#  cells    cell width   datum
Xcells=120   dx=0.  Xdatum=0.    # input number of cells from Grid.out
Zcells=128  dz=0.  Zdatum=0.     # input number of cells from Grid.out
gemgrid/grid.asc                 # calls the grid specified in GEMGRID
<END GRID>

<BOUNDARY CONDITIONS>
# lower     upper    in each direction
Xmin=wall  Xmax=free       # b/c use of symmetry, the X min is fixed
Zmin=wall  Zmax=free       # the 'free' allows for minimal reflection
<END BOUNDARY CONDITIONS>
```

```
<BLOCKED CELLS>
# imin imax  jmin jmax  kmin kmax
<END BLOCKED CELLS>

#   ++++++ FLOW FIELD SPECIFICATION ++++++
<EOS FILES>   # Equation of State Files
# .... matl number  matl file name ......
TNT             D:\Seth\Tools\Eos_Lib\TNT.eos         # EOS file for
#                                                       TNT
Tillwater       D:\Seth\Tools\Eos_Lib\Tillwater.eos   # EOS file for
#                                                       Water
Air             D:\Seth\Tools\Eos_Lib\air.eos         # EOS file for
#                                                       Air
<END EOS FILES>

<HYDROSTATIC FIELD>    # creates a hydrostatic field
 zref=0.     pref=1.e+6     zmax=max     # Reference line
#   matl name     matl zmin     matl int energy     [EOS V1..Vn]
    air           zmin=0.       ei=eref
    Tillwater     zmin=min      ei=eref
<END HYDROSTATIC FIELD>

<INITIAL STATES>
#state   matl    g      rho              e         p   u   v   w
1     TNT     rho=rhoref     ei=eref
<END INITIAL STATES>

<FLOWFIELD>
option=hydrostatic               # initializes hydrostatic field
# option   State
                 # imin/max  jmin/max  kmin/max state
option=ball   state=1   mass=50     x=0    z=-207341  # charge
#                                                       parameters
<END FLOWFIELD>
```

3. GEMINI

```
<CASE>
..\Pregemini\restart_000000.bin         # start file (from PreGemini)
IED Cylinder Pre-calc                   # TITLE (Limit 40 characters)
Fluid                                   # Fluid or Structure
<END CASE>

<TERMINATE>
300                          # maximum step number
0.003                        # termination time
1.E-12                       # terminate if step size is less than this
value
# i/r  j/y  k/z  variable  change (+/-)    This is a TRAP STOP
x=30  j=1  z=-207341   var=p  dif=0.1
x=30  j=1  z=-207341   var=u  dif=10.
x=1   j=1  z=-207355   var=p  dif=0.1
x=1   j=1  z=-207355   var=w  dif=10.
x=1   j=1  z=-207327   var=p  dif=0.1
x=1   j=1  z=-207327   var=w  dif=10.
<END TERMINATE>
```

```
<INTEGRATION>
.45                 # CFL safety factor
.05                 # initial step CFL factor
2.                  # limiter setting
0                   # equalize after lagrange step (1=yes,0=no)
1                   # equalize after remap step (1=yes,0=no)
1                   # protect (0=off, 1 = on)
<END INTEGRATION>

<CELL HISTORY>
#x=7.62  z=-21.59    # 3.0 in r-dir
<END CELL HISTORY>

<CONTOUR PLOTS>
 1000            #  step increments between plotting
 .5e-5           #  time increments between plotting

<target plot steps>
<end target plot steps>

<target plot times>
<end target plot times>

<END CONTOUR PLOTS>

<RESTART>
100          #  restart tape write interval
  5          #  restart file save frequency

<target restart steps>
<end target restart steps>

<target restart times>
<end target restart times>

<END RESTART>

<TEXT OUTPUT>
1000000             # step increments between printing [Gemini Only]
1000.           # time increments between printing [Gemini Only]
 standard     # options: DEBUG or STANDARD,  ELEMENTS is optional
# imin imax  jmin jmax  kmin kmax
  imin=1  imax=1  jmin=1  jmax=1  kmin=10  kmax=1
<END TEXT OUTPUT>


      ***** END *****
```

B. 3-DIMENSIONAL COORDINATE SYSTEM

The 2-D portion of this problem consisted of setting up the environment and letting the charge explode. The 2-D portion was stopped when the pressure wave from the explosion was about to reach the cylinder structure. At this point, the calculation was 'rezoned' into three dimensions in order to incorporate the structure. By doing a 2-D 'pre-calc', the computational time was decreased.

1. GEMGRID

```
# This grid input is for a three dimensional Cartesian coordinate
simulation.


# The X BLOCK displays the cell properties for the X direction.
# In this case, there are 4 lines of input.  There are 20 cells
# of constant width (0.6 cm).  Three are 35 cells that begin at a
# width of 0.65 cm and increase to 1.4 cm in width.  There are
# 5 cells that start with a width of 1.4 cm and end with 5.0 cm.
# There are 7 cells that begin with a width of 7.0 cm and end
# with a width of 62.8 cm.
                    <X BLOCK>
#             +++++ r,x    mesh +++++
1                      idatum
0.                     xdatum
#number  xs       xe         ratio        width
20      0.6       NA           1.           NA
35      0.65     1.4           NA           NA
 5      1.4      5.0           NA           NA
 7      7.0      62.8          NA           NA
                  <END X BLOCK>


# Like the X BLOCK, the Y BLOCK inputs indicate a nonuniform grid
# in the Y direction.
                    <Y BLOCK>
#             ++++++ y   mesh ++++++
1                      idatum
0.                     ydatum
#number  xs       xe         ratio        width
23      0.5       NA          1.           NA
12      1.0       NA          1.           NA
 5      1.5       4.0         NA           NA
 5      4.0      16.0         NA           NA
 3      18.0    106.7         NA           NA
                  <END Y BLOCK>




# Like the X BLOCK, the Z BLOCK inputs indicate a non-uniform grid
```

```
# in the Z direction.  In addition, the zdatum is given to be at
# Zmin.


    <Z BLOCK>
#              +++++++ z   mesh  +++++++
1                     idatum
-207469                    zdatum
#number  xs       xe        ratio        width
  NA     2.0       NA         1.0         50
  NA     1.0      1.0         NA          15
  NA     0.5      0.5        NA           50
  NA     0.5      NA         1.0          15
  NA     1.0      NA         1.0          50
  NA     2.0      NA         1.0          70
                   <END Z BLOCK>

                      <POST>
Standard       # Half, Standard or double

                <END POST>
```

2. PREGEMINI

```
<OPTIONS>
 REZONE           # Rezone of the 2-D Precalc
 BODYFILL         # Allows a structure to be filled with property
     0.           # initial time (<0 then use value in restart file)
-980.665          # gravity constant(e.g. -981cm/sec**2 ; z-direction)
<END OPTIONS>

<REZONE>               # section necessary for rezone runs only
D:\Seth\Cylinder_Tests\Explosion_95\Gemini2D\Gemini\restart_000080.bin
2                 # cell subdivision in each direction
5                 # subdivision refine in mixed cells
4.                # new flow field conservation scaling factor
0.  0.  0.        # location of old grid origin in new grid
<END REZONE>

<SUBGRIDS>
2  auto         # Prepares for parallel processing
1 auto          # There are 2 subgrids created in X and Z direction
2 auto
<END SUBGRIDS>

<GRID>
CARTESIAN    # coordinate (0 = Cartesian; 1 = cylindrical; 2 =
spherical)
#     cells    cell width   datum
    Xcells=67      dx=0.     Xdatum=0.    #  x or r cells
    Ycells=48      dy=0.     Ydatum=0.    #     y cells
    Zcells=255      dz=0.     Zdatum=0.    #     z cells
grid\grid.asc    # calls the Grid.out file
<END GRID>


<BOUNDARY CONDITIONS>
#  lower upper    direction
```

```
Xmin=wall Xmax=free    # x or r
Ymin=wall Ymax=free    # y
Zmin=free Zmax=free    # z
 <END BOUNDARY CONDITIONS>

<BLOCKED CELLS>
 # imin imax  jmin jmax  kmin kmax
<END BLOCKED CELLS>

#   ++++++ FLOW FIELD SPECIFICATION ++++++
<EOS FILES>
# .... matl number  matl file name ......
TNT             D:\Seth\Tools\Eos_Lib\TNT.eos
Tillwater       D:\Seth\Tools\Eos_Lib\Tillwater.eos
air             D:\Seth\Tools\Eos_Lib\air.eos
<END EOS FILES>

<INITIAL STATES>
#state   matl    g      rho              e         p   u   v   w
1     TNT        rho=rhoref     ei=eref
2     Air        rho=rhoref     ei=eref
3     Tillwater  rho=rhoref     ei=eref
<END INITIAL STATES>

<BURN>
# unburned to burned         Det.time[s]      x0    y0    z0
#Pentolitesolid to Pentolite   Tburn=0.        x=0.  y=0.  z=-21.59
<END BURN>

<HYDROSTATIC FIELD>
 zref=0.     pref=1.e+6     zmax=max     # Reference line
#   matl name     matl zmin     matl int energy     [EOS V1..Vn]
    air           zmin=0.       ei=eref
    Tillwater     zmin=min      ei=eref
<END HYDROSTATIC FIELD>


<FLOWFIELD>
# option   State
option=hydrostatic
<END FLOWFIELD>
```

```
# The structure that is filled with a property is input in this
# section.
# The interface elements and node file are needed.  In addition, the
# location of the origin of the structure needs to be located in the
# flow field coordinate system.
<BODY>
Cylinder.ifa    (I5)      #interface element file (format identifer)
Cylinder.nod              #node file
0.   0.   -207326.2              #location of body coordinate system in
#                                 fluid mesh
1.   0.   0.                 #vector along body coord sys x axis in fluid
#                           coord
0.   1.   0.                 #vector along body coord sys y axis in fluid
#                           coord
0.   0.   1.                 #vector along body coord sys z axis in fluid
#                           coord
<END BODY>

# In BODYFILL, seeds need to be created that will fill the above
# mentioned
# structure.  These seeds will be the starting point of the fill, and
# will
# continue until a computational boundary, structural boundary, or
# subgrid boundary is reached.
<BODYFILL>
state=2       x=20.   y=15.0    z=-207380.
state=2       x=40.   y=15.0    z=-207380.
state=2       x=22.5  y=2.0    z=-207357.
state=2       x=40.   y=2.0    z=-207357.
<END BODYFILL>


<TEXT OUTPUT>
# imin imax  jmin jmax  kmin kmax
  imin=1  imax=1  jmin=1  jmax=1  kmin=1  kmax=1
<END TEXT OUTPUT>
```

3. GEMINI

```
<CASE>
PreGemini_Rezone\rezone_000000_xxx.bin       # start file
Aluminum Cylinder Implosion                  # TITLE (Limit 40
characters)
Coupled                                      # Fluid or Coupled
<END CASE>

<TERMINATE>
999999                      # maximum step number
.008                        # termination time
1.E-12                      # terminate if step size is less than this
value
# i/r   j/y   k/z   variable  change(+/-)
#  115    80    55      u          10.
<END TERMINATE>

<INTEGRATION>
```

```
.45                 # CFL safety factor
.05                 # initial step CFL factor
2.                  # limiter setting
0                   # equalize after lagrange step (1=yes,0=no)
1                   # equalize after remap step (1=yes,0=no)
1                   # protect (0=off, 1 = on)
<END INTEGRATION>

<TEXT OUTPUT>
     1000             # step increments between printing [Gemini Only]
     1000.            # time increments between printing [Gemini Only]
 standard           # options: DEBUG or STANDARD,  ELEMENTS is optional
   # imin imax  jmin jmax  kmin kmax
      1    1     1    1     1   1
<END TEXT OUTPUT>

#   -----history-----
<CELL HISTORY>
#  i    j    k
#  x    y    z
x=0.1    y=0.1    z=-207331   # 25cm above center
x=0.1    y=0.1    z=-207356   # 50 cm above center
x=0.1    y=0.1    z=-207306   # 100 cm above center
x=0.1    y=0.1    z=-207428    # 25 cm below center
x=0.1    y=0.1    z=-207453    # 50 cm below center
x=0.1    y=0.1    z=-207503    # 100 cm below center
x=22.85    y=0.1    z=-207331   # 25cm above 3/4 length
x=22.85    y=0.1    z=-207356   # 50 cm above 3/4 length
x=22.85    y=0.1    z=-207306   # 100 cm above 3/4 length
x=22.85    y=0.1    z=-207428    # 25 cm below 3/4 length
x=22.85    y=0.1    z=-207453    # 50 cm below 3/4 length
x=22.85    y=0.1    z=-207503    # 100 cm below 3/4 length
x=0.1    y=48.3    z=-207380   # 25cm athwart at center
x=0.1    y=73.3    z=-207380   # 50 cm athwart at center
x=0.1    y=123.3    z=-207380   # 100 cm athwart at center
x=22.85    y=48.3    z=-207380    # 25 cm athwart at 3/4 length
x=22.85    y=73.3    z=-207380    # 50 cm athwart at 3/4 length
x=22.85    y=123.3    z=-207380    # 100 cm athwart at 3/4 length
x=0.1    y=0.1       z=-207380     # center of cylinder
x=22.85   y=0.1      z=-207380    # center of cylinder at 3/4 length
#x=0.1   y=7.9375  z=-566.9   #  4" freefield gage
#x=0.1  y=16.51    z=-573.29   #  6.5" freefield gage
#x=0.1  y=46.99    z=-573.29   #  18.5" freefield gage
#x=0.1    y=0.1    z=-574.5   #  contact gage at cylinder crown, axial
dist=0 (ctr)
#x=11.43  y=0.1    z=-574.5   #  contact gage at cyl. crown, 4.5"
axially from ctr
#x=22.86  y=0.1    z=-574.5   #  contact gage at cyl. crown, 9.0"
axially from ctr
#x=0.1   y=11.66   z=-585.0  #  contact gage at 30 deg. down.
#x=0.1   y=23.6172 z=-605.5 #  contact gage at mid-draft, 90 deg.
#x=0.1    y=0.1    z=-636   #  contact gage at cylinder keel
#x=0.1    y=0.1    z=-475   # one meter above top
#x=0.1    y=0.1    z=-525   # half meter above top
#x=0.1    y=0.1    z=-605.5  # center of imploded cylinder
<END CELL HISTORY>
```

```
<CONTOUR PLOTS>
20000       #   step increments between plotting
100.e-6      #  time increments between plotting

<target plot steps>
1
<end target plot steps>

<target plot times>
<end target plot times>

<END CONTOUR PLOTS>

# +++++ RESTART FILES +++++
<RESTART>
1000         #  restart tape write interval
5            #  restart file save frequency

  <target restart steps>
  <end target restart steps>

  <target restart times>
  <end target restart times>
<END RESTART>

#   +++++++++++++++ Required for Coupled Runs Only +++++++++++++++
<COUPLED>
1.e+6        # back pressure
.true.       # Load Failed SWI elements
0. 0. -207326.2     # location of Body coordinate system in Fluid Mesh
1. 0. 0.     # vector along Body coordinate system x axis in Fluid
#             coordinates
0. 1. 0.     # vector along Body coordinate system y axis in Fluid
#             coordinates
0. 0. 1.     # vector along Body coordinate system y axis in Fluid
#             coordinates
<END COUPLED>

<ELEMENT HISTORY>
 4224     # contact gage at cylinder crown, axial dist=0 (ctr)
 4213     # contact gage at cyl. crown, 4.5" axially from ctr
 4203     # contact gage at cyl. crown, 9.0" axially from ctr
 3804     #  contact gage at 30 deg. down.
 2922     #  contact gage at mid-draft, 90 deg.
 1578     #  contact gage at cylinder keel
<END ELEMENT HISTORY>




<NODE HISTORY>
```

```
  3   # crown node
 1122 # movin around mid-length circumference
 1154
 1186
 1218
 1250
 1282
 1314
 1346
 1378
 1410
 1442
 1474
 1506
 1538
 1570
    2 # mid-draft node
    4 # keel node
#   3 # crown node
  4292 # nodes along crown moving toward rear
  4294
  4296
  4298
  4300
  4302
  4304
  4306
  4308
  4312
  4316
  4320
  4324
  4328
  1604
<END NODE HISTORY>
```

4. GEMHIS

```
   <Case>
all             # Process number (3 digits, "all", or "none")
.               # Subdirectory for output files (must previously exist)
                # (don't use "/", use "." for current working dir)
none            # Series: Output file identifier (1-10 characters or
                  "none")
                # (Series cannot end with "b" for DysmasP files)
1               # IVerbose: Screen output (0=no, 1=some, 2=lots)
-1.000   1.00   # tBeg,tEnd: Time window for output (sec)
0.000   1.00    # tOffset, tScale: Offset and scaling for time
                # t <== tScale*(tOffset+t)
ascii           # FileType ("ascii" or "binary")
Tecplot         # FileFormat ("plain", "Tecplot", "DysmasP")
<End Case>

<Files>
1           # IFileSplitGbl: Output file type (Global variable files)
```

```
                    # 1= single file
                    # 2= one file for each variable
3             # IFileSplitPt: Output file type  (Point variable files)
                    # 1= single file
                    # 2= one file for each variable
                    # 3= one file for each history point
                    # 4= one file for each variable and history point
<End Files>

<Options>
1         # ChargeScale: Scaling for specie (EnergyInt, Energy, Mass,
              Volume, Radius)
-5.00e7          # pRefImp: Impulse intensity ref pressure (dynes/cm^2)
                 # (make <0 to use value from 1st record in file)
0                # IRmOverlap (flag for removing oldest data if there is
                   a time overlap)
<End Options>



####################################
#The remaining sections are optional
####################################

<Undocumented Options>
#GageSymSize=8.                #Size (cm) of symbols in file gages.dat
<End Undocumented Options>

<Global Variables>
#  Key    MatNum  VarOffset  VarScale     #Note: MatNum=0 is for cell
avg
 radius     1        0.        1.
<End Global Variables>

<Point Variables>
#  Key    MatNum  VarOffset  VarScale     #Note: MatNum=0 is for cell
avg
#   u       0        0.         1.
#   v       0        0.         1.
#   w       0        0.         1.
    p       0        0.         0.0001   # converts to kPa
#   r       0        0.         1.
#   r       1        0.         1.
#   r       2        0.         1.
#   e       0        0.         1.
#   e       1        0.         1.
#   e       2        0.         1.
#   eint    0        0.         1.
#   eint    1        0.         1.
#   eint    2        0.         1.
#   ekin    0        0.         1.
#   f       1        0.         1.
#   f       2        0.         1.
#  eos       1        0.        1.
<End Point Variables>
```

```
<Body Global Variables>
#  Key    VarOffset  VarScale
 force-x      0.        1.
 force-y      0.        1.
 force-z      0.        1.
 force        0.        1.
<End Body Global Variables>

<Body Element Variables>
#  Key    VarOffset  VarScale
   p          0.        1.
<End Body Element Variables>

<Body Node Variables>
#  Key    VarOffset  VarScale
 force-x      0.        1.
 force-y      0.        1.
 force-z      0.        1.
 force        0.        1.
   u          0.        1.
   v          0.        1.
   w          0.        1.
 vel          0.        1.
   x          0.        1.
   y          0.        1.
   z          0.        1.
<End Body Node Variables>




# The following is a Key to the Global Variables
#########################################################
#   Variable:                     allowed MatNum (0...NMat)
# energykin                          any
# energyint    energy      mass      any
#       vol    radius                >0
#    volcav                          >0
#
#########################################################
# The following is a Key to the Point Variables
#########################################################
#   Variable:                     allowed MatNum (0...NMat)
# all =  all point variables             NA
#   u = velocity in r,x-dir              0
#   v = velocity in y,theta-dir          0
#   w = velocity in z-dir                0
#   p = pressure                         0
#   r = density                          any
#   e = total energy                     any
# eint= internal energy                  any
# ekin= kinetic energy                   0
#   f = volume fraction                  >0
#   i = impulse intensity                0
```

```
# eos#= EOS variable number #           NA

#########################################################
# The following is a Key to the Body Global Variables
#########################################################
# force-x = Total body force in r,x-dir
# force-y = Total body force in y,theta-dir
# force-z = Total body force in z-dir
# force   = Total body force magnitude
#       i = Impulse

#########################################################
# The following is a Key to the Body Element Variables
#########################################################
#   p = Element pressure
#   i = Impulse intensity
#

#########################################################
# The following is a Key to the Body Node Variables
#########################################################
# force-x = Node force in r,x-dir
# force-y = Node force in y,theta-dir
# force-z = Node force in z-dir
# force   = Node force magnitude
#   u = Node velocity in r,x-dir
#   v = Node velocity in y,theta-dir
#   w = Node velocity in z-dir
# vel = Node velocity magnitude
#   x = Node position (r,x-dir)
#  y = Node position (y,theta-dir)
#  z = Node position (z-dir)
```

5. GEMFIELD

```
<Case>
all             # Process number (3 digits, "all", or "none")
.               # Subdirectory for output files (must previously exist)
                # (don't use "/", use "." for current working dir)
none            # Series: Output file identifier
                # (Series cannot end with "b" for DysmasP files)
1               # IVerbose: Screen output (0=no, 1=some, 2=lots)
-1.000   1.00   # tBeg,tEnd: Time window for output (sec)
 0.000   1.00   # tOffset, tScale: Offset and scaling for time
                # t <== tScale*(tOffset+t)
ascii           # FileType ("ascii" or "binary")
Tecplot         # FileFormat ("plain", "Tecplot", "DysmasP")
<End Case>

<File Output>
3                # IFileSplit: Output file type
                 # 1= single file
                 # 2= one file for each variable
                 # 3= one file for each time step
                 # 4= one file for each variable and time step
5000             # NTimeRecLimit: Max number of time records to generate
```

```
<End File Output>

<Time Step Targets>
#1815 6000
<End Time Step Targets>

<Plot Variables>
#  Key    MatNum  VarOffset  VarScale     #Note: MatNum=0 is for cell
avg
#   all       0        0.         1.
#   all includes the next nine variables
#   u         0        0.         1.
#   v         0        0.         1.
#   w         0        0.         1.
    p         0        0.         0.0001   # Convert to kPa
#   r         0        0.         1.
#   r         1        0.         1.
#   r         2        0.         1.
#   e         0        0.         1.
#   e         1        0.         1.
#   e         2        0.         1.
#   eint      0        0.         1.
#   eint      1        0.         1.
#   eint      2        0.         1.
#   ekin      0        0.         1.
#   f         1        0.         1.
#   f         2        0.         1.
#   f         3        0.         1.
#  stat       0        0.         1.
<End Plot Variables>



<Subdomain>
 xMin=0.    xMax=0.    iDelta=1
 yMin=-99999.     yMax=999999.    jDelta=1
 zMin=-9999999.     zMax=999999.    kDelta=1
       0                #NPtsRay
0. 0. 0.                # xOffset, yOffset, zOffset (cm)
1.e0                    # xyzScale   [xyz] <==
[xyz]Scale*([xyz]Offset+[xyz])
<End Subdomain>



####################################
#The next 2 sections are optional
####################################

<Options>
F          # Show parallel subdomain boundaries (default "F")
F          # Show failed body elements (default "T")
           # (Use "T" to preserve correct element numbering in Tecplot)
<End Options>

<Undocumented Options>
```

```
#addgeo=1  node1=1  node2=69
#addgeo=1  node1=0  node2=2
#ShowBlocked=T                    #logical flag to show values in cells
blocked by body
<End Undocumented Options>



#########################################################
# The following is a Key to the Plottable Variables
#########################################################
#   Variable:                     allowed MatNum (0...NMat)
# all =  all point variables             NA
#   u = velocity in r,x-dir              0
#   v = velocity in y,theta-dir          0
#   w = velocity in z-dir                0
#   p = pressure                         0
#   r = density                          any
#   e = total energy                     any
# eint= internal energy                  any
# ekin= kinetic energy                   0
#   f = volume fraction                  >0
# eos#= EOS variable number #            NA  [currently, only for P-
alpha EOS]
# stat= status of cell (active/blocked)  0
```

LIST OF REFERENCES

1. Hicks, A.N., "Explosion Induced Hull Whipping," Advances in Marine Structures: Proceedings of an International Conference held at the Admiralty Research Establishment, Dunfermline, 20-23 MAY 1986.

2. Kusano, H.M., "Implosions in Pressure Vessels, Experimental Results," Naval Civil Engineering Laboratory, Point Hueneme, California, FEB 1970.

3. Shin, Y.S., "Naval Ship Shock and Design Analysis," Course Notes for Underwater Shock Analysis, Naval Postgraduate School, Monterey, CA, 2004.

4. Snay, H.G., "Hydrodynamics of Underwater Explosions," U.S. Naval Ordinance Laboratory, 1957.

5. Hicks, A.N., "Effect of Bubble Migration of Explosion-Induced Whipping of Ships," Report 3301, Naval Ship Research and Development Center, Washington, D.C., FEB 1970.

6. Chertock, G., "The Flexural Response of a Submerged Solid to a Pulsating Gas Bubble," Journal of Applied Physics, Vol. 24, No. 2, FEB1953.

7. Hicks, A.N., "The Whipping Forces Experienced by a Ship Very Close to an Underwater Explosion," Department of the Navy, Naval Ship Research and Development Center, Washington, D.C., JAN 1970.

8. Chahine, G.L. and Harris, G.S., "Multi-cycle Underwater Explosion Bubble Model. Part II: Validation Examples for Hull Girder Whipping Problems," Indian Head Division, Naval Surface Warfare Center, Indian Head, MD, 1998.

9. USA+ Keyword User's Manual, Release 6.21, Anteon Corporation, Mystic, CT, NOV 2003.

10. Drimmer, B.E., "Method for Improving the Performance of Underwater Explosive Warheads," United States Patent #5450794, SEP 1995.

11. Lee, J.H., "Theory of Explosions," McGill University, Montreal, Quebec, NOV 1969.

12. Gemini User's Manual, Release 4.30, Naval Surface Warfare Center, Indian Head, MD, JUN 2005.

13. Price, R. S., "Sounds from Implosions of Steel Cylinders Under Water," Naval Ordnance Laboratory, White Oak, Maryland, SEP 1974.

14. Reader, W.T. and Chertock, R.J., “Transient Sounds Due to Implosion of Simple Structures under Hydrostatic Pressure,” Journal of the Acoustical Society of America, 1972.

15. Urick, R.J., “Implosions as Sources of Underwater Sound,” Journal of the Acoustical Society of America, 1963.

16. Turner, S.E., “Small-Scale Implosion Testing of Glass and Aluminum Cylinders,” Naval Undersea Warfare Center Division, Newport, Rhode Island, AUG 2004.

17. Turner, S.E., “Summary of Analytical Prediction of Implosion with Glass Test Samples,” Naval Undersea Warfare Center Division, Newport, Rhode Island, OCT 2004.

18. Roark, R.J. and Young, W.C., *Formulas for Stress and Strain 5th Edition,* McGraw-Hill Book Company, 1975.

INITIAL DISTRIBUTION LIST

1. Defense Technical Information Center
   Ft. Belvoir, Virginia

2. Dudley Knox Library
   Naval Postgraduate School
   Monterey, California

3. Mechanical Engineering Department Chairman, Code ME
   Naval Postgraduate School
   Monterey, California

4. Naval/Mechanical Engineering Curriculum Code 74
   Naval Postgraduate School
   Monterey, California

5. Distinguished Professor Young S. Shin, Code ME/Sg
   Department of Mechanical and Astronautical Engineering
   Naval Postgraduate School
   Monterey, California

6. Research Assistant Professor Jarema M. Didoszak, ME/Di
   Department of Mechanical and Astronautical Engineering
   Naval Postgraduate School
   Monterey, California

7. Reid M. McKeown
   Naval Surface Warfare Center – Indian Head Division
   Indian Head, Maryland

8. Frederick A. Costanzo
   Underwater Explosion Research Department (UERD)
   Naval Surface Warfare Center – Carderock Division
   West Bethesda, Maryland

9. Gregory S. Harris
   Naval Surface Warfare Center – Indian Head Division
   Indian Head, Maryland

10. Roger Ilamni
    Naval Surface Warfare Center – Indian Head Division
    Indian Head, Maryland

11. Steven E. Turner
Naval Undersea Warfare Center – Newport Division
Newport, Rhode Island

12. Hans U. Mair
Institute for Defense Analysis
Alexandria, Virginia

13. Ken C. Kiddy
Naval Surface Warfare Center – Indian Head Division
Indian Head, Maryland

14. Andrew Wardlaw
Naval Surface Warfare Center – Indian Head Division
Indian Head, Maryland

15. Alan Luton
Naval Surface Warfare Center – Indian Head Division
Indian Head, Maryland

16. Professor Nick Vlahopoulos
Naval Architecture & Marine Engineering Department
University of Michigan
Ann Arbor, Michigan

17. Robert Wunderelick
Naval Surface Warfare Center – Carderock Division
West Bethesda, Maryland

18. Jay Warren
Northrop Grumman Corporation
Newport News, Virginia

19. Thomas Moyer
Northrop Grumman Ship Systems
Pascagoula, Mississippi

20. Travis Kerr
Northrop Grumman Corporation
Newport News, Virginia

21. Luise Couchman
Naval Research Laboratory
Washington, District of Columbia

22. Angela Maggioncalda
ROI Consulting LLC
Washington, District of Columbia